Evaluating the Impact Reduced *RBX1* Expression has on Chromosome Instability and Colorectal Cancer

by

Emerson Davi do Nascimento Brazil

A Thesis submitted to the Faculty of Graduate and Postdoctoral Studies of
the University of Manitoba
in partial fulfillment of the requirements of the degree of

Master of Science

Department of Biochemistry and Medical Genetics

University of Manitoba

Winnipeg

Copyright © 2026 by Emerson Davi do Nascimento Brazil

ABSTRACT

Colorectal cancer (CRC) was ranked the fourth most commonly diagnosed cancer type and third leading cause of death in Canada in 2025. Although CRC is associated with high morbidity and mortality rates, the molecular mechanisms driving CRC development remain poorly understood. Therefore, understanding aberrant genetic and molecular mechanisms driving CRC development is crucial for the development of novel therapeutic strategies that can ultimately improve prognosis and survival of CRC patients. Chromosome instability (CIN) is a predominant genome instability in CRC, and it is defined by the increase of rate in which whole chromosomes or chromosome fragments are gained or lost and are a known driver of ongoing cell-to-cell heterogeneity. CIN is associated with ~85% of CRC cases and is suggested to be a driver of CRC pathogenesis. Previous studies have identified *RBX1,* a core member of the SCF complex, as a strong CIN gene candidate as its reduced expression resulted in increases in nuclear areas relative to non-targeting control. *RBX1* encodes a core member of the SCF complex that ubiquitinates proteins for proteolytic degradation via the 26S proteasome; however, the role of *RBX1* in inducing CIN in CRC remains to be elucidated. Therefore, this study evaluated the effect of reduced *RBX1* expression on CIN and early CRC development. Short-term siRNA approaches coupled with quantitative imaging microscopy techniques were employed to assess changes in CIN-associated phenotypes. Analysis showed that reduced *RBX1* expression corresponded with increases in CIN phenotypes (significant changes to nuclear areas, micronucleus formation, and chromosome numbers) in both non-malignant colonic epithelial and CRC cell lines relative to non-targeting control. Collectively, our findings identify *RBX1* as a novel CIN gene and may provide new insights into the molecular origins and pathogenic events in CRC.

ACKNOWLEDGEMENTS

To my advisor, Dr. Kirk McManus, for his guidance and mentorship throughout my program. I am also grateful to my committee members, Dr. Yale Michaels and Dr. Joel Pearson, for their thoughtful feedback, constructive criticism, and continued encouragement throughout this journey.

This research was made possible by generous financial support from Research Manitoba in the form of a master's studentship award, as well as funding and scholarship support from the Department of Biochemistry and Medical Genetics and the University of Manitoba, including the graduate entrance scholarship and the recognition of research excellence award. I also extend my sincere appreciation to the CancerCare Manitoba Foundation and the Paul Albrechtsen Research Institute for their support.

I would like to thank the members of the McManus laboratory for their collaboration. A special thank you to Nicole Gerber, who walked beside me through this entire journey and provided constant encouragement and friendship. I am also grateful to Dr. Helen Chen for her unwavering support, thoughtful conversations, and enduring friendship, and to my summer student Francesco Caligiuri for reminding me to keep "rolling the dice" and never lose sight of curiosity and perseverance.

Finally, I would like to thank my parents Benedito Brazil and Maria de Fatima Brazil, my brother Douglas Brazil, and all my family and friends in Canada and in Brazil for their love, understanding, and encouragement.

And to myself, for having the courage to leave my home country and pursue my dreams.

TABLE OF CONTENTS

ABSTRACT ..... **ii**

ACKNOWLEDGEMENTS ..... **iii**

LIST OF TABLES ..... **vi**

LIST OF FIGURES ..... **vii**

LIST OF ABBREVIATIONS ..... **viii**

CHAPTER 1. INTRODUCTION **1**

1.1. COLORECTAL CANCER OVERVIEW **1**

1.1.1. Initiation and Progression of Colorectal Cancer 1

1.1.2. Risk Factors 3

1.1.3. Screening and Survival 4

1.1.4. Diagnosis and Staging 5

1.1.5. Treatment Strategies 6

1.2. MOLECULAR PATHOGENESIS OF COLORECTAL CANCER **7**

1.2.2. Genome Instability in Colorectal Cancer 10

1.2.3. Chromosome Instability 11

1.3. THE SCF COMPLEX AND F-BOX PROTEINS **12**

1.3.1. The SCF Complex is Implicated in Chromosome Instability 14

1.3.2. RING-Box 1 (*RBX1*) 15

CHAPTER 2. RATIONALE, HYPOTHESIS AND RESEARCH AIMS **17**

2.1. RATIONALE **17**

2.2. HYPOTHESIS AND RESEARCH AIMS **17**

CHAPTER 3. MATERIALS AND METHODS **18**

3.1. BIOINFORMATIC APPROACHES **18**

3.1.1. Genomic Alterations and Survival Analyses 18

3.2 REAGENTS **19**

3.3 CELL CULTURE **19**

3.3.1. Cell Passaging 20

3.3.2. Cell Counting and Seeding 21

3.3.3. Short-Interfering RNA Transfection 22

3.4 WESTERN BLOT ANALYSES **23**

3.4.1. Whole Cell Protein Extraction and Quantification via Bicinchoninic Acid Assay 23

3.4.2. Gel Electrophoresis and Western Blot 24

3.4.3. Semi-Quantitative Western Blot Analysis 25

3.5 SINGLE-CELL QUANTITATIVE IMAGING MICROSCOPY (QuantIM) **26**

3.5.1. Cell Fixation and DNA Counter-staining for Nuclear Area and Micronucleus Formation Analyses 26
3.5.2. Image Acquisition and Analysis 26
3.5.3. Mitotic Chromosome Spreads and Chromosome Enumeration 27
3.6. STATISTICAL ANALYSES 28
3.6.1. Two-Sample Kolmogorov-Smirnov Test 28
3.6.2. Mann-Whitney Test 28
3.6.3. Student's t-Test 28
CHAPTER 4. RESULTS 29
4.1. Bioinformatic Analyses Reveal Heterozygous Loss of *RBX1* is Frequent in CRC and is Associated with Poor Patient Outcomes 29
4.2. Establishing *RBX1* Silencing Efficiencies Using Short-Interfering RNA Duplexes 32
4.3. AIM 1: To Determine the Impact Reduced *RBX1* Expression has on CIN in Non-malignant Colonic Epithelial Cell Contexts 33
4.3.1. *RBX1* is Efficiently Silenced in 1CT and A1309 Cells, and its Reduced Expression Induces Substrate Accumulation 33
4.3.2. Reduced *RBX1* Expression Underlies Increases in CIN-Associated Phenotypes in Non-Malignant Colonic Epithelial Cells 34
4.4. AIM 2: To Determine the Impact Reduced *RBX1* Expression has on CIN in a Malignant Colorectal Cancer Context 42
4.4.1. *RBX1* can be Efficiently Silenced in HCT116 Cells, and its Reduced Expression Corresponds with Substrate Accumulation 42
4.4.2. Reduced *RBX1* Expression Underlies Increases in CIN-Associated Phenotypes in Malignant Colonic Epithelial Cells 43
CHAPTER 5. SUMMARY AND DISCUSSION 47
5.1. SUMMARY 47
5.2 DISCUSSION 47
5.2.1. *RBX1* Silencing Corresponds with Larger Increases in Nuclear Areas that may be Induced by Endoreduplication 47
5.2.2. *RBX1* Silencing Corresponds with Variable CIN Phenotypes in Non-Malignant and Malignant Colonic Epithelial Cell Lines 50
5.2.3. *RBX1* Silencing may Induce CIN-associated Phenotypes through Aberrant Increases in Cyclin E1 51
CHAPTER 6. FUTURE DIRECTIONS, CONCLUSIONS AND SIGNIFICANCE 53
6.1. FUTURE DIRECTIONS 53
6.1.1. Determining the Long-term Impact Reduced *RBX1* Expression has on CIN Using *RBX1*$^{+/-}$ Clones 53
6.1.2. Evaluating Cellular Transformation Phenotypes Using *RBX1*$^{+/-}$ Clones 54

6.1.3. Exploiting Reduced *RBX1* Expression in Novel Diagnostic and Therapeutic Strategies 55
6.2. CONCLUSION AND SIGNIFICANCE 56
REFERENCES 57
APPENDIX A: SOLUTIONS 66
APPENDIX B: SUPLEMENTARY TABLES 72

LIST OF TABLES

Table 3-1. Properties of Human Colonic Epithelial Cell Lines Employed in CIN Assays. 20
Table 3-2. Cell Seeding Densities and Volume Medium Employed in Corresponding CIN Assays. 21
Table 3-3. Volumes Employed for *RBX1* Silencing Experiments using siRNA. 22
Table 3-4. List of Antibodies Employed for Western Blot Analysis. 25
Table S1. Two-sample KS Test Reveals Significant Increases in Nuclear Area Distributions Following *RBX1* Silencing in 1CT 72
Table S2. MW Tests Identify Significant Increases in the Frequencies of Micronucleus Formation Following *RBX1* Silencing in 1CT 73
Table S3. Student's T-Tests Identify Significant Increases in the Frequency of Aberrant Chromosome Numbers Following *RBX1* Silencing in 1CT 74
Table S4. Two-sample KS Test Reveals Significant Increases in Nuclear Area Distributions Following *RBX1* Silencing in A1309 74
Table S5. MW Tests Identify Significant Increases in the Frequencies of Micronucleus Formation Following *RBX1* Silencing in A1309 75
Table S6. Student's T-Tests Identify Significant Increases in the Frequency of Aberrant Chromosome Numbers Following *RBX1* Silencing in A1309 76
Table S7. Two-sample KS Test Reveals Significant Increases in Nuclear Area Distributions Following *RBX1* Silencing in HCT116 76
Table S8. MW Tests Identify Significant Increases in the Frequencies of Micronucleus Formation Following *RBX1* Silencing in HCT116 77
Table S9. Student's T-Tests Identify Significant Increases in the Frequency of Aberrant Chromosome Numbers Following *RBX1* Silencing in HCT116 78

LIST OF FIGURES

Figure 1-1. Anatomy of the Colon 2
Figure 1-2. The Adenoma to Carcinoma Pathway 8
Figure 1-3. CIN Drives Genetic and Cell to Cell Heterogeneity. 11
Figure 1-4. The SCF complex targets proteins for degradation via 26S proteasome. 14
Figure 4-1. RBX1 Copy Number Losses Are Prevalent in CRC and are Associated with Diminished RBX1 mRNA Expression and Increases in Genome Instability. 30
Figure 4-2. Heterozygous Loss of RBX1 is Associated with Worse CRC Patient Outcomes. 31
Figure 4-3. *RBX1* is Efficiently Silenced in HCT116 cells. 32
Figure 4-4. *RBX1* Silencing is Associated with Increases in Cyclin E1 Levels in Non-Malignant Colonic Epithelial Cell Lines 34
Figure 4-5. *RBX1* Silencing Induces Significant Increases in Nuclear Areas in 1CT. 35
Figure 4-6. *RBX1* Silencing Corresponds with Significant Increases in Micronucleus Formation in 1CT. 36
Figure 4-7. *RBX1* Silencing Induces Increase in Aberrant Chromosome Numbers in 1CT. 38
Figure 4-8. Reduced *RBX1* Expression Corresponds with Significant Increases in Nuclear Areas in A1309 Cells. 39
Figure 4-9. Diminished *RBX1* Expression Underlies Significant Increases in Micronucleus Formation in A1309. 40
Figure 4-10. Reduced RBX1 Expression Induces Increase in Aberrant Chromosome Numbers in A1309. 41
Figure 4-11. *RBX1* is Effectively Silenced in HCT116 and is Associated with Increases in Cyclin E1 Levels. 42
Figure 4-12. *RBX1* Silencing Underlies Significant Increases in Nuclear Areas in HCT116. 43
Figure 4-13. Reduced *RBX1* Expression is Associated with Significant Increases in Micronucleus Formation in HCT116 44
Figure 4-14. *RBX1* Silencing Underlies Increase in Aberrant Chromosome Numbers in HCT116. 46

LIST OF ABBREVIATIONS

~	Approximately
ºC	Degrees Celsius
>	Greater than
<	Less than
%	Percent
µg	Microgram(s) (weight)
µL	Microliter(s) (volume)
µm	Micrometer(s) (length)
µM	Micromolar (concentration)
2D	Two-dimension
3D	Three-dimension
5-FU	5-Fluorouracil
AJCC	American Joint Committee on Cancer
ATP	Adenosine triphosphate
APC	Adenomatous Polyposis Coli
APC	Anaphase Promoting Complex (Cyclosome)
ATCC	American Type Culture Collection
BCA	Bicinchoninic Acid
BFP	Blue Fluorescent Protein
bp	Base Pair(s)
BRCA1	Breast Cancer Type 1 Susceptibility Protein
BRCA2	Breast Cancer Type 2 Susceptibility Protein
BSA	Bovine Serum Albumin
c-JUN	cellular Jun
Cas9	CRISPR Associated Protein 9
CRL	Cullin-RING ligase
CCND1	Cyclin D1
CCNE1	Cyclin E1
CCS	Cosmic Calf Serum
CIMP	CpG Island Methylator Phenotype
CIN	Chromosome Instability
cm	Centimeter(s) (length)
c-MYC	MYC Proto-oncogene Protein
CO_2	Carbon Dioxide
CPTS	Copper phthalocyanine 3, 4', 4'', 4'''-tetrasulfonic acid tetrasodium salt
CRC	Colorectal Cancer
CRISPR	Clustered Regularly Interspaced Short Palindromic Repeats
CTLA-4	Cytotoxic T-Lymphocyte-Associated Protein 4
CUL1	Cullin 1
DAPI	4', 6-Diamidino-2-Phenylindole
DDB1	Damage Specific DNA Binding Protein 1
DMEM	Dulbecco's Modified Eagle Medium
dNTP	Dinucleotide Triphosphates
DSB	Double-strand Break
E1	Ubiquitin-activating Enzyme
E2	Ubiquitin-conjugating Enzyme

E3	Ubiquitin Ligase
EDTA	Ethylenediaminetetraacetic Acid
EGF	Endothelial Growth Factor
EGFR	Endothelial Growth Factor Receptor
EPCAM	Epithelial Cell Adhesion Molecule
ECL	enhanced chemiluminescence
EMI1	Early Mitotic Inhibitor 1
FACS	Fluorescence-activated Cell Sorting
FAP	Familial Adenomatous Polyposis
FBS	Fetal Bovine Serum
FBXO28	F-box Only Protein 28
FBXO5	F-box Only Protein 5 (also known as EMI1)
FBXO7	F-box Only Protein 7
FIT	Fecal Immunochemical Test
FOLFIRI	Folinic acid, 5-fluorouracil, irinotecan
FOLFOX	Folinic acid, 5-fluorouracil, oxaliplatin
g	Gram(s) (weight)
GFP	Green Fluorescent Protein
GTP	Guanosine 5'-triphosphate
h	Hour(s) (time)
HRP	Horseradish Peroxidase
HRR	Homologous Recombination Repair
H2A	Histone H2A
HGSC	High-grade serous carcinoma
kb	Kilobase(s)
kDa	Kilodalton(s)
KCl	Potassium Chloride
KEAP1	Kelch-like ECH-associated protein 1
KM	Kaplan-Meier
KRAS	Kirsten Rat Sarcoma Proto-Oncogene
KS	Kolmogorov-Smirnov
MAPK	Mitogen Activated Protein Kinase
min	Minute(s) (time)
mL	Milliliter(s) (volume)
mm	Millimeter(s) (length)
mM	Millimolar (concentration)
MMR	Mismatch Repair
MLH1	MutL homolog 1
MSH2	MutS homolog 2
MSH6	MutS homolog 6
mTOR	Mechanistic Target of Rapamycin Kinase
mRNA	messenger RNA
MW	Mann-Whitney
NEDD8	Neural precursor cell Expressed, Developmentally Downregulated 8
n	Number of Technical Replicates
N	Number of Experimental Replicates
N-CIN	Numerical Chromosome Instability
ng	Nanogram(s) (weight)

NHEJ	Non-homologous End Joining
nm	Nanometer(s) (length)
nM	Nanomolar (concentration)
NOTCH1	Notch Receptor 1
O_2	Oxygen
PARP1	Poly (ADP-Ribose) Polymerase 1
PALB2	Partner and Localizer of BRCA2
PBS	Phosphate Buffered Saline
PCR	Polymerase Chain Reaction
PD-1	Programmed Death
PD-L1	Programmed Death Ligand-1
P-value	Probability Value
QuantIM	Quantitative Imaging Microscopy
RAD51	RAD51 Recombinase
RBX1	RING Box Protein 1
RBX2	RING Box Protein 2
RING	Really Interesting New Gene
ROC1	Regulator of Cullins 1
RING-H2	RING finger domain with aH2-type zinc-binding motif
RIPA	Radioimmunoprecipitation assay
RT	Room Temperature
s	Second(s) (time)
SCF	SKIP1-CUL1-F-box
S-CIN	Structural Chromosome Instability
siRNA	short interfering ribonucleic acid
SDS	Sodium Dodecyl Sulfate
siRNA	Short-interfering RNA
SKP1	S-phase Kinase-associated Protein 1
SKP2	S-phase Kinase-associated Protein 2
SMAD4	Mothers Against Decapentaplegic Homology Family Member 4
TBS	Tris-buffered Saline
TBST	Tris-buffered Saline with Tween-20
TCGA	The Cancer Genome Atlas
TGFβ	Transforming Growth Factor Beta
TP53	Tumour Protein P53
TNM	tumor size, lymph node involvement, and metastasis
V	Volt(s)
VEGF	Vascular Endothelial Growth Factor
vs.	Versus
WB	Western Blot
WNT	Wingless-related Integration Site
w/v	Weight per volume
×g	Acceleration

CHAPTER 1. INTRODUCTION

1.1.COLORECTAL CANCER OVERVIEW

Cancer remains a public health problem, and it represents one of the leading causes of death worldwide. The latest global burden of cancer released by the World Health Organization in 2022 revealed an estimate of 20 million new cases and 9.7 million deaths in that year[1]. Colorectal cancer (CRC) represents 9.6% of those new cases with approximately 2 million cases[1, 2]. CRC was ranked the 4th most commonly diagnosed cancer type (~26,400 new cases) and 3rd leading cause of death (~9,100 cases) in men and women in Canada in 2025, which represented 830 new cases and 320 deaths in Manitoba in the same year[3]. In general, patients with CRC have a 5-year survival rate of 67% in Canada; however, this number can be as low as 11-13% in stage IV tumours[4]. Thus, it is essential to understand the molecular pathways underlying early CRC development, which will provide novel insights into the development of new therapeutic strategies to improve patient prognosis and decrease poor patient outcomes related to this disease.

1.1.1. Initiation and Progression of Colorectal Cancer

CRC is classified as a heterogeneous group of malignances rather than a single disease[5]. Such heterogeneity on CRC classification is a consequence of variations regarding both the anatomical localization of the tumors and the distinct developmental origins of the colon, which results in different characteristics regarding disease progression and overall patient survival[5, 6]. In general, the anatomy of the large intestine is categorized into seven distinct parts (cecum; ascending; transverse; descending; sigmoid colon; rectum; anus) and is ~150 cm in length[7]. According to its embryological origins, the colon is classified into two groups: midgut and hindgut. Together, the midgut gave origin to the proximal colon (right side), which is comprised of the cecum, ascending colon and two thirds of the transverse colon, whereas the hindgut (left side) is comprised of the remaining one third of the transverse colon, as well as descending and sigmoid colon, rectum and anus (***Figure 1-1***)[7, 8]. Right- and left-sided tumors also exhibit differences in morphology and histology. Sessile serrated tumors tend to appear in right-side regions, and their flat morphology makes them difficult to detect in standard CRC diagnostic imaging techniques (*i.e.,* colonoscopy)[7, 8]. On the other hand, left-side regions tend to exhibit polypoid morphology, which are more likely to be detected in early stages of tumor development[7, 8].

Furthermore, it is estimated that approximately 20–30% of colorectal cancers (CRCs) arise from sessile serrated lesions, which are precursor lesions that can progress into a malignancy. Because sessile serrated lesions are most frequently found in the proximal (right-sided) colon, the CRCs that develop through this pathway frequently exhibit a genomic profile characterized by high levels of microsatellite instability (*i.e.* MSI-high)[7, 9]. Alternatively, polyps found on the left side of the colon tend to exhibit chromosome instability (CIN)[7, 9]. CIN is another type of genome instability that is present in ~85% of all CRC cases[10, 11]. It is characterized by the increase of rate in which whole chromosomes or chromosome fragments are gained or lost[10, 11] (see *Section 1.2.3*). Although most polyps do not evolve into adenocarcinomas, it is well established that the onset and evolution of a tumorigenic process require the accumulation of multiple genetic alterations overtime[5, 7]. This process, known as adenoma to carcinoma pathway (see *Section 1.2.1*), was first described by Fearon and Vogelstein and it is proposed to occur over 10 to 15 years[12, 13]. Therefore, understanding the etiology and distinct biological mechanisms each tumor type express is fundamental for the development of prognosis and novel therapeutic strategies.

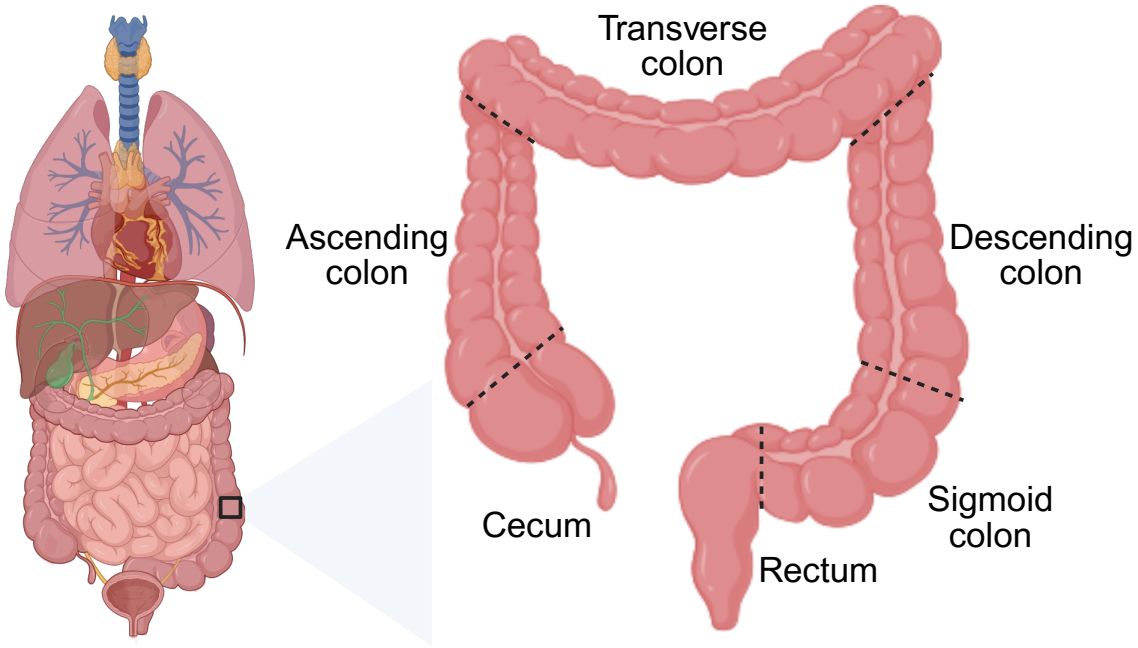

Figure 1-1. Anatomy of the Colon
Schematic illustration of the colon and rectum. Proximal or right-side colon is comprised by the cecum, ascending colon and 2/3 of the transverse colon. Distal or left-side colon is comprised by the final 1/3 of the transverse colon, descending colon, sigmoid colon and rectum. Adapted from Campos Gudiño et al[14] and created with BioRender.com.

1.1.2. Risk Factors

As a multifactorial disease, there are many different variables that can contribute to the development of CRC[15]. Although the mechanisms that give rise to CRC have not been fully understood, there are many risk factors that may increase the chances of developing this disease, which could be associated with genetics, sex, age, lifestyle and environmental factors[3, 15]. In general, CRC cases are classified into two main categories: familial and sporadic. The familial component of CRC diagnosis is linked to patients with family history of CRC or polyps in first degree relatives, which represents ~30% of all CRC diagnosis[16, 17]. However, only 10% of those CRC cases are linked to specific mutations that will eventually increase the susceptibility to develop not only CRC but other cancer types as well[18]. Lynch syndrome, or hereditary non-polyposis colon cancer, is the most common hereditary cause of CRC[18]. This disease is linked to mutations in mismatch repair genes (MMR), particularly *MutL Homolog 1* (*MLH1*), *MutS Homolog 2* (*MSH2*), *MutS Homolog 6* (*MSH6*) and *Postmeiotic Segregation Increased 2* (*PMS2*). Also, mutations in the *Epithelial Cellular Adhesion Molecule Gene* (*EPCAM*) may result in epigenetic silencing and eventual loss of expression of the *MSH2* gene[18, 19]. Familial Adenomatous Polyposis (FAP), which is another type of inherited CRC, is characterized by a loss of function in the *Adenomatous Polyposis Coli* gene (*APC*)[20]. This mutation is responsible to disrupt the Wnt/β-catenin pathway, which is involved in both initiation and progression of CRC[20, 21].

Regarding sex-based CRC incidence, men are 1.5x more likely to develop CRC than women regardless of age or ethnicity[22]. Although CRC is more prevalent in adults over 50 years of age, recent studies have reported an increase in CRC incidence among adults younger than 50 years in many high-income countries, including Canada[22, 23]. Such contrasts might be attributed to generational differences in diet, lifestyle and environmental factors. Low fiber intake, lack of physical activity and increase in the consumption of red meat and saturated fat are also linked to increases in the risk of developing CRC[24]. Furthermore, overweight and obesity are strongly associated with an overall increase of 36% in CRC cases, which can be partially explained by the disruption of metabolic pathways that may eventually play a role in CRC progression and development[25].

Lastly, epidemiological data also demonstrates an association between CRC and well-stablished risk factors for cancer, such as alcohol consumption and smoking[24]. Moderate to heavy alcohol consumption increases the risk of developing colorectal cancer by 1.5 times; smoking, on

the other hand, can increase the chances of developing CRC up to 60% when compared to people who do not consume tobacco products[24, 26].

1.1.3. Screening and Survival

According to the Canadian Cancer Registry (CCR) database ~49% of all CRC cases are diagnosed at stages III and IV combined, while stage I diagnosis represents only ~20% of the cases[27]. In the USA these numbers may be even higher; ~60% of the CRC cases are diagnoses at late stages, where the 5-year survival can be as low as 11-13% (stage IV tumors)[28]. Low incidence rates in early CRC stages may be partially explained by the lack of signs and symptom. Detecting cancer at an early stage can prevent the development of advanced stages and reduce the mortality rates in the population[29, 30]. Therefore, screening individuals for detection of precancerous polyps or curable early-stage tumors may increase their chances of having a good prognosis and increased survival outcomes[30].

Most screening programs in the world use non-invasive faecal occult blood tests (FOBTs) as their primary screening tool[31]. In Canada, fecal immunohistochemical test (FIT) is the most commonly employed CRC stool screening test and it has gradually replaced the Guaiac-based fecal occult blood (gFOBT) test[32]. The FIT test is based on the use of antibodies that specifically detect human hemoglobin, rather than an unspecific peroxidase reaction[31, 33]. Additionally, the FIT test only requires one stool sample collection, and it is not affected by diet or the use of specific medications, representing a more effective alternative when compared to the gFOBT test[31, 33].

In most CRC screening programs, patients with a positive FIT test are required to do a colonoscopy[31]. Colonoscopy is considered the gold standard tool for both screening and early CRC diagnosis, consisting on the use of a flexible endoscope that is capable to evaluate the entire colon and rectum[31]. This method has an 89-95% detection sensitivity for adenomas and CRC ≥ 1cm, and 86-89% specificity; false positive cases are mostly attributed to non-malignant polyps that were biopsied[33]. Colonoscopy is the most used CRC screening method in the USA, where 61% of the screened population used this method[34]. In Canada, colonoscopy is only used as a follow-up exam after a positive stool test or in cases when the patient is at high risk for developing CRC (see *Section 1.1.2*); for the general population, a FOBT test is recommended every two years starting at the age of 50[35].

1.1.4. Diagnosis and Staging

As mentioned on the previous section, colonoscopy is the gold standard procedure for both CRC screening and diagnosis[33]. Once a precancerous polyp or a CRC tumour is detected, a specimen is collected for biopsy and confirmation of the diagnosis[36]. The American Joint Committee on Cancer (AJCC) Tumour, Node and Metastasis system (TNM) is the most used classification system in the world, and it is essential to determine disease extent, guide clinical decisions and predict prognosis and survival outcomes[37, 38]. This classification system is based on tumour size and localization, invasion of regional lymph nodes and the presence or absence of metastasis[38]. In summary, the T (Tumour) category describes the size and invasiveness of the tumour. It ranges from T1, in which the tumour in only in the inner layer of the bowel, up to T4 when tumor cells have spread outside of the primary tissue[38, 39].

The N (Node) category describes whether or not the tumour has spread to the lymph nodes, ranging from N0 when the cancer has not spread to nearby lymph nodes, to N2, when cancer infiltrates into four or more nearby lymph nodes[38, 39]. And lastly the M (Metastasis) category, which evaluates if the cancer has spread to other parts of the body, being divided into M0, when no spread has been detected, and M1 when cancer has spread to distant parts of the body[38, 39]. The combination of the characteristics described in the TNM classification system is used to define the overall CRC tumour staging and it is categorized as follows: stage 0 indicates carcinoma in situ, stage I refers to tumours that haven't grown outside the primary organ, stages II and III describe larger tumours or tumours that have started to invade nearby tissues, and stage IV that indicates tumours that have undergone metastatic spread.[38, 39]

CRC staging is also used to estimate 5-year net survival. In Canada, the overall 5-year net survival for patients with CRC is approximately 67%[3]. More specifically, stage I tumours have the highest 5-year survival rate, ranging from 91-92%; stages II and III typically exhibit a 79-88% and 68-74% survival rate, respectively, while stage IV tumours have the lowest 5-year survival rate, ranging from 11-13%[3]. Therefore, the earlier CRC is diagnosed and treated, the better the survival outcomes, which strongly highlights the importance of CRC screening programs and diagnosis to mitigate the high incidence of morbidity and mortality associated with CRC[40].

1.1.5. Treatment Strategies

As a heterogeneous disease, CRC treatment requires personalized regimens based on multidisciplinary approaches encompassing tumour staging (see *Section 1.1.4*) and localization, surgical techniques, molecular profiling, immunotherapy and chemotherapy[41, 42]. Accordingly, for stage 0 and I tumours, surgery represents the main therapeutical strategy, and it normally consists of the excision of polyps or tumours followed by the removal of a small amount of adjacent tissue[41]. For CRC tumours at stages II and III, surgery is also the main choice of treatment and chemotherapy may be associated with surgery in cases with a high risk of malignancy recurrence[41, 43]. Lastly, stage IV CRC treatment consists of the surgical removal of primary and metastatic resectable tumours as well as chemotherapy, which can be used either before surgery to shrink the tumours, or after surgery to treat unresectable or metastatic areas[43].

The combination of multiple compounds has been proven to improve therapeutic response and reduce side effects[44]. FOLFOX is a chemotherapeutic combination comprised of three drugs: folinic acid (leucovorin), 5-fluorouracil (5-FU) and oxaliplatin[45]. Briefly, 5-FU is a fluoropyrimidine that disrupts DNA replication and repair, resulting in DNA double-strand break and apoptosis while leucovorin acts by stabilizing the 5-FU molecule, and oxaliplatin impacts DNA replication and transcription[46, 47]. FOLFIRI is another chemotherapy regimen that replaces oxaliplatin with irinotecan, which is a topoisomerase I inhibitor that also causes DNA double-strand break and cell death[48].

Alongside combined therapies, targeted agents are used as a second line treatment for advanced cases[49]. They are another treatment regimen that can be used in combination with chemotherapy, by themselves or in combination with another targeted therapy[48, 49]. For example, cetuximab and panitumumab are both FDA-approved targeted therapies. They are an anti-EGFR (Endothelial Growth Factor Receptor) agent that are beneficial to patients with RAS-wild-type tumors (*i.e. KRAS*), which are normally found in left-sided tumours[50]. Bevacizumab is another targeted therapy used for the treatment of CRC tumours that overexpress VEGF (Vascular Endothelial Growth Factor), which is responsible to promote angiogenesis and tumour growth[50].

In addition to the methods mentioned above, immune checkpoint inhibitors are another example of targeted therapy. However, instead of blocking important pathways that are linked to tumour growth and spread, they work by targeting pathways that enhance immunorecognition and response against malignant cells and are more effective in tumours harbouring deficiencies in DNA mismatch repair genes or high frequency of microsatellite instability (MSI high)[50]. Ipilimumab, a

CTLA-4 (Cytotoxic T-Lymphocyte-Associated Protein 4) inhibitor was the first FDA-approved immune checkpoint therapy. Pembrolizumab and nivolumab are also immune checkpoint inhibitors, which are responsible to block PD-1 (Programmed Death Ligand-1) activity[50]. Although immune checkpoint inhibitors produce an efficient therapeutic response, they are effective in only 5-15% (MSI-high) of all CRC cases[51]. Therefore, novel treatment strategies are necessary to improve patient prognosis and survival outcomes in CRC tumours both early and late stages.

1.2. MOLECULAR PATHOGENESIS OF COLORECTAL CANCER

The mechanisms underlying CRC heterogeneity normally differ according to the precursor lesions, anatomical site and distinct genetic alterations. Thus, sporadic tumours represent ~85% of all CRC cases, whose onset and development are proposed to follow the adenoma to carcinoma pathway. This pathway was described by Fearon and Vogelstein and its multistep process is detailed below[12, 52].

1.2.1. The Adenoma to Carcinoma Pathway

The Fearon and Vogelstein adenoma to carcinoma pathway describes the process in which normal colonic epithelial cells acquire genetic alterations that are linked to the progression from benign polyps to invasive carcinomas[12, 52]. In this pathway, CRC evolution is coordinated by the mutational activation or inactivation of oncogenes and tumour suppressor genes, respectively[12, 53]. In general, proto-oncogenes regulate normal processes linked to cellular growth and division; thus, mutation, amplification or overexpression of these genes may contribute to tumour development due to uncontrolled cell proliferation signals. By contrast, tumour suppressor genes regulate cellular processes linked to the cell cycle, DNA damage repair and apoptosis[53]. In the adenoma to carcinoma pathway model, at least four genes are associated with CRC development: *Adenomatous Polyposis Coli* (*APC*), *Kirsten Rat Sarcoma Proto-oncogene* (*KRAS*), *Mothers Against Decapentaplegic Homology Family Member 4* (*SMAD4*) and *Tumor Protein 53* (*TP53*)[54].

As presented in ***Figure 1-2***, the adenoma formation is initially characterized by the hyperproliferation of colonic epithelial cells that result in the benign growth and formation of polyps, which is followed by changes in tumour size and cellular morphology[12, 54]. Lastly, adenomas continue to progress and begin to invade adjacent tissue layers, which eventually may lead to metastasis in both proximal and distant sites[12, 54].

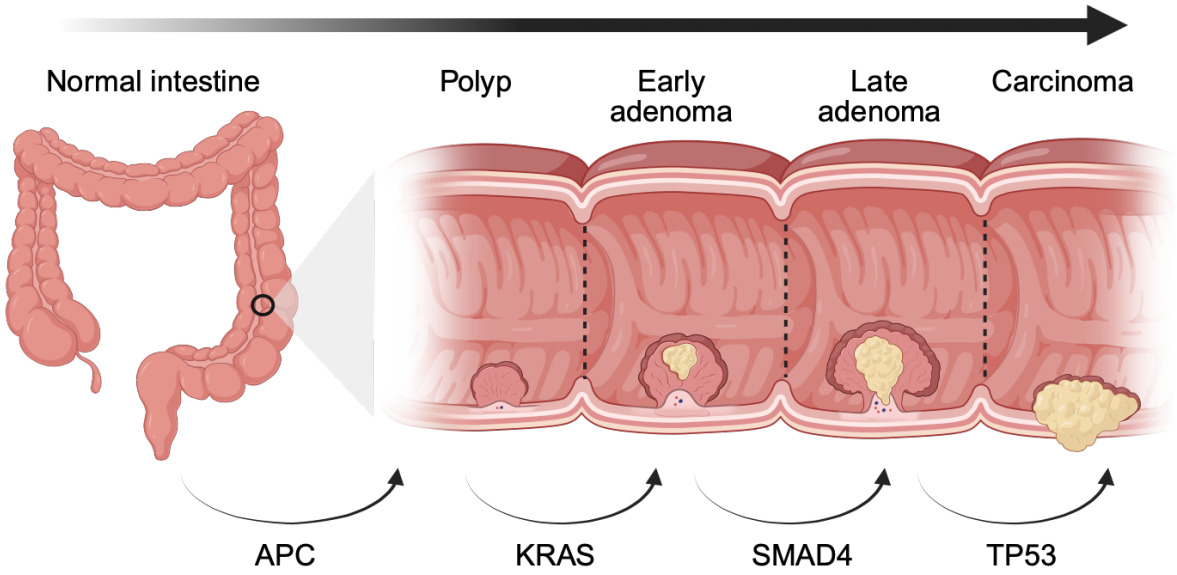

Figure 1-2. The Adenoma to Carcinoma Pathway
Schematic illustrating the progressive acquisition of genetic alterations related to sporadic CRC development. As described by Fearon and Vogelstein[12, 52], specific mutations in tumor suppressor genes and oncogene (*APC* inactivation, *KRAS* mutation, and loss of *SMAD4* and *TP53*) promote the development of normal colon into malignant carcinoma. Adapted from De Palma *et al*[55] and created with BioRender.com.

The tumour suppressor gene *Adenomatous Polyposis Coli* (*APC*) plays an important role in controlling regular cellular processes, such as cell proliferation, and encodes a protein that regulates ubiquitination and degradation of β-catenin[56, 57]. Therefore, *APC* mutations result in the subsequent accumulation of β-catenin, which upregulates proto-oncogenes such as *MYC* (*Helix-loop-helix Transcription Factor*) and Cyclin D1 (*CCND1*)[56, 57]. Additionally, it is proposed that *APC* mutations may promote epithelial hyperproliferation and the development of adenomas and adenocarcinomas[58]. *APC* mutations were first identified based on its association with FAP syndrome; however, *APC* mutations are proposed to have a higher frequency in CRC, ranging from ~45%-80% of the cases[58]. More specifically, frameshift mutations at codon 1309 (the encoded β-catenin binding site) will result in a truncated form of the APC protein, which may eventually promote CIN through mechanisms linked to defects in microtubule formation and errors in chromosome segregation[58, 59].

Mutations in the proto-oncogene *KRAS* are proposed to be the second key genetic alteration in the adenoma to carcinoma pathway. This gene encodes a guanosine 5'-triphosphate (GTP)-binding protein, whose mutation adversely impacts downstream signalling pathways related to cell proliferation, differentiation and apoptosis[12, 60]. More specifically, mutations in

codons 12 and 13 (more frequent), and 61, 117 and 146 (less frequent) will impact the hydrolysis of Guanosine Triphosphate (GTP) into Guanosine Diphosphate (GDP), resulting in constitutive RAS activation and persistent downstream signalling involving Mitogen-Activated Protein Kinase (MAPK) activity, promoting cell survival and uncontrolled proliferation[12, 60]. KRAS mutations occur in ~38% of CRC cases worldwide and are present in 58% of adenomas larger than 1cm, 9% of adenomas smaller than 1cm, and 47% of carcinomas[12, 60].

SMAD4 (*Mothers Against Decapentaplegic Homolog 4*) is a tumour suppressor gene that plays a central role in the TGF-β pathway regulating cell proliferation, differentiation and apoptosis[61]. It is proposed that mutations in this gene can cause Juvenile Polyposis Syndrome, a disease marked by the development of polyps in the gastrointestinal tract with a high risk of malignancy[61]. *SMAD4* alterations are present in ~30% of CRC cases and in 25% of early-onset CRC cases, typically as homozygous deletions or truncating mutations[62]. Such alterations are suggested to be a late-stage event in CRC oncogenesis, arising after inactivation of genes such as *APC*, and playing a role in tissue dysplasia and invasiveness. Additionally, *SMAD4* localizes to chromosome 18q, and the loss of this chromosome arm occurs in ~75% of all CRC and precedes *TP53* mutations in the adenoma to carcinoma pathway[61, 62].

TP53, also referred as "the Guardian of the Genome", is the most commonly mutated gene in human cancers[63]. *TP53* is a critical tumour suppressor that plays a critical role in DNA double-strand break repair, proliferation control and apoptosis. Therefore, mutations in this gene will allow the uncontrolled growth and proliferation of cells with damaged DNA[63]. *TP53* mutations are present in ~75% or CRC cases and ~30% of late adenomas, representing a fundamental late-stage event in the adenoma to carcinoma pathway model[63, 64]. Although mutations in *APC*, *KRAS*, *SMAD4* and *TP53* genes are linked to the adenoma to carcinoma pathway, it is important to highlight that these mutations alone may not play a role on the development of CRC. Thus, studies that assess additional mechanisms linked to CIN and CRC are essential to shed a light on the development of new therapeutic strategies that will eventually improve patient prognosis and survival outcomes.

1.2.2. Genome Instability in Colorectal Cancer

Genome instability refers to the increase of genetic alterations that are commonly observed in distinct cancer types[65]. Also known as a hallmark of cancer, these alterations often enable the acquisition of characteristics required for oncogenesis and tumour progression including CpG island methylator phenotype (CIMP), MSI and CIN[65]. CIMP represents an epigenetic subtype of genome instability characterized by the widespread hypermethylation of CpG islands associated with promoters, which are short segments of DNA containing high frequency of cytosine and guanine[66, 67]. Patients harbouring this methylator phenotype are associated with poor prognostic features, such as worse disease-free and overall survival, and it affects DNA repair, cell cycle and apoptosis and is present in ~10-15% of sporadic CRC cases[66, 67].

MSI is another subset of genome instability that originates from defects in DNA mismatch repair genes (MMR), which leads to uncontrolled errors in short, repeated DNA sequences known as microsatellites. MSI alterations result from defects in genes such as *MLH1*, *MSH2*, *MSH6*, and *PMS2*. MSI-high profiles are linked to the onset of both hereditary (Lynch syndrome - see *Section 1.1.2*) and sporadic CRC cases, and it is present in ~15% of all CRC cases[18 19, 65]. Finally, CIN is a type of genome instability phenotype that induces cell-to-cell heterogeneity and contributes to different stages of tumour evolution[11] (*see Section 1.2.3*). Recent evidence suggests these subtypes of genome instability are not mutually exclusive in sporadic colon cancer, where ~12% of MSI tumours may also present a varying degree of CIN[68, 69]. Therefore, gaining new insights into aberrant genes and molecular pathways is fundamental for the understanding of the tumour biology and eventually the development of novel therapeutic strategies.

1.2.3. Chromosome Instability

As mentioned above, CIN is a predominant genome instability in CRC and it is defined by the increase of rate in which whole chromosomes or chromosome fragments are gained or lost and is a known driver of ongoing cell-to-cell heterogeneity[11, 70, 71] (***Figure 1-3***), promoting early CRC events such as cellular transformation as well as late events including metastasis, drug resistance and worse patient outcomes[11, 70, 72]. These chromosome alterations are normally categorized into two distinct subtypes: numerical CIN (N-CIN) and structural CIN (S-CIN). N-CIN generally refers to either the gain or loss of chromosomes, leading to an aneuploid state states[73, 74], and it is normally associated with chromosome segregation errors that arise during mitosis, which are a consequence of alterations in mitotic spindle formation, defects in sister chromatid cohesion, improper microtubule attachment, chromosome condensation errors and abnormal cytokinesis[75-78].

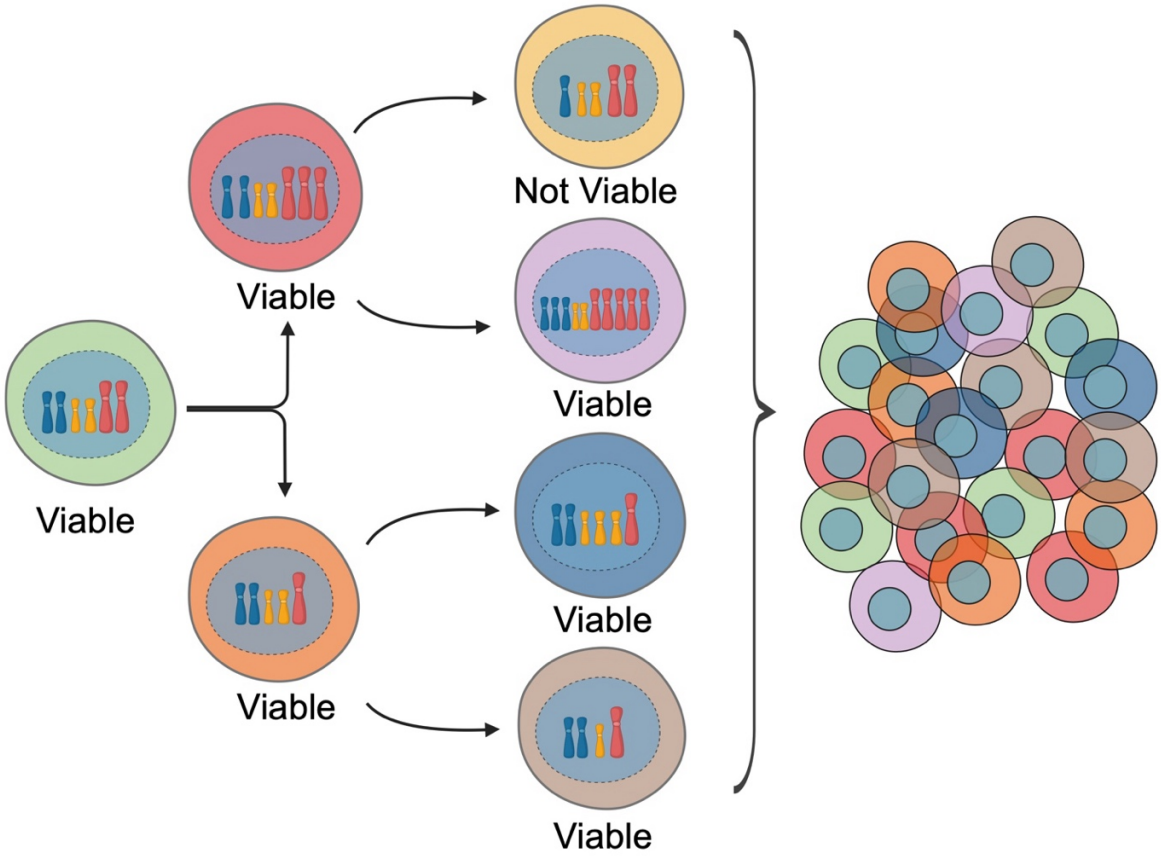

Figure 1-3. CIN Drives Genetic and Cell to Cell Heterogeneity.
Schematic model depicting N-CIN driving ongoing genetic and karyotypic heterogeneity. For illustration purposes, cells only contain three pairs of chromosomes. Chromosomes are gained or lost throughout multiple rounds of cell division, resulting in genetically distinguished cells and intratumoral heterogeneity. Adapted from Lepage *et al*[70] and created with BioRender.com.

On the other hand, S-CIN results in structural changes in chromosomes, including chromosome rearrangements, amplification, deletions and translocations, which are commonly associated with replication stress, errors in DNA double-strand break repair mechanisms and telomere dysfunction[73, 79-81]. Although N-CIN and S-CIN arise from distinct mechanisms, both variations of CIN tend to coexist in tumours and are considered an early etiological event in CRC pathogenesis[73, 79]. Interestingly, it is postulated that moderate levels of CIN are still viable to the cells, while high CIN levels can lead to genomic imbalance, growth arrest and cell death in both simple and more complex organisms[82]. Understanding different cellular mechanisms and characterizing aberrant genes that underly the complex interplay between CIN, tumour progression and treatment response is crucial for the development of novel therapeutic strategies (*i.e.* synthetic lethality)[82, 83]. More specifically, synthetic lethality is known to exploit genetic interactions between a loss of function gene and a drug that will target a remaining functional gene, such as poly-ADP ribose polymerase (PARP) inhibitors in *BRCA1/BRCA2* deficient tumours[83, 84].

Additional studies have demonstrated that CIN is also linked to mechanisms that control protein degradation in ubiquitin-proteasome system. Research from the McManus laboratory identified members of the S-phase Kinase associated Protein 1 (SKP1), Cullin 1 (CUL1), F-box protein (SCF) complex as novel CIN genes[10, 85]. More specifically, they determined that reduced expression of core members of the SCF complex (*RBX1*, *CUL1*, *SKP1*) induce CIN, and the aberrant expression of CIN genes are linked to pathogenic implications in cancer development[10, 85]. It has also been demonstrated that reduced *RBX1* expression induces CIN in cellular models of tubo-ovarian, high-grade serous carcinoma (HGSC), strongly suggesting that reduced *RBX1* expression may also induce CIN in CRC contexts[86]. Thus, it is essential to determine the impact reduced *RBX1* expression has on CIN in colonic epithelial cell contexts to gain novel insight into the mechanisms underlying CRC development.

1.3. THE SCF COMPLEX AND F-BOX PROTEINS

Ubiquitination is a mechanism that plays a central role in the post-translational modification of proteins, controlling many distinct cellular processes including protein localization and degradation, DNA repair, chromatin remodulation and cell cycle control[87, 88]. The SCF complex is an E3 ubiquitin ligase that targets proteins for proteolytic degradation via the 26S proteasome. The SCF complex is comprised of three central proteins RBX1, CUL1 and SKP1, and a variable F-Box protein that confers target specificity to the complex[89]. The ubiquitination process is performed by three distinct enzymes: 1) E1 ubiquitin-activating enzyme; 2) E2

ubiquitin-conjugating enzyme; and 3) E3 ubiquitin ligase[87, 89]. More specifically, the E1 enzyme activates free ubiquitin molecules, which are recruited to the E2 conjugating enzyme. E2 is subsequently recruited to the E3 ligase, resulting in eventual binding to RBX1 and the consecutive transfer of a ubiquitin moiety onto the substrate protein[89, 90]. The functional outcome for targeted proteins varies according to specific lysine (K) residue attachment site, the number of ubiquitin molecules attached (*i.e.* mono-ubiquitination or poly-ubiquitination) and the spatial arrangement of the ubiquitin subunits. Accordingly, the attachment of one ubiquitin molecule (mono-ubiquitination) frequently regulates protein localization and remodelling[90, 91]. By contrast, poly-ubiquitination refers to the attachment of consecutive ubiquitin molecules into one of seven K residues (*i.e.,* K6, K11, K27, K29, K33, K48, K63), and subsequent formation of poly-ubiquitinated chains. For instance, proteolytic degradation can be induced via the 26S proteosome upon poly-ubiquitination of the K48 residue, while DNA repair, signalling and apoptosis are regulated by the polyubiquitination of the K63 residue[90, 92, 93].

The human genome encodes ~600 E3 ubiquitin ligase complexes, which collectively provide substrate specificity to ubiquitin dependent systems[94]. As presented in ***Figure 1-4***, the SCF complex is comprised of three invariable core members SKP1, CUL1 and RBX1, and one of 69 variable F-box proteins[10, 85]. The SCF complex belongs to the RING-type E3 ubiquitin ligase family, which represents the largest E3 ligase complex group, and targets proteins for proteasomal degradation, protein localization and activity[95]. As previously mentioned, RBX1 is responsible for regulating the ligase activity by facilitating the conjugation with the charged E2 ubiquitin conjugating enzyme and the SCF complex, while CUL1 works as a scaffolding protein. Lastly, SKP1 works as an adapter protein responsible to bind to both CUL1 and one out of the 69 F-box proteins[95, 96]. These F-box subunits recognize specific regions on target proteins and thereby confer substrate specificity to the complex[95, 96]. Protein substrates that are known to be regulated by the SCF complex may integrate mechanisms linked to cell cycle regulation (*e.g*., Cyclin E1), transcription factors, and apoptotic and DNA repair proteins. Therefore, dysregulation of SCF complex activity has been linked to the pathogenesis of multiple cancer types, including CRC[10, 85, 97, 98]. Consequently, it is essential to understand the roles of SCF complex members as well as the mechanistic pathways that underly the dysregulation of substrate protein units and how they may be implicated to CRC pathogenesis.

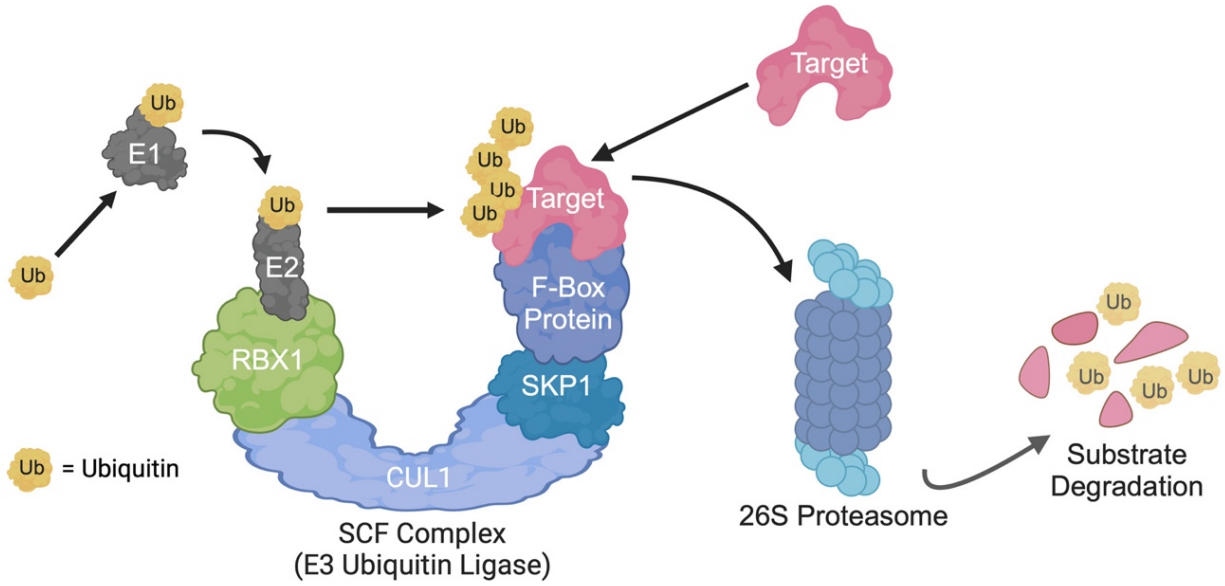

Figure 1-4. The SCF complex targets proteins for degradation via 26S proteasome. Schematic illustration of poly-ubiquitination and degradation of protein targets by the SCF complex. The SCF complex is comprised of three invariable core proteins (SKP1, CUL1, RBX1) and one of 69 variable F-Box proteins that confer substrate specificity to the complex. Figure created with BioRender.com.

1.3.1. The SCF Complex is Implicated in Chromosome Instability

The McManus laboratory has previously identified that the disruption of SCF complex core members drives CIN through distinct mechanisms associated with ubiquitination and proteolytic degradation. More specifically, it has been demonstrated that reduced *SKP1* expression leads to Cyclin E1 accumulation, replication stress, DNA double-strand breaks, micronucleus formation, nuclear area heterogeneity, and aneuploidy[99, 100]. Furthermore, the reduced expression of *CUL1* disrupts overall SCF complex activity, resulting in lagging chromosomes during mitosis, chromosome missegregation errors, centrosome amplification and increased aneuploidy states[101]. Lastly, reduced *RBX1* expression also resulted in the onset of dynamic CIN phenotypes in HGSC, mirroring disease progression and demonstrating Cyclin E1 accumulation[86].

To gain novel insight into how silencing of SCF complex members affected CIN, our research team performed a genetic screen investigating members of the SCF complex as potential CIN gene candidates[10]. Briefly, SCF complex core members and F-box proteins were individually silenced in HCT116 cells and QuantIM was employed to assess nuclear area changes relative to siControl[10]. Accordingly, *RBX1* silencing induced increases in nuclear area, providing new insights into the role decreased *RBX1* expression plays in CRC context[10]. F-box proteins target hundreds to

thousands of proteins for proteolytic degradation due its substrate-recognition characteristic, impacting mechanisms related to cell cycle progression, centrosome duplication, and DNA repair[102, 103]. For instance, *SKP2* and *EMI1* (*FBXO5*) were identified as novel CIN genes in CRC context, where their reduced expression disrupted SCF complex function, resulting in CIN phenotypes and long-term cellular transformation characteristics[10, 85].

Disruption in F-box proteins has also been linked to different cancer types. For instance, in breast cancer, *FBX028* overexpression plays a role in the ubiquitination of the oncoprotein MYC, resulting in MYC-dependent transcription errors, abnormal proliferation and tumorigenesis[104]. Similarly, studies revealed that reduced *FBXW7* expression impacts the ubiquitination and degradation of cell cycle regulators and oncogenic proteins such as c-MYC, mTOR, Cyclin E, Notch, and c-JUN, resulting in cell cycle defects, abnormal cell proliferation and eventual tumorigenesis[105, 106]. Despite ongoing efforts, the identification of novel CIN genes including the role of SCF complex members in CRC remains poorly understood. Therefore, it is essential to understand how reduced *RBX1* expression impacts both non-malignant and malignant colonic epithelial cell lines, which will eventually provide novel insights into the early events related to CRC pathogenesis.

1.3.2. RING-Box 1 (*RBX1*)

RBX1 encodes a 12 kilodalton (kDa) RING-finger protein comprised of 108 amino acids[107]. Also known as RING-Box protein 1, or Regulator of Cullin 1 (*ROC1*), *RBX1* is located on chromosome 22q13 and is highly expressed across multiple organs including placenta, muscle, heart and liver[107, 108]. The RBX1 protein in humans is localized in both the nucleus and the cytoplasm, suggesting its role in proteolytic degradation of nuclear and cytoplasmic proteins[108]. The animo-terminal portion of the RBX1 protein binds to CUL1, while its carboxy-terminal zinc-binding RING-H2 domain binds E2 enzymes.[108, 109]. As an essential gene, *RBX1* is highly conserved throughout eukaryotic evolution, with homologs identified in species ranging from yeast to humans.[108]. For instance, the deletion of *RBX1* homolog in *Saccharomyces cerevisiae* (*Hrt1*) results in lethality[110]. Also, *RBX1* homolog deletion in *Caenorhabditis elegans* (*RBX-1*), *Drosophila melanogaster* (*Roc1a*), and mice (*Rbx1*) is associated with the disruption of cell proliferation and embryonic development mechanisms, which may also lead to lethality[108, 111]. Studies revealed that out of the ~600 E3 ubiquitin ligase complexes encoded by the human genome, ~250-300 comprise the Cullin-RING ligases (CRLs) family, which are known to interact with *RBX1*[109, 112-114]. *RBX1* has a paralog, *RBX2*, and both proteins share a related zinc-binding domain[108]. However, *RBX2* responds primarily to cellular stress, while *RBX1* responds to regular

physiological conditions[115]. Additionally, *RBX2* only interacts with one CRL family (CRL5), whereas *RBX1* interacts with all seven CRL members (CRL1, 2, 3, 4A, 4B, 5 and 7)[109, 116]. *RBX1* also plays a role in neddylation, a post-translational modification process that consists of the attachment of NEDD8 (Neural precursor cell Expressed, Developmentally Downregulated), a ubiquitin-like protein modifier essential to the proper activation and function of the SCF complex[95, 117]. More specifically, NEDD8 in linked to the K residue of the SCF core member CUL1[95, 117].

RBX1 contributes to genome stability by regulating DNA double-strand break repair pathways, and it has been linked to the ubiquitin regulation of PALB2 by the KEAP1-CUL3-RBX1 E3 ligase[118, 119]. PALB2 acts as a molecule adapter between BRCA1 and BRCA2, forming a complex that is essential for recruiting RAD51 and resulting in downstream DNA double-strand break repair through the homologous recombination (HR) repair pathway[118, 120, 121]. RBX1 is also a subunit of the DDB1–CUL4–RBX1 E3 ubiquitin ligase complex, which plays a role in ubiquitination of histone H2A and promotion of UV-induced break DNA repair through Nucleotide Excision Repair (NER) mechanisms[122].

RBX1 alterations are present in multiple malignancies and its dysregulation impacts tumor development and resistance[86, 123]. As previously mentioned, *RBX1* heterozygous loss is highly prevalent in HGSC (~83% of patient samples), and its reduced expression results in an increase of CIN-associated phenotypes[86]. *RBX1* shallow deletion is also prevalent in CRC cases, as ~34% of patients harbor *RBX1* shallow deletions[124] (*see* ***Figure 4-1***). Additionally, disruption in *RBX1* expression is linked to tumour metastasis in triple-negative breast cancer and is also associated with poor prognosis and survival in patients with non-small cell lung cancer[125, 126]. Therefore, studies aimed at investigating the impact reduced *RBX1* expression has on CIN and CRC are essential to provide new insights into the underlying mechanisms associated with this disease.

CHAPTER 2. RATIONALE, HYPOTHESIS AND RESEARCH AIMS

2.1. RATIONALE

CRC was the fourth most diagnosed and third most lethal cancer in Canada in 2025[3]. Despite ongoing efforts to develop new diagnostic and treatment strategies, the 5-year survival rate of CRC can be as low as 11-13% (Stage IV)[127]. Therefore, understanding the mechanisms underlying CRC development and progression is crucial for designing novel therapeutic strategies aimed at reducing the high morbidity and mortality rates associated with this disease. CIN is a genome instability hallmark that is highly prevalent in many cancer types, and it is present in ~85% of CRC cases[85]; however the molecular determinants (*i.e.* aberrant genes, proteins, and pathways) responsible for driving CIN remain poorly understood. In this regard, a previous siRNA-based library screen[10] performed by the McManus laboratory identified *RBX1* as a potential CIN gene candidate, suggesting that its reduced expression may contribute to the development of CRC.

TCGA data extracted from the cBioPortal revealed that ~34% of CRC patients exhibit *RBX1* shallow deletions, which is associated with increases in genome instability markers and poor patient outcomes[124, 128, 129]. Recent studies have also revealed that reduced *RBX1* expression induces CIN in tubo-ovarian high-grade serous carcinoma (HGSC)[86]; however, the impact reduced *RBX1* expression has on CIN and early CRC development has not been investigated. Thus, it is essential to determine the impact reduced *RBX1* expression has in relevant cellular contexts, which will offer a better understanding of the potential mechanisms underlying CIN, providing novel insights into the development of new therapeutic strategies. Therefore, my project aims to understand the role of *RBX1* on the molecular origins of CIN in CRC by investigating the impact of reduced *RBX1* expression on CIN in both non-malignant colonic epithelial and CRC cell lines.

2.2. HYPOTHESIS AND RESEARCH AIMS

Hypothesis: Reduced *RBX1* expression induces CIN that contributes to early CRC development. This hypothesis was tested through the execution of two research aims.

Aim 1: To determine the impact reduced *RBX1* expression has on CIN in non-malignant colonic epithelial cell contexts.

Aim 2: To determine the impact reduced *RBX1* expression has on CIN in a malignant colorectal cancer context.

CHAPTER 3. MATERIALS AND METHODS

3.1. BIOINFORMATIC APPROACHES

All bioinformatic data regarding *RBX1* copy number alteration (CNA), survival and mRNA expression were collected from The Cancer Genome Atlas (TCGA; Pan-Cancer Atlas data)[124]. Data extraction and visualization were performed using cBioPortal (www.cbioportal.org)[128, 129], an open source and freely accessible platform designed for multidimensional cancer genomics datasets analysis. All patient-derived data extracted for this study are publicly available and does not require human ethics approval.

3.1.1. Genomic Alterations and Survival Analyses

To assess the prevalence of *RBX1* copy number losses in cancer, CNA data from eight common solid tumors (breast, cervical, colorectal, glioblastoma, head and neck, liver, lung and prostate) were extracted from TCGA Pan-Cancer Atlas[124], and the following Onco Query Language commands were used: (1) HOMDEL, representing deep deletions (loss of two alleles); (2) HETLOSS, shallow deletions (loss of one allele); (3) GAIN (gain of one allele); (4) AMP, large amplifications (gain of two or more alleles); and (5) MUT (mutation). All *RBX1* CNA data was exported to Prism v10 (GraphPad) to plot deep and shallow deletions across the eight specified cancer types listed above.

All CRC patient sample data regarding individual *RBX1* CNA frequencies (*i.e.*, deep deletions, shallow deletions, diploid, gains and amplifications) and mRNA expression levels were extracted using cBioPortal[128, 129]. Afterwards, CNA data were compared with their corresponding mRNA expression z-score (z = expression in tumor sample - mean expression in reference sample[diploid])/standard deviation of expression in reference sample[diploid]) and imported into Prism v10 (GraphPad), where shallow deletions and normal cases (*i.e.*, diploid) were statistically compared by two-sample Mann-Whitney (MW) test (detailed in *Section 3.6.2*).

TCGA patient data were used to compare patient survival outcomes[124]. Data were imported into Prism v10 (GraphPad) to generate and statistically analyze Kaplan-Meier (KM) curves for overall survival, progression free survival and disease-specific survival. Log-rank tests were applied to assess statistically significant differences between patient sample with *RBX1* shallow deletions relative to diploid, and tests with a p-value <0.05 were considered statistically significant. Figures were generated using Adobe Photoshop 2025.

3.2 REAGENTS

In general, solutions and reagents (see Appendix A) employed in this study were purchased from Thermo Scientific, Sigma-Aldrich, Gibco, HyClone, Corning and Sarstedt.

3.3 CELL CULTURE

The three colonic epithelial cell lines employed in this study are characterized in ***Table 3-1***. Non-malignant cell lines, 1CT and A1309, were provided by Dr. Jerry Shay (University of Texas Southwestern Medical Center, USA), while the malignant cell line, HCT116, was purchased from American Type Culture Collection (Rockville, MD). 1CT and A1309 cells were cultured on surface treated (with oxygen and nitrogen functional groups) Primaria tissue culture plates (Corning) in X-medium (Dulbecco's Modified Eagle Medium [DMEM] with High Glucose Medium 199) (HyClone) supplemented with 2% cosmic calf serum (CCS) (HyClone) (Appendix A). HCT116 cells were cultured in 10 cm tissue culture plates (Sarstedt) with McCoy's 5A medium (HyClone) supplemented with 10% fetal bovine serum (FBS) (Sigma-Aldrich) (Appendix A). Both non-malignant and malignant cell lines were grown in an incubator at 37 degrees Celsius (ºC). However, 1CT and A1309 cells were grown in sealed chambers containing 2% O2, 7% CO2 and 91% nitrogen, as low-oxygen conditions have been shown to extend the lifespan of epithelial cells by delaying stress-induces senescence that results from regular atmospheric oxygen conditions (21% O2)[130]. A tray with Milli-Q water containing cupric sulfate pentahydrate (Appendix A) was placed in the bottom of the incubator to maintain humidity and prevent microbial and fungal growth. All cell lines used in this study are karyotypically stable[85] and confirmed to express RBX1 protein, making them suitable for subsequent analyses.

Table 3-1. Properties of Human Colonic Epithelial Cell Lines Employed in CIN Assays.

	1CT	A1309	HCT116
Source	Dr. Jerry Shay (University of Texas)	Dr. Jerry Shay (University of Texas)	American Type Culture Collection (Rockville, MD)
Culture Properties	Adherent	Adherent	Adherent
Transformed or Immortalized	Immortalized (human telomerase and CDK4[A])	Immortalized (human telomerase and CDK4[A])	Transformed
Karyotype	Diploid 46 XY, Male Stable	Diploid 46 XY, Male Stable	Near Diploid 45 X, Male Stable
Growth Medium	X-media + 2% CCS	X-media + 2% CCS	McCoy's 5A +10% FBS
Doubling Time	~22 hours (h)	< 22 h	< 22 h
Protein Expression Profiling			
KRAS	Wild-type[C]	G12V[B]	G13D[B]
TP53	Wild-type[C]	Wild-type[C], ~50% knockdown[D]	Wild-type[C]
APC	Wild-type[C]	Expression of truncated protein[E], ~70% knockdown[D]	Wild-type[C]

[A]Cyclin Dependent Kinase 4.
[B]Amino acid substitutions are denoted by their single letter code.
[C]Refers to expression of wild-type protein.
[D]Extent of knockdown relative to endogenous 1CT levels
[E]APC truncated at codon 1309

3.3.1. Cell Passaging

Cell cultures were maintained under sub-confluent conditions and were passaged in a biological safety cabinet every 2–4 days. Briefly, cell culture medium was aspirated from tissue culture dishes and cells (adhered) were rinsed once with 1× PBS (Phosphate-Buffered Saline; Appendix A). To detach adherent cells, 1 mL of 0.05% trypsin-EDTA ([Ethylenediaminetetraacetic Acid]; Gibco, Life Technologies) was added to tissue culture dishes and incubated for ~ 5 minutes (min) (HCT116 and 1CT cells), or ~2 min (A1309 cells) at room temperature. Cell detachment was monitored using an inverted Zeiss ID03 microscope equipped with a 10× objective (Zeiss). After detachment, trypsin was diluted using 4mL of 1x sterile PBS for HCT116 cells or 1mL of trypsin neutralizer with 2mL of 1x sterile PBS for both 1CT and A1309 cells. Cells suspensions were collected, transferred to 15 mL conical tubes (Sarstedt) and centrifuged at 140 times gravitational acceleration (x g) for 5 min at 21 °C in a Legend XFR centrifuge (Thermo Scientific). After aspirating the supernatant, cell pellets were resuspended in 1x sterile PBS (8mL for HCT116

and 3mL for 1CT and A1309). Cell suspension was reseeded into a 10 cm plate (~1mL) containing 10mL of fresh cell culture medium and placed in the incubator as described in *Section 3.3*.

3.3.2. Cell Counting and Seeding

Cells were prepared for seeding CIN assays according to *Section 3.3.1*. After pelleting and resuspension, HCT116 cells were filtered through a 40 μm Falcon mesh filter into a 50 mL Sarstedt conical tube to remove cellular aggregates; filtration was not required for 1CT and A1309 cell lines, as they do not form cell aggregates. For enumeration, 40 microliter (μL) aliquots of each cell suspension were combined at a 1:1 ratio with 0.2% trypan blue dye (Gibco) within a 0.5 mL microcentrifuge tube, and 20 μL of this mixture was added in duplicate onto a Cedex Smart Slide (Roche). The number of viable cells in the suspension (cells/mL) was quantified automatically using a Cedex XS cell counter. Once the average number of viable cells (cells/mL) was determined, it was used to calculate the precise volume of cell suspension required for dilution in complete medium, ensuring accurate seeding densities for all subsequent experiments (see **Table 3-2**).

Table 3-2. Cell Seeding Densities and Volume Medium Employed in Corresponding CIN Assays.

Cell Line	Assays[A]	Plate Format	Cell Seeding Density (cells/well)	Volume Medium in Well
1CT	WB	6-well	30,000	2,000 μL
	NA/MN	96-well	1,000	200 μL
	MS	6-well	20,000	2,000 μL
A1309	WB	6-well	30,000	2,000 μL
	NA/MN	96-well	1,000	200 μL
	MS	6-well	20,000	2,000 μL
HCT116	WB	6-well	30,000	2,000 μL
	NA/MN	96-well	1,000(Control) 2,000(Transfected)	200 μL
	MS	6-well	30,000	2,000 μL

[A]WB, western blot; NA, nuclear area; MN, micronucleus; MS, mitotic chromosome spreads.

3.3.3. Short-Interfering RNA Transfection

RBX1 silencing experiments were performed using four distinct siRNA duplexes (siRBX1-1, -2, -3, -4; ON-TARGETplus [Dharmacon]). Individual siRNAs targeted different regions of the *RBX1* coding sequence, along with a non-targeting siRNA control (siControl) were employed. Each siRNA duplex and the control were reconstituted in 1× siRNA buffer (Appendix A) to prepare 20 µM stock solutions and 10 µM working solutions. An siRNA pool (siRBX1-P) was made by combining equal concentrations of the individual siRBX1 duplexes (siRBX1-1, -2, -3, -4) at 10 µM. The siRNAs were aliquoted into 10 µL portions and stored at -80 ºC. To limit RNA degradation, aliquots were subjected to no more than five freeze/thaw cycles. Cells were seeded approximately 24 h before siRNA transfection and incubated at 37 ºC to allow adhesion (cell densities are described in ***Table 3-2***). Lipid-mediated transfection was performed using RNAiMAX (Invitrogen). Transfection reagent and siRNA were gently mixed in a 1:1 ratio in cell culture media solution, and volumes were adjusted based on the plate format (see ***Table 3-3***). After a 20 min incubation period, the transfection solution was added into the wells and plates were rocked gently and incubated for a period of four days.

Table 3-3. Volumes Employed for *RBX1* Silencing Experiments using siRNA.

Cell Line	Assays[A]	siRNA Volume[B]	RNAiMAX Volume[B]	Volume Medium in Well[B]	Total Volume
1CT	WB	0.5 µL in 250 µL medium	6 µL in 250 µL medium	2,000 µL	2,500uL
	NA/MN	0.05 µL in 10 µL medium	0.3 µL in 10 µL medium	200 µL	220 µL
	MS	0.33 µL in 250 µL medium	4 µL in 250 µL medium	2,000 µL	2,500uL
A1309	WB	0.5 µL in 250 µL medium	6 µL in 250 µL medium	2,000 µL	2,500uL
	NA/MN	0.05 µL in 10 µL medium	0.3 µL in 10 µL medium	200 µL	220 µL
	MS	0.33 µL in 250 µL medium	4 µL in 250 µL medium	2,000 µL	2,500uL
HCT116	WB	1 µL in 250 µL medium	6 µL in 250 µL medium	2,000 µL	2,500uL
	NA/MN	0.1 µL in 10 µL medium	0.3 µL in 10 µL medium	200 µL	220 µL
	MS	1 µL in 250 µL medium	6 µL in 250 µL medium	2,000 µL	2,500uL

[A]WB, western blot; NA, nuclear area; MN, micronucleus; MS, mitotic chromosome spreads. [B]siRNAs and RNAiMAX were dilute in complete medium.

3.4 WESTERN BLOT ANALYSES

Western blots were employed to assess *RBX1* silencing efficiency and to evaluate changes in Cyclin E1 protein abundance following *RBX1* silencing.

3.4.1. Whole Cell Protein Extraction and Quantification via Bicinchoninic Acid Assay

Briefly, whole-cell protein lysates were collected four days after siRNA transfection. Cell culture medium was aspirated, and cells were washed with 1 mL of cold (4 ºC) 1× PBS (three times). Cells were treated with 80 µL of RIPA (radioimmunoprecipitation assay) lysis buffer (Appendix A) supplemented with 25× protease inhibitor (Appendix A). Cells were incubated for 15 min on ice (~4 ºC) and mixed by tapping half-way through. Cell scrapers were used to collect protein lysates, which were transferred into 1.5mL microcentrifuge tubes (~4 ºC). Lysates were sonicated twice (3 seconds each) using a Sonifier Cell Disrupter (Branson Sonic Power Co.) set at 50% duty cycle, and output control set at level 6. Tubes were centrifuged (Biofuge Fresco; Thermo Scientific) at 16,000 x G for 2 min at 4 ºC in order to remove remaining cell debris. Resulting supernatant was removed, transferred into fresh 1.5 mL microcentrifuge tubes, and stored at -20 ºC for short-term (< 2 weeks) or -80 ºC for long-term (> 2 weeks) storage. Prior to western blot experiments, protein concentrations were quantified using a Thermo Scientific BCA (Bicinchoninic Acid) Assay Kit according to the protocol provided by the manufacturer. Working reagent was prepared by mixing reagent A (BCA reagent) and reagent B (4% cupric sulfate solution) at a 50:1 ratio; 200 µL was dispensed into each well of a clear 96-well plate (Corning). A series of nine bovine serum albumin (BSA) standards ranging from 0 to 2,000 µg/mL were prepared to establish a standard curve. 25 µL aliquots from each BSA standard were loaded in duplicates, while test protein lysates were added in triplicate at 5 µL per well, supplemented with 20 µL of RIPA buffer. The plate was mixed for 10 seconds on a Multi-Microplate Genie shaker (Scientific Industries) to ensure homogeneity and incubated at 37 ºC for 30 min. Absorbance at 562 nm was measured using the SpectraMax iD3 plate reader (Molecular Devices). A standard curve was generated based on BSA concentration standards. To determine the final protein concentrations, three absorbance readings per sample were averaged and the result was multiplied by 5 (dilution factor).

3.4.2. Gel Electrophoresis and Western Blot

Equimolar amounts of protein samples (20 µg/well) were prepared by mixing appropriate volumes of 6× sodium dodecyl sulfate (SDS) Sample Loading Buffer (Appendix A) with RIPA buffer. Samples were denatured by incubating at 99 ºC in a heating block (Eppendorf) for 5 min and chilled on ice for at least 1 min. A Mini-PROTEAN electrophoresis tank (BioRad) was assembled with a 4–20% Mini-PROTEAN TGX gel (BioRad) and filled with 1× Running Buffer (Appendix A). To help identify the molecular weight of proteins, 4 µL of FroggaBio molecular weight marker (BLUelf Prestained Protein Ladder) was loaded into one well. Subsequent wells were loaded with 20 µL of denatured protein samples (20 µg/well). Electrophoresis was conducted at 140 V for 67 min at 4 ºC using a PowerPac HC power supply (BioRad). For protein transfer, a 0.45 µm nitrocellulose membrane (Biorad) along with blotting pads (BioRad) were soaked in 1× Transfer Buffer (Appendix A) prior to the transfer. Gel, membrane and blotting pads were assembled in a Trans-Blot Turbo Transfer System with 1× Transfer Buffer, and constant 25 volts (V) was applied for 7 min at room temperature to transfer proteins electrophoretically onto the membrane. Total protein transfer was assessed by staining the membrane with 5 mL of total protein stain copper phthalocyanine 3,4',4",4"'-tetrasulfonic acid tetrasodium salt (CPTS; Appendix A) for 5 min at room temperature using a Belly Dancer shaker (Stovall Life Science Inc.). Tris-buffered saline (TBS) containing 0.1% Tween 20 (TBST; Appendix A) was used to de-stain the membrane. Afterwards, the membrane was blocked for 1hour (room temperature) using 5% non-fat milk (w/v) diluted in 1× TBST (Appendix A) under gentle rocking. Primary antibodies against the target protein (*e.g.*, RBX1) and the loading control (*e.g.*, Cyclophilin B or α-Tubulin) were diluted in 5% non-fat milk (according to concentrations detailed in ***Table 3-4***) and incubated overnight at 4 ºC with gentle rocking. On the following day, membranes were washed with 1× TBST (three 10-min washes) on the Belly Dancer shaker set to medium speed (dial speed '5'). Horseradish peroxidase (HRP)-conjugated secondary antibodies were also diluted in 5% non-fat milk (see ***Table 3-4***) and incubated with the membrane for 1 hour at room temperature with gentle rocking. Finally, membranes were rinsed briefly with TBST followed by three 10 min washes in TBST.

Table 3-4. List of Antibodies Employed for Western Blot Analysis.

Primary Antibodies				
Antibody	**Catalogue Number**	**Source**	**Species**	**Dilution**
RBX1	ab86862	Abcam	Rabbit	1:30,000
Cyclin E1	ab3927	Abcam	Mouse	1:4,000
α-Tubulin	ab7291	Abcam	Mouse	1:4,000
Cyclophilin B	ab16045	Abcam	Rabbit	1:150,000
Secondary Antibodies				
Goat α Mouse HRP[A]	115-035-146	Jackson ImmunoResearch	Goat	1:10,000
Goat α Rabbit HRP[A]	111-035-144	Jackson ImmunoResearch	Goat	1:10,000

[A]HRP (Horseradish peroxidase)

3.4.3. Semi-Quantitative Western Blot Analysis

The UltraSense Western Substrate kit (FroggaBio) was used to visualize the antibody-conjugated proteins according to the manufacturer's instructions. Visualization solution was prepared by mixing the luminol solution with the peroxide solution at a 1:1 ratio and protected from light to prevent signal degradation. The membrane edges were carefully blotted on a Kimwipe (Kimberly Clark) to remove excess TBST and were placed on a clear page protector where approximately 1000 µL of luminol/peroxide solution was applied on the membrane, followed by a 5 min incubation at room temperature (in the dark). Chemiluminescent signals were captured using a ChemiDoc Imaging System (Bio-Rad). Exposure times were empirically optimized for each antibody to ensure strong signals without pixel saturation. Images were imported into ImageJ software (National Institutes of Health) for semi-quantitative analysis of protein expression. Band intensities were first normalized against their respective loading controls (*i.e.* Cyclophilin B or α-Tubulin) and normalized relative to a control sample (*i.e.*, Non-Targeting Control [siControl]), which was set to 100%, allowing the comparison of protein expression between control and experimental groups. Figures were generated using Adobe Photoshop 2025.

3.5 SINGLE-CELL QUANTITATIVE IMAGING MICROSCOPY (QuantIM)

QuantIM techniques were applied to *RBX1* silenced cells to assess CIN phenotypes, including changes in nuclear area and micronucleus formation[85, 86]. Mitotic chromosome spreads, which is a standard cytogenetic technique, were generated and enumerated to assess the impact reduced *RBX1* expression has on chromosome complements.

3.5.1. Cell Fixation and DNA Counter-staining for Nuclear Area and Micronucleus Formation Analyses

To evaluate changes in nuclear area and micronucleus formation, established QuantIM[85, 86] techniques were employed. After a four days post-transfection period (see *Section 3.3.3*), cell culture medium was aspirated from 96-well plates and cells were fixed with 200 µL of 4% paraformaldehyde (Appendix A) for 15 min at room temperature. Paraformaldehyde was discarded, and cells were washed twice with 200 µL of 1× PBS. Cells nuclei were counterstained using 200 µL of 200 ng/mL Hoechst 33342 (Thermo Scientific) in 1× PBS (Appendix A) per well. Plates were stored in the dark at 4 ºC overnight to ensure uniform nuclear staining before imaging on the following day.

3.5.2. Image Acquisition and Analysis

To acquire sufficient cell counts for quantitative analysis, non-overlapping two-dimensional (2D) images were captured from each well in 3×3 or 4×4 matrices using ImageXpress HT.ai Imaging System (Molecular Devices) equipped with a 20x Water Immersion CFI Apochromat objective lens (0.95 numerical aperture). Image acquisition and analyses were optimized using the IN-Carta Image Analysis Software (Molecular Devices) for both nuclear area and micronucleus formation analysis. Filters based on size, fluorescence intensity, and image periphery exclusion were derived from parameters previously established in our research pipeline[131, 132]. Filters were applied to eliminate small debris, mitotic or apoptotic bodies, and partial nuclei located at the edges of the wells. These parameters were individually optimized and consistently applied throughout experiments. For nuclear areas quantification, primary masks were applied automatically to identified interphase nuclei, which were counter-stained with Hoechst (see *Section 3.5.1*). Partial nuclei near image borders (<50 µm from edges) were excluded using a periphery filter. Masks were also applied for micronuclei detection, which included micronuclei with a maximum diameter of 30 µm. A secondary mask with a 15 µm ring width was applied to define the cellular boundary, and micronuclei were identified as dots situated outside the primary mask but within the secondary mask. Micronuclei count data

(well/condition) were normalized to total number of nuclei imaged and presented as the frequency of micronucleus formation per condition. Data from at least 1000 nuclei per condition were used and results were imported into Prism v10 (GraphPad) to perform two-sample Kolmogorov-Smirnov [KS] test for nuclear area cumulative distribution frequency and Mann-Whitney [MW] test for micronucleus formation frequency (see *Section 3.6*). Cumulative distribution frequency graphs were used to present nuclear area data, while dot plot graphs were used to represent micronuclei data. Figures were generated in Adobe Photoshop 2025, and all experiments were performed at least three times (N = 3).

3.5.3. Mitotic Chromosome Spreads and Chromosome Enumeration

Mitotic chromosome spreads were generated by seeding cells (see ***Table 3-2***) onto sterile coverslips, followed by silencing with siRNAs (see ***Table 3-3***). On the fourth post-transfection day, cells were treated with KaryoMAX Colcemid (Gibco) at 100 ng/mL (Appendix A) in complete medium for 1.5 h (HCT116) or 3.5 h (1CT, A1309) at 37 ºC to enrich for mitotic population. Following incubation, Colcemid and medium were aspirated, and 2 mL of hypotonic solution (75 mM potassium chloride [KCl]; Appendix A) was added to each well for approximately 20 min (1CT, A1309) or 17min (HCT116). Cells were fixed with a 3:1 methanol: acetic acid solution (Appendix A), which were applied in 3 x 10 min intervals. After fixation, coverslips were placed on the side of the wells to dry overnight and mounted on the following day on glass microscope slides using 4’,6-diamidino-2-phenylindole (DAPI) Mounting Medium (Vector Laboratories; Appendix A), followed by incubation at 4 ºC in the dark. A minimum of 100 mitotic chromosome spreads per condition were imaged on a Zeiss Axio Imager Z2 microscope equipped with a 63× oil-immersion plan apochromat objective (numerical aperture 1.4) and Zeiss Axiocam 820 CMOS camera (20 megapixel). Images were acquired as 16-bit TIFF files and analyzed in FIJI software for visual assessment and manual chromosome counting. Chromosome spreads deviating from the modal karyotype of the respective cell line (see ***Table 3-1***) were categorized as: 1) losses (< modal chromosome number); 2) small-scale gains (< 10 additional chromosomes); and 3) large-scale gains (10 or more additional chromosomes). Three biological replicates were analyzed per condition, and data were imported into Prism v10 (GraphPad) for graph generation and descriptive statistical analyses. Figures were assembled using Adobe Photoshop 2025.

3.6. STATISTICAL ANALYSES

The number of experimental replicates (N) and technical replicates (n) is reported for all experiments included in this thesis. Data from three biological replicates for each cell line are presented. All statistical analyses were performed using Prism v10 (GraphPad).

3.6.1. Two-Sample Kolmogorov-Smirnov Test

The two-sample Kolmogorov-Smirnov (KS) test is a non-parametric statistical test that was used to assess differences in nuclear area cumulative frequency distributions of two datasets, such as control and silenced conditions. The test calculates a p-value corresponding to the largest deviation observed between the respective distributions. Two-sample KS test results (p-value<0.05) are presented as follows: p-value < 0.05 (*), p-value < 0.01 (**), p-value < 0.001 (***), and p < 0.0001 (****).

3.6.2. Mann-Whitney Test

The Mann-Whitney test is a non-parametric statistical test employed to compare the micronucleus formation rank orders of two independent datasets, such as control and silenced conditions. Results are calculated based on the difference in mean ranks between the conditions under investigation. Results considered statistically significant are presented as follows: p-value < 0.05 (*), p-value < 0.01 (**), p-value < 0.001 (***), and p < 0.0001 (****).

3.6.3. Student's t-Test

The Student's t-test is a parametric statistical test employed to compare the means of two independent aberrant chromosome groups, such as control and silenced conditions. P-values are presented based on the probability that the difference between the two means occurred by chance, and results that were considered statistically significant are presented as follows: p-value < 0.05 (*), p-value < 0.01 (**), p-value < 0.001 (***), and p < 0.0001 (****).

CHAPTER 4. RESULTS

4.1. Bioinformatic Analyses Reveal Heterozygous Loss of *RBX1* is Frequent in CRC and is Associated with Poor Patient Outcomes

Publicly available TCGA data[124] extracted from cBioPortal[128, 129] were used to determine the prevalence and potential clinical relevance of *RBX1* copy number losses, and copy number alteration (CNA) data from eight common solid tumor types (breast, cervical, colorectal, glioblastoma, head and neck, liver, lung and prostate) were assessed. As presented in ***Figure 4-1A***, patient data from all eight cancer types exhibit *RBX1* shallow deletions (*i.e.,* heterozygous loss), ranging from ~10% in prostate cancer to ~45% in breast cancer. Regarding CRC, ~34% of cases present *RBX1* shallow deletions, which is associated with statistically significant (Student's t-test; **** p-value <0.0001) reduction of mRNA expression (***Figure 4-1B***) relative to samples with diploid *RBX1* copy numbers. Additionally, patient samples harbouring *RBX1* shallow deletions presented statistically significant increases (Student's t-test; ****; p-value <0.0001) in genome instability markers relative to those with diploid copy numbers. More specifically, according to ***Figure 4-1C***, patients with *RBX1* shallow deletions presented increases in fraction genome altered (percent of gains or losses of copy numbers in the genome), aneuploidy score (number of altered chromosome arms) and tumor break load (chromosome breaks and rearrangements). To evaluate how *RBX1* shallow deletions impact patient outcomes in CRC, three distinct survival curves (KM curves) were generated and assessed: 1) overall survival; 2) progression free survival; and 3) disease-specific survival (***Figure 4-2***). Log-rank tests revealed that patients with *RBX1* shallow deletions exhibited worse outcomes (p-value < 0.05) relative to those with diploid copies. Collectively, these finding support the hypothesis that decreased *RBX1* expression may have a role in CRC pathogenesis. Therefore, it is essential to determine the impact reduced *RBX1* expression has in relevant cellular contexts, which will offer a better understanding of the potential mechanisms underlying CIN in CRC contexts.

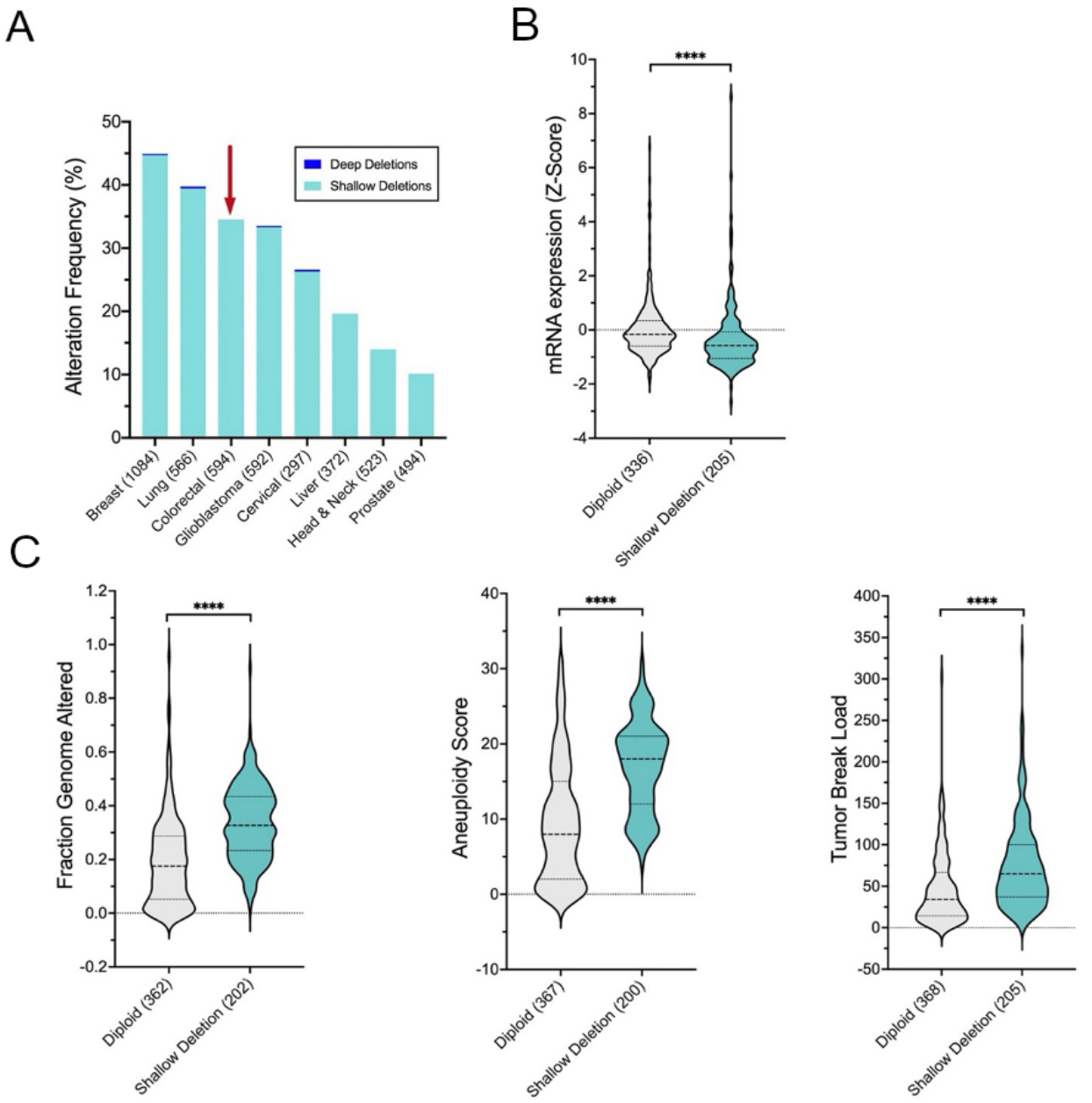

Figure 4-1. RBX1 Copy Number Losses Are Prevalent in CRC and are Associated with Diminished RBX1 mRNA Expression and Increases in Genome Instability.
(A) TCGA[124] data showing *RBX1* copy number losses including deep deletions (*i.e.*, homozygous loss) or shallow deletions (*i.e.*, heterozygous loss). ***(B)*** CRC cases with shallow *RBX1* deletions correspond with significant decreases in mRNA expression. Number of cases indicated in brackets, black dotted lines indicate the 1st and 3rd quartiles, and dashed black line identifies the median (Student's t-test; **** p-value < 0.0001). ***(C)*** CRC cases with shallow *RBX1* deletions are associated with a significant increase in fraction genome altered, aneuploidy score and tumor break load when compared to cases with diploid *RBX1* copy numbers. Number of cases indicated in brackets, black dotted lines indicate the 1st and 3rd quartiles, and dashed black line identifies the median (Student's t-test; **** p-value < 0.0001).

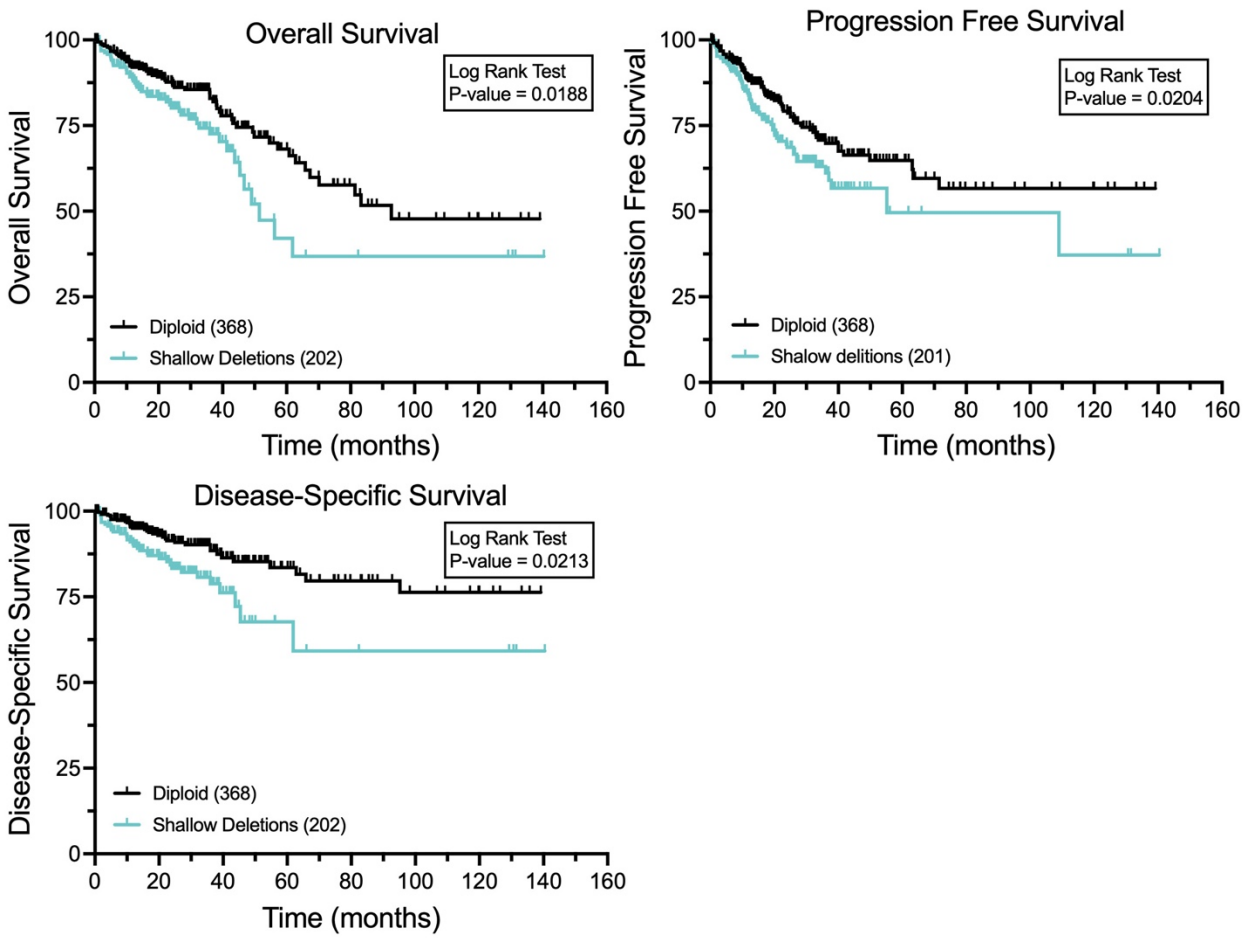

Figure 4-2. Heterozygous Loss of RBX1 is Associated with Worse CRC Patient Outcomes. KM curves showing significantly worse Overall, Disease-Specific and Progression Free Survival for CRC patients with *RBX1* shallow deletions compared to patients with diploid *RBX1* copy numbers (Log-rank test; p-value < 0.05)[128, 129]. Numbers in brackets indicate number of cases.

4.2. Establishing *RBX1* Silencing Efficiencies Using Short-Interfering RNA Duplexes

To evaluate *RBX1* silencing efficiency (see *Section 3.3.3*) and minimize potential off-target effects, four individual siRNAs duplexes (siRBX1-1, -2, -3, -4) and an siRBX1-Pool (siRBX1-P) comprised of equimolar concentrations of the individual siRBX1 duplexes were used along with a non-targeting siRNA duplex (siControl). HCT116, a well stablished and karyotypically stable CRC cell line[10, 85, 86], was used to assess *RBX1* silencing efficiencies using semi-quantitative western blot analysis (see *Section 3.4*). Protein expression was quantified according to band intensities, which were normalized to their respective loading control (α-Tubulin) and are presented relative to the siControl that was set to 100%. As shown in ***Figure 4-3***, *RBX1* was efficiently silenced in all silencing conditions, showing ~ 0% abundance (*i.e.*, below level of detection) following silencing with siRBX1-1, -2, -3, -4, and siRBX1-P. Although all siRNAs demonstrated similar silencing efficiency, siRBX1-2, -4 and siRBX1-P were selected for subsequent studies as they exhibited the greatest decrease in RBX1 protein abundance in a ovarian cancer study[86], and were purposefully selected to maintain experimental consistency. Collectively, western blotting revealed that *RBX1* is efficiently silenced in HCT116 cells.

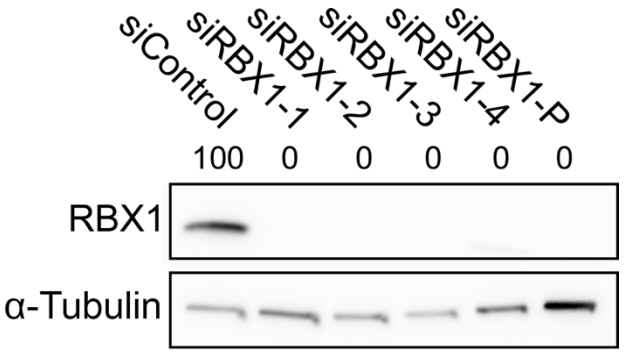

Figure 4-3. *RBX1* is Efficiently Silenced in HCT116 cells.
Semi-quantitative western blot showing decreased *RBX1* expression relative to siControl in HCT116 cells (one biological replicate) following transfection with four individual (siRBX1-1, -2, -3, -4) and pooled (siRBX1-Pool; equimolar amounts of siRBX1-1 to -4) siRNAs. RBX1 abundance is normalized to the corresponding loading control (α-Tubulin) and is presented relative to siControl, which is set to 100%.

4.3. AIM 1: To Determine the Impact Reduced *RBX1* Expression has on CIN in Non-malignant Colonic Epithelial Cell Contexts

4.3.1. *RBX1* is Efficiently Silenced in 1CT and A1309 Cells, and its Reduced Expression Induces Substrate Accumulation

Prior to evaluating the impact reduced *RBX1* expression has on CIN, *RBX1* silencing efficiencies were first assessed in two non-malignant cell lines, namely 1CT and A1309, using the siRNA duplexes (siRBX1-2, -4 and -P) identified above (see *Section 4.2*). In agreement with the silencing observed in HCT116, semi-quantitative western blots revealed effective *RBX1* silencing within both 1CT and A1309 cells (***Figure 4-4***); however, residual protein abundance varied across the silencing conditions in both lines. RBX1 abundance was reduced to ~3% to 5% in 1CT and ~1% to 4% in the A1309 cell line relative to siControl (***Figure 4-4***). To determine whether *RBX1* silencing impacts SCF complex function, Cyclin E1 abundance, an established target of the SCF complex, was assessed[86]. As expected, *RBX1* silencing corresponded with an increase in Cyclin E1 levels ranging from 204% to 534% in 1CT and ~108% to 223% in A1309 (***Figure 4-4***), indicating that reduced *RBX1* expression adversely impacts the SCF complex function. Collectively, these findings demonstrate that *RBX1* can be efficiently silenced in non-malignant colonic epithelial cell contexts and, therefore underscores the utility of this approach in determining the short-term impact reduced *RBX1* expression has on CIN.

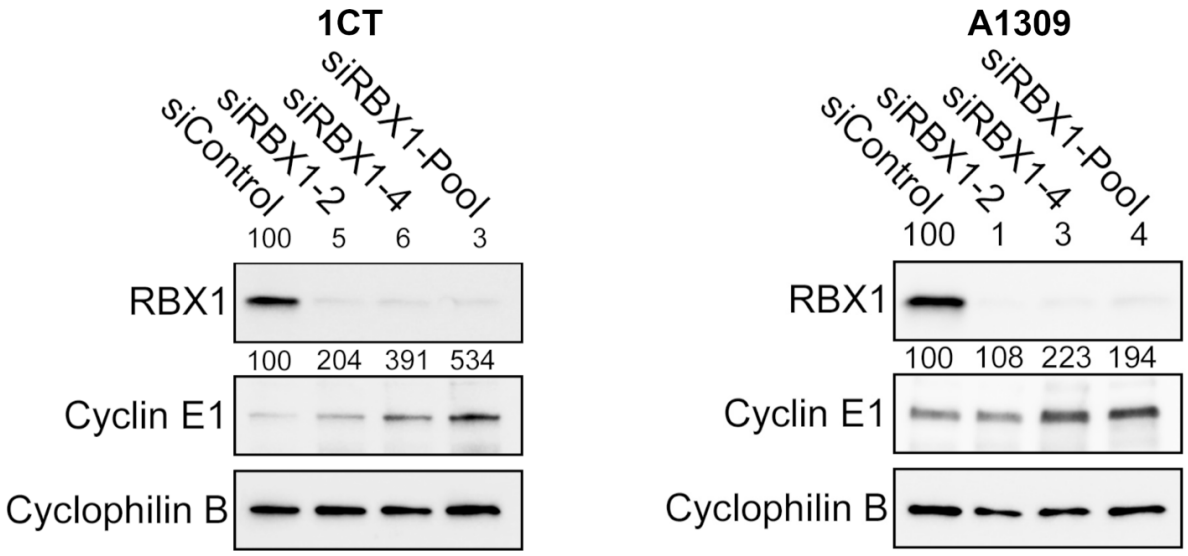

Figure 4-4. *RBX1* Silencing is Associated with Increases in Cyclin E1 Levels in Non-Malignant Colonic Epithelial Cell Lines
Semi-quantitative western blot depicting *RBX1* silencing efficiency relative to siControl in 1CT (left) and A1309 cells (right). Two individual (siRBX1-2, -4) and pooled (siRBX1-Pool; equimolar amounts of siRBX1-1 to -4) siRNAs were used to silence *RBX1* expression. RBX1 and Cyclin E1 abundance levels are normalized to the loading control (Cyclophilin B) and are presented relative to siControl above each column (N = 3).

4.3.2. Reduced *RBX1* Expression Underlies Increases in CIN-Associated Phenotypes in Non-Malignant Colonic Epithelial Cells

Having established our ability to silence *RBX1*, we sought to investigate the potential impact reduced *RBX1* expression has in early CRC development using the 1CT and A1309 cellular models. QuantIM approaches[85, 86] were employed to assess changes in nuclear areas and micronucleus formation, and to enumerate chromosomes in mitotic chromosome spreads. Qualitative analysis of nuclear areas in 1CT revealed an overall increase in nuclear areas and a prevalence of nuclear area heterogeneity in all *RBX1* silenced conditions relative to siControl (***Figure 4-5A***). Subsequent statistical analyses (two-sample KS test; p-value <0.0001; ***Table S1***, page 72) revealed significant increases in nuclear area distributions (*i.e.,* rightward shifts) in the silenced conditions relative to siControl in all three biological replicates (***Figure 4-5B***).

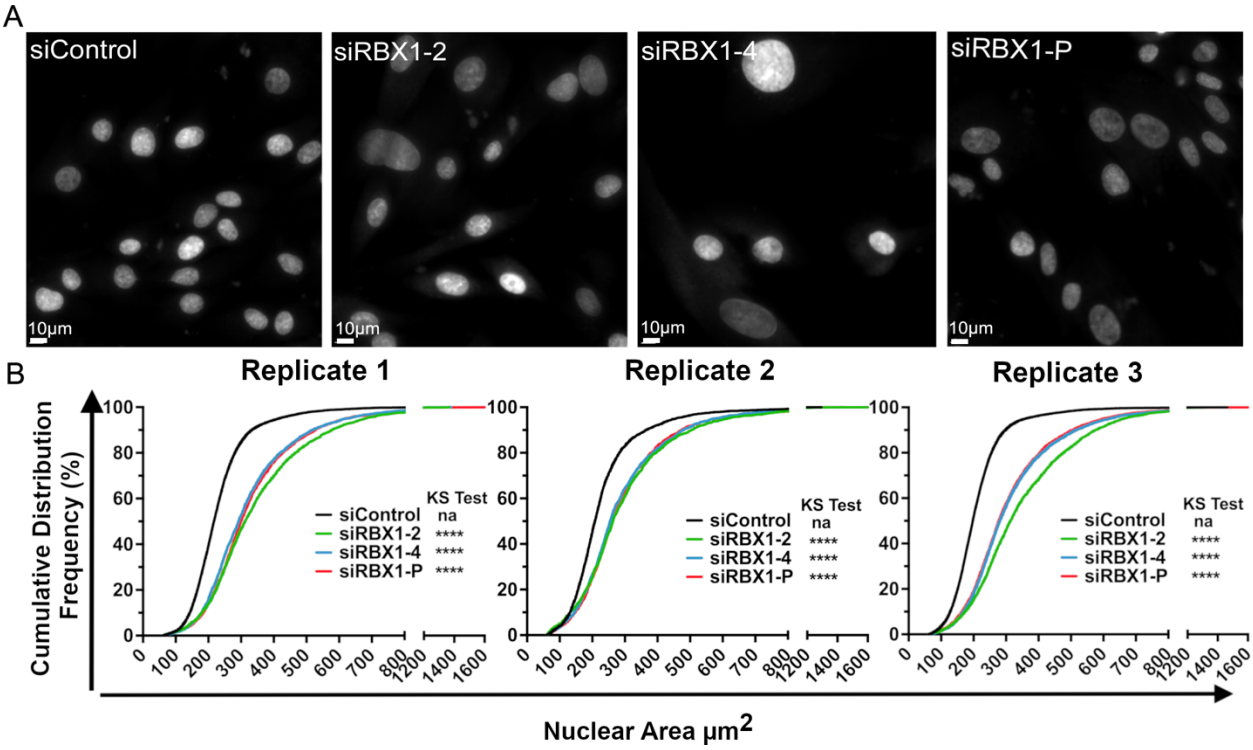

Figure 4-5. *RBX1* Silencing Induces Significant Increases in Nuclear Areas in 1CT.
(A) Low-resolution images of Hoechst-counterstained nuclei showing visual increases in nuclear areas following *RBX1* silencing relative to siControl. ***(B)*** Cumulative nuclear area distribution frequency graphs of three biological replicates reveal statistically significant increases in nuclear areas following *RBX1* silencing relative to siControl (two-sample KS test; na = not applicable; **** p-value < 0.0001; N = 3, n=6; >1000 nuclei imaged/silencing condition).

QuantIM approaches[85, 86] were also used to determine whether decreased *RBX1* expression impacts micronucleus formation (***Figure 4-6A***). Following *RBX1* silencing, 1CT cells demonstrated statistically significant increases (MW test; p-value<0.05; ***Table S2***, page 73) in micronuclei in all biological replicates. More specifically (***Figure 4-6B***), a ~2- to ~4-fold increase in micronuclei was observed across all silenced conditions relative to siControl.

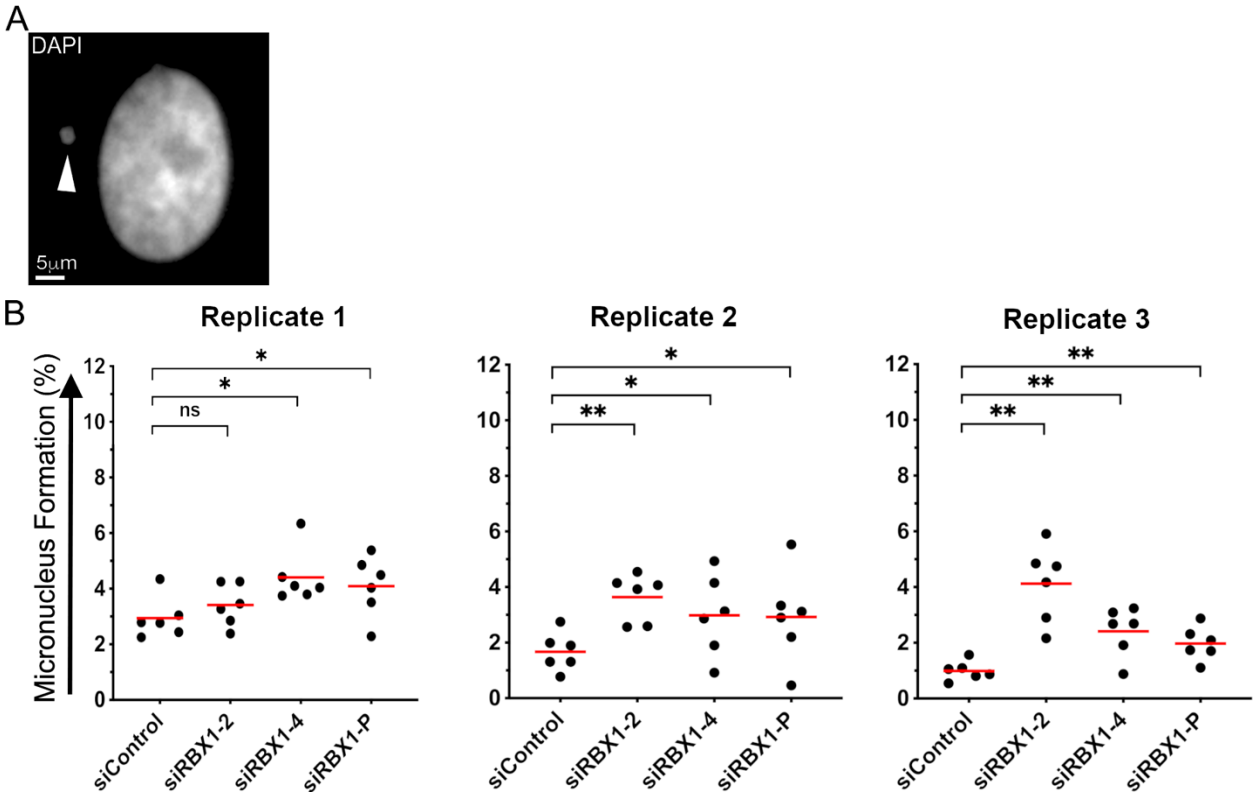

Figure 4-6. *RBX1* Silencing Corresponds with Significant Increases in Micronucleus Formation in 1CT.
(A) Low-resolution image of a Hoechst-counterstained nucleus with an associated micronucleus (arrowhead). ***(B)*** Dot plots from three biological replicates depicting increases in the frequency of micronucleus formation following *RBX1* silencing. Statistically significant increases were observed following *RBX1* silencing relative to siControl (MW test; ns = non-significant; * p-value < 0.05; ** p-value < 0.01). Red bars identify median values. (N = 3, n=6; >1000 nuclei imaged/silencing condition).

The QuantIM experiments[85, 86] described above do not directly assess chromosome numbers, but rather aberrant phenotypes associated with CIN. Accordingly, we next sought to determine the impact diminished *RBX1* expression has on chromosome numbers by enumerating chromosomes in mitotic chromosome spreads generated from *RBX1* silenced and control conditions. Spreads with 46 chromosomes were classified as modal, while spreads with divergent chromosome counts were classified as aberrant and sub-categorized into one of three categories (***Figure 4-7A***): 1) losses (<46 chromosomes); 2) small-scale gains (47-55 chromosomes), and 3) large-scale chromosome gains (≥ 56 chromosomes). A minimum of 100 mitotic chromosome spreads per *RBX1* silenced condition were assessed and repeated three times (N=3, ***Figure 4-7B***). Overall, losses and small-scale gains were the most prevalent phenotypes relative to siControl across all replicates with Replicate 1 inducing the largest fold increases (ranging from 2.8- to 3.1-fold), followed by Replicate 2 (2.3- to 2.5-fold increase) and Replicate 3 (1.9- to 2.2-fold increase). Analyses of all three Replicates combined (***Figure 4-7C***) revealed statistically significant differences (Student's t-test; p-value<0.05; ***Table S3***, page 74) in the numbers of aberrant chromosomes. More specifically, siRBX1-2 exhibited the greatest fold increase relative to siControl (2.5- fold increase), followed by siRBX1-4 and siRBX1-P with a 2.4- fold increase each.

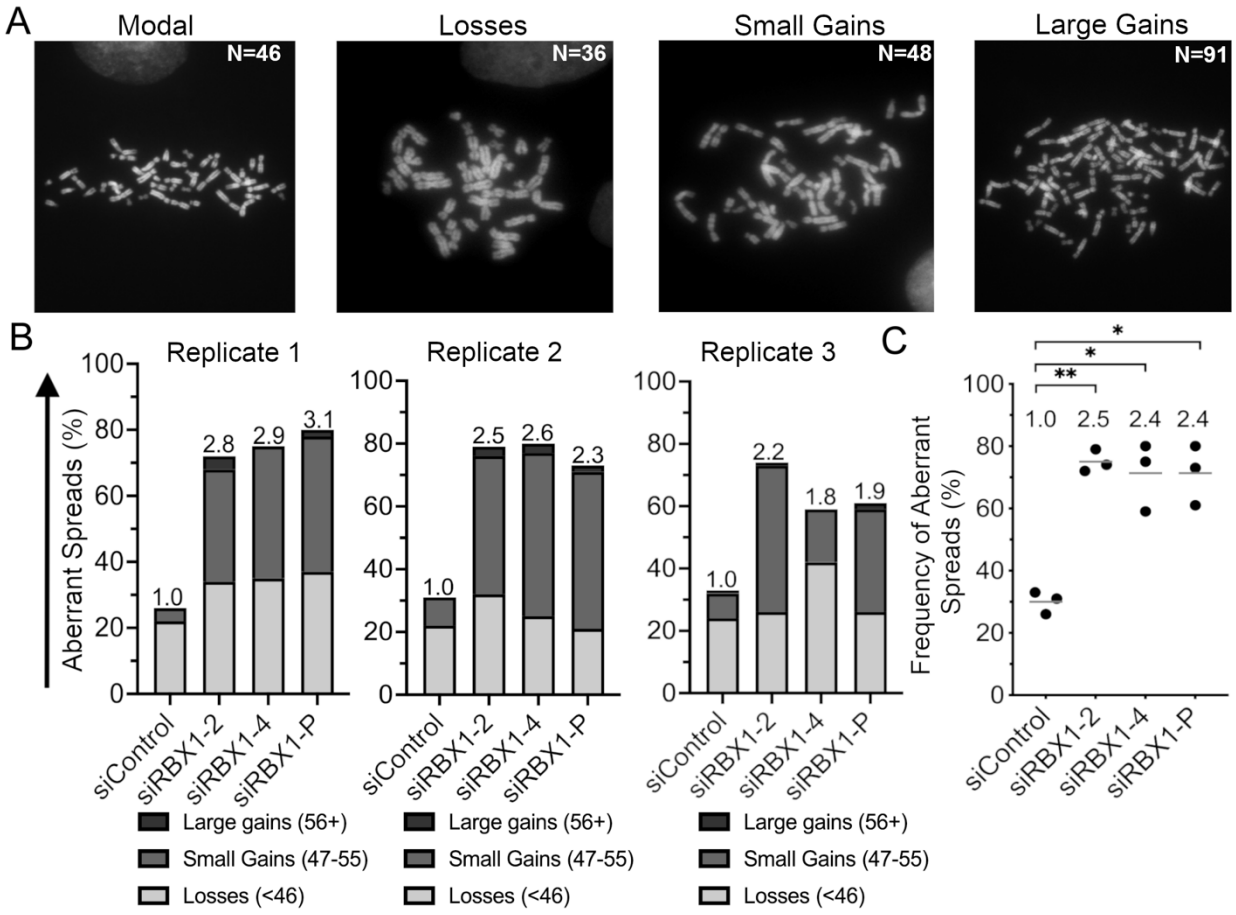

Figure 4-7. *RBX1* Silencing Induces Increase in Aberrant Chromosome Numbers in 1CT. ***(A)*** Representative images of DAPI-counterstained mitotic chromosome spreads displaying the modal number of 46 chromosomes, chromosome losses (<46 chromosomes), small scale gains (47-55 chromosomes) and large-scale gains (≥56 chromosomes). **(*B*)** Bar graphs presenting three biological replicates of the frequencies of aberrant chromosome spreads following *RBX1* silencing (N = 3; ≥ 100 spreads analysed/condition). The total fold increase in aberrant chromosome spreads is presented above each bar. ***(C)*** Dot plot reveals significant increases in the frequencies of aberrant chromosome complements following *RBX1* silencing in three biological replicates. The fold increase in aberrant spreads relative to siControl is presented at the top of each column (Student's t-test; p-value < 0.05, * p-value < 0.05; ** p-value < 0.01). Red bars identify mean values.

Next, we determined the impact reduced *RBX1* expression has on CIN-associated phenotypes in the A1309 cell line. Overall, qualitative assessment of nuclear areas revealed increases in nuclear areas in the silenced populations relative to siControl (***Figure 4-8A***). Further analyses of nuclear area cumulative distribution frequencies (***Figure 4-8B***) revealed statistically significant increases (two-sample KS test; p-value <0.0001; ***Table S4***, page 74) in nuclear areas in all A1309 silenced conditions relative to siControl.

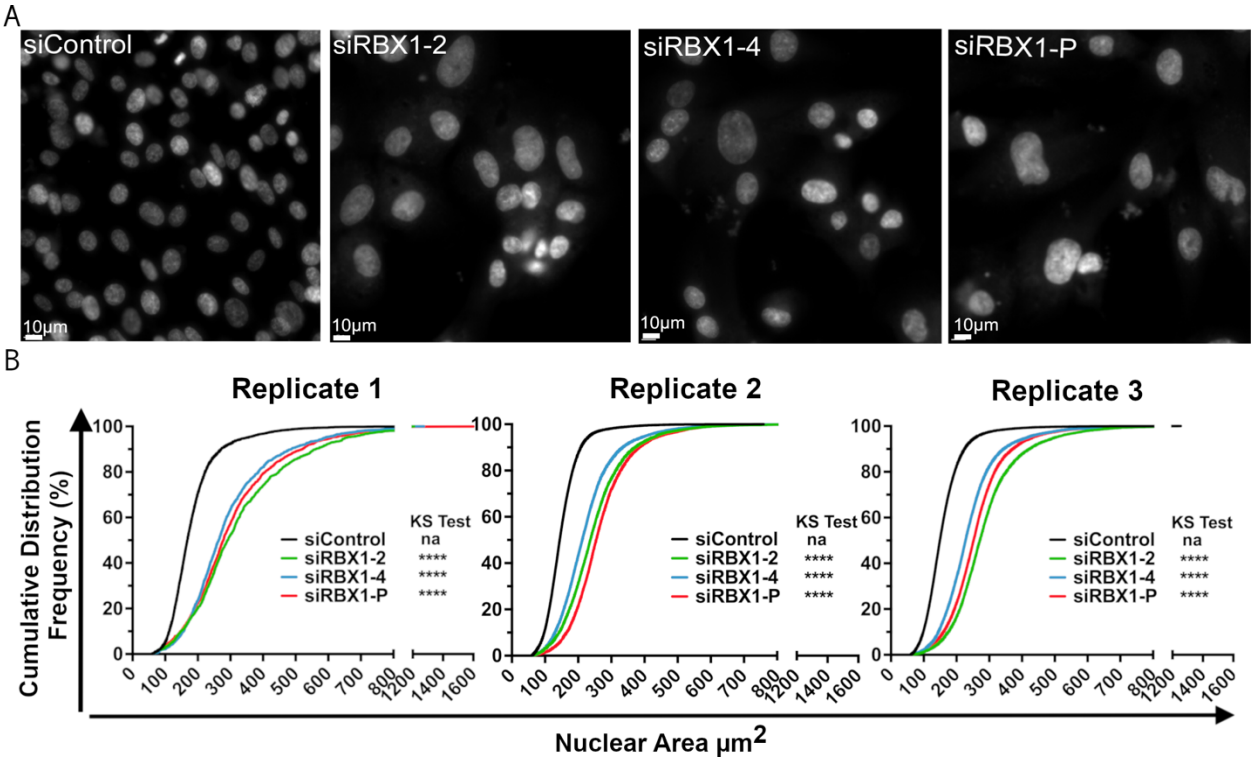

Figure 4-8. Reduced *RBX1* Expression Corresponds with Significant Increases in Nuclear Areas in A1309 Cells.
(A) Hoechst-counterstained images of nuclei depicting qualitative increases in nuclear areas following *RBX1* silencing relative to siControl. ***(B)*** Statistically significant increases in cumulative nuclear area distribution frequencies in three biological replicates following *RBX1* silencing relative to siControl (two-sample KS test; na = not applicable; ****p-value < 0.0001; N = 3, n=6; >1000 nuclei imaged/silencing condition).

Next, we performed micronucleus formation analyses that revealed reduced *RBX1* expression corresponds with increases in micronuclei (***Figure 4-6A***). More specifically, statistically significant increases (MW test; p-value <0.05; ***Table S5***, page 75) in micronucleus formation was observed in all three biological replicates in the A1309 cell line. Accordingly, *RBX1* silencing resulted in a ~3- to ~10-fold increase in micronucleus formation relative to siControl in A1309 cells (***Figure 4-9***).

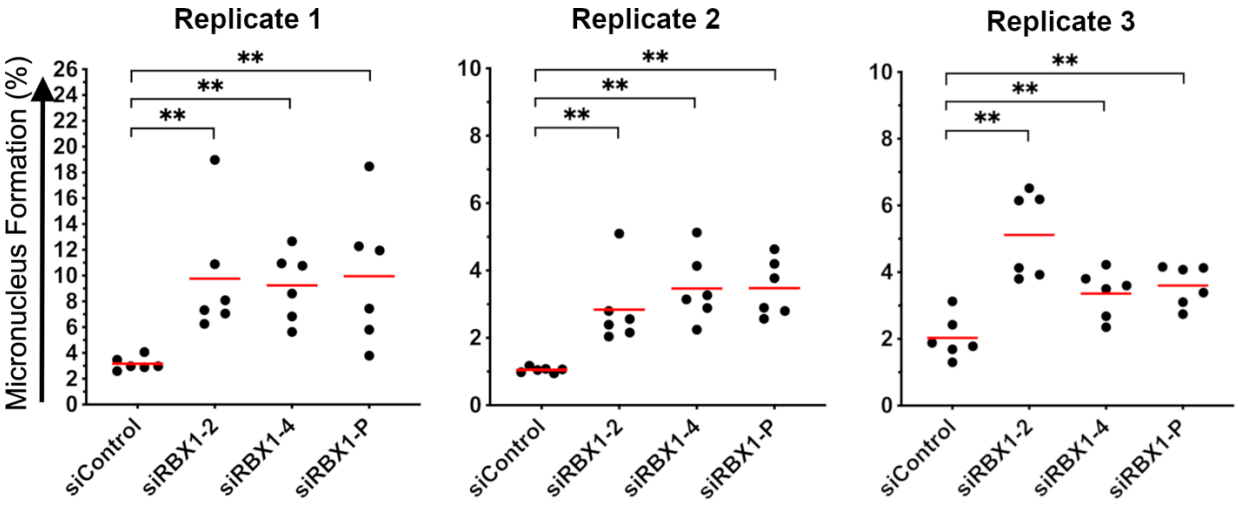

Figure 4-9. Diminished *RBX1* Expression Underlies Significant Increases in Micronucleus Formation in A1309.
Dot plots of three biological replicates reveal an overall increase in the frequency of micronucleus formation following *RBX1* silencing. Increases are statistically significant in all replicates relative to siControl (Mann-Whitney [MW] test; ** p-value < 0.01). Median values are indicated by the red bars. (N = 3, n=6; >1000 nuclei imaged/silencing condition).

To directly assess chromosome numbers, a minimum of 100 mitotic chromosome spreads were generated and analyzed per silencing condition. The A1309 cell line also has a modal number of 46 and aberrant chromosome spreads were subcategorized as losses, small gains and large gains (***Figure 4-10A***). According to (***Figure 4-10B***), Replicate 1 exhibited variation ranging from 2.1- to 2.6-fold increase, while Replicate 2 demonstrated the largest increase in aberrant spreads (2.6- to 2.7-fold increase) relative to siControl. Replicate 3 showed the smallest range in aberrant spreads, with 2.0- to 2.2-fold increase. Overall analyzes of all three replicates (***Figure 4-10C)*** revealed a 2.3- and 2.5-fold increase in aberrant chromosome numbers in siRBX1-4 and siRBX1-2 respectively, while siRBX1-P presented a 2.4- fold increase, which were determined to be statistically significant when compared to siControl (Student's t-test; p-value<0.05; ***Table S6***, page

76).

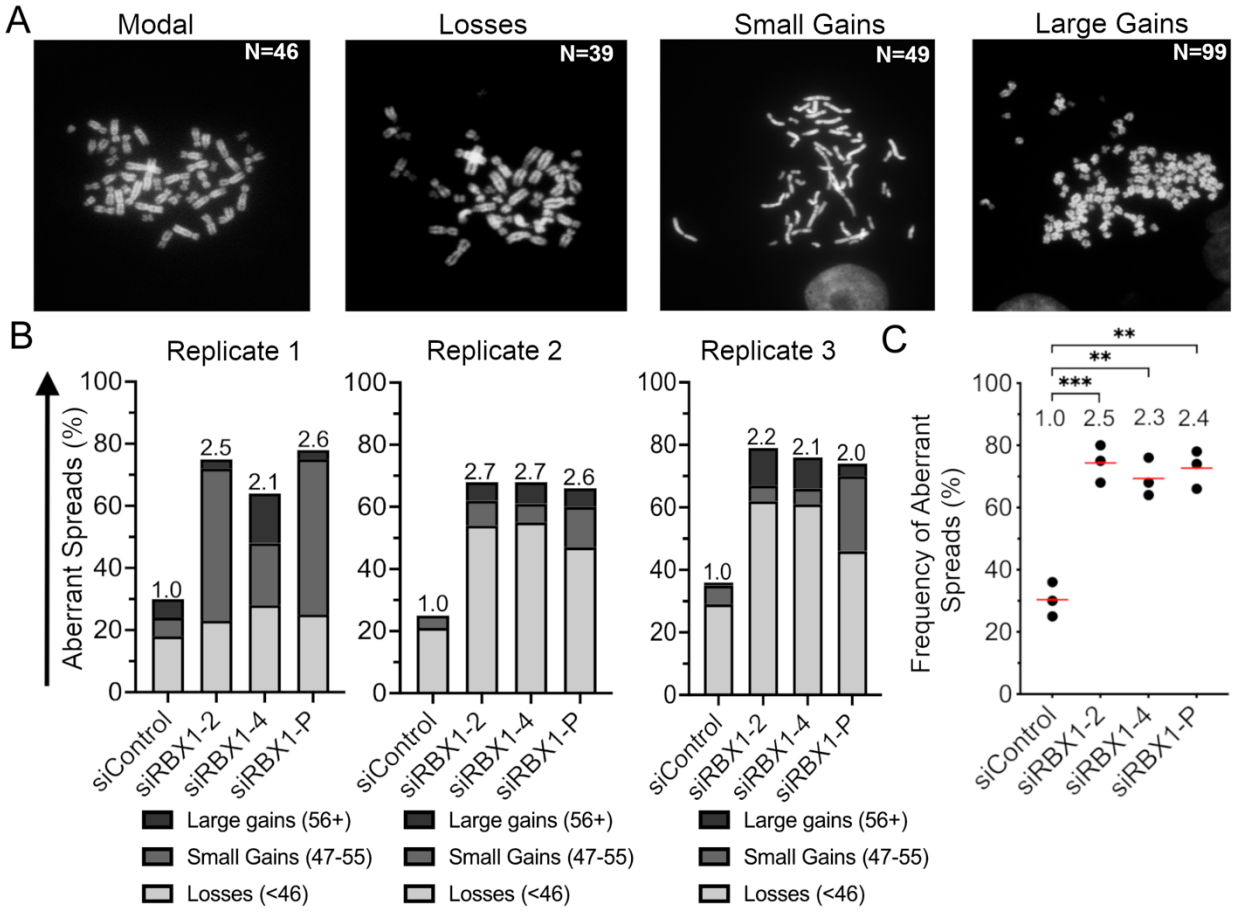

Figure 4-10. Reduced RBX1 Expression Induces Increase in Aberrant Chromosome Numbers in A1309.
(A) DAPI-counterstained mitotic chromosome spreads displaying the modal number of 46 chromosomes, chromosome losses (<46 chromosomes), small scale chromosome gains (47-55 chromosomes) and large chromosome gains (≥56 chromosomes). **(*B*)** Bar graphs depicting frequencies of aberrant chromosome spreads from three biological replicates after *RBX1* silencing (N = 3; ≥100 spreads per condition), with fold increases indicated above each bar. ***(C)*** Dot plot reveals significant increases in the frequencies of abnormal chromosome complements following *RBX1* silencing in three biological replicates. The fold increase in aberrant spreads relative to siControl is presented at the top of each column (Student's t-test; N = 3, n ≥100 spreads/condition; ** p-value < 0.01, *** p-value < 0.001). Red bars represent mean values.

Collectively, the above data establish that *RBX1* silencing induces increases in nuclear areas, micronucleus formation and aberrant chromosome numbers in two non-malignant colonic epithelial cell contexts. Thus, these findings are consistent with *RBX1* being a novel CIN gene that may contribute to early CRC pathogenesis.

4.4. AIM 2: To Determine the Impact Reduced *RBX1* Expression has on CIN in a Malignant Colorectal Cancer Context

4.4.1. *RBX1* can be Efficiently Silenced in HCT116 Cells, and its Reduced Expression Corresponds with Substrate Accumulation

Western blot analysis was also performed in HCT116 cells to assess *RBX1* silencing efficiency. According to ***Figure 4-11***, *RBX1* silencing corresponded with decreases in RBX1 protein abundance, ranging from ~1 to ~3% of endogenous protein levels in the silenced conditions relative to siControl. Decreased *RBX1* expression in a malignant CRC context also revealed striking increases in Cyclin E1 protein levels (~960% to ~1801%) relative to siControl, which indicates a disruption in the normal function of the SCF complex. Together, these findings demonstrate that *RBX1* can be effectively silenced in HCT116 cells, making it a relevant malignant cell line model to assess the impact diminished *RBX1* expression has on CIN in CRC.

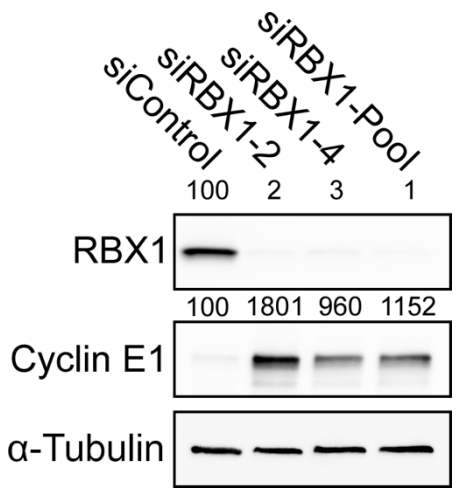

Figure 4-11. *RBX1* is Effectively Silenced in HCT116 and is Associated with Increases in Cyclin E1 Levels.
Semi-quantitative western blot showing *RBX1* silencing efficiency in HCT116 relative to siControl. RBX1 and Cyclin E1 abundance levels are normalized to the loading control (α-Tubulin) and are presented relative to siControl above each column (N = 3).

4.4.2. Reduced *RBX1* Expression Underlies Increases in CIN-Associated Phenotypes in Malignant Colonic Epithelial Cells

To determine the impact reduced *RBX1* expression has on CIN in a malignant context, QuantIM techniques[85, 86] were employed to assess changes in CIN-associated phenotypes in HCT116. Overall, decreased RBX1 protein abundance in this cell line was associated with visual increases in nuclear areas (***Figure 4-12A***) and corresponded with statistically significant increases in nuclear area distribution frequencies (two-sample KS test; p-value <0.0001; ***Table S7***, page 76) in three biological replicates (***Figure 4-12B***).

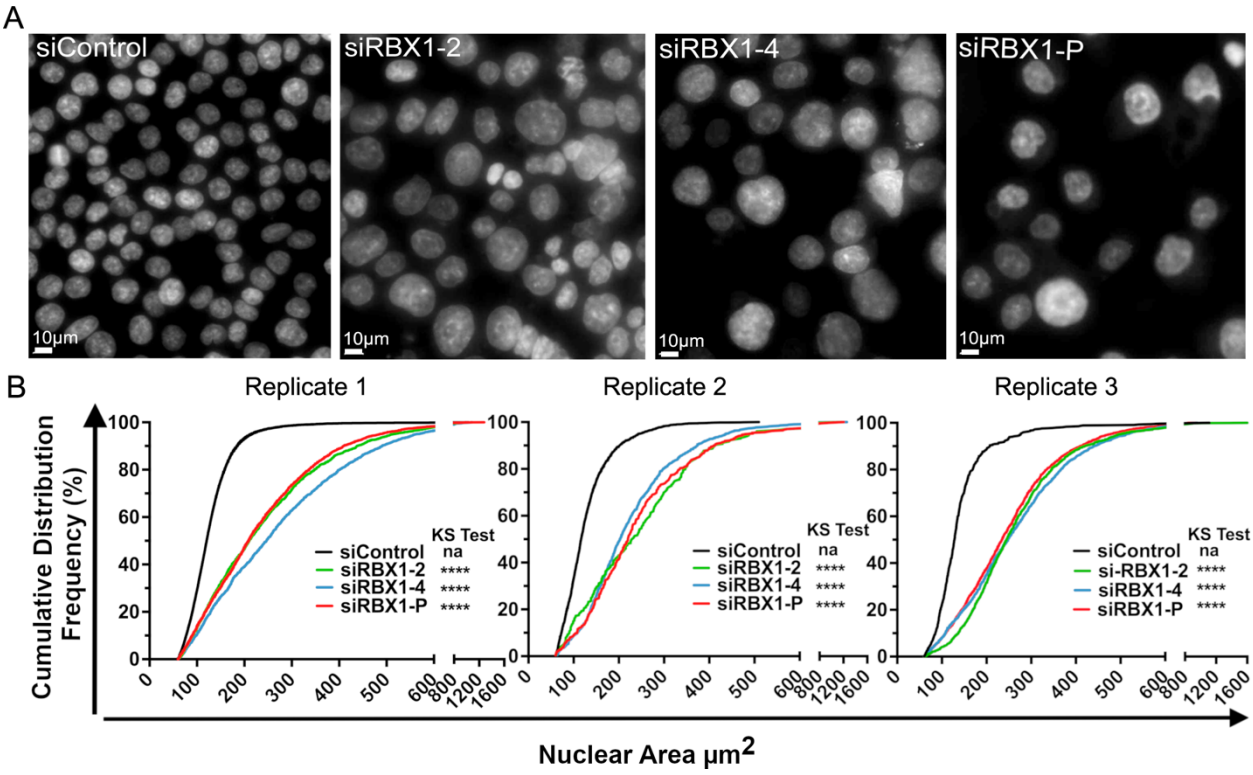

Figure 4-12. *RBX1* Silencing Underlies Significant Increases in Nuclear Areas in HCT116. ***(A)*** Low-resolution images of Hoechst-counterstained nuclei exhibiting visual increases in nuclear areas following *RBX1* silencing relative to siControl. ***(B)*** Cumulative nuclear area distribution frequency graphs from three biological replicates identify statistically significant increases in nuclear areas following *RBX1* silencing relative to siControl (two-sample KS test; na = not applicable; ****p-value < 0.0001; N = 3, n=6; >1000 nuclei imaged/silencing condition).

Subsequent micronucleus formation analyses revealed a lower frequency in micronucleus formation in HCT116 (***Figure 4-13A***), which ranged from ~3- to ~5% in the silenced conditions relative to siControl across all biological replicates (***Figure 4-13B***). More specifically, only 2 silenced conditions in replicates 1 (siRBX1-2 and siRBX1-P) and 3 (siRBX1-2 and siRBX1-4) displayed statistically significant increases in micronucleus formation frequency relative to siControl, while in Replicate 2 none of the silenced conditions were determined as statistically significant (MW test; p-value<0.05; ***Table S8***, page 77).

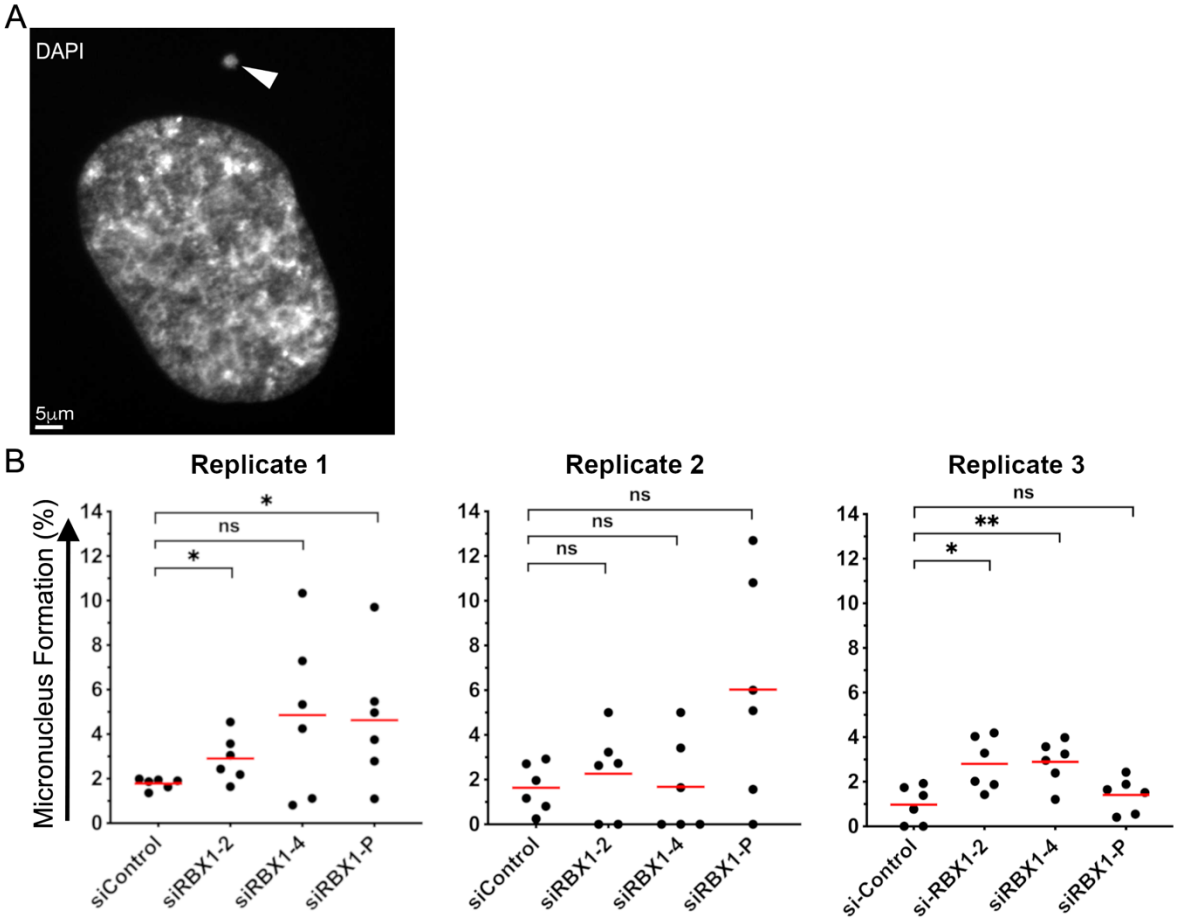

Figure 4-13. Reduced *RBX1* Expression is Associated with Significant Increases in Micronucleus Formation in HCT116
(A) Image of a Hoechst-counterstained nucleus with an associated micronucleus (arrowhead). **(*B*)** Dot plots reveal increases in the frequencies of micronuclei formation in replicates 1 and 3 following *RBX1* silencing. Statistically significant increases were observed in two replicates following *RBX1* silencing relative to siControl (Mann-Whitney [MW] test; ns = non-significant; * p-value < 0.05; ** p-value < 0.01). Red bars represent median values. (N = 3, n=6; >1000 nuclei imaged/silencing condition).

Chromosome enumeration analysis revealed a similar trend in a malignant context. Recall that HCT116 has a modal chromosome number of 45 and therefore, spreads with aberrant numbers were subcategorized (***Figure 4-14A***) as losses (<45 chromosomes), small-scale gains (46-54 chromosomes), and large-scale chromosome gains (≥55 chromosomes). Interestingly, losses were the most prevalent aberrant phenotype observed across all three biological replicates, followed by spreads with small and large number of chromosomes gains, respectively (***Figure 4-14B***). More specifically, replicate 1 had the largest increase in aberrant spreads (2.4- to 2.6-fold increase) relative to siControl, followed by Replicate 2 (2.0- to 2.2-fold increase) and Replicate 3 (1.8- to 2.2-fold increase). Silenced conditions (***Figure 4-14C***) revealed a 2.2- fold increase in aberrant chromosome numbers in siRBX1-2, while siRBX1-4 and siRBX1-P had 2.1-fold increases that were statistically significant (Student's t-test; p-value<0.05; ***Table S9***, page 78).

The data presented above demonstrate that reduced *RBX1* expression induced increases in nuclear areas, micronucleus formation and aberrant chromosome numbers in HCT116. Collectively, the above findings coupled with those observed in non-malignant 1CT and A1309 cells, demonstrate that *RBX1* silencing induces increase in the frequencies of CIN-associated phenotypes suggesting that *RBX1* is a novel CIN gene that may contribute to CRC pathogenesis.

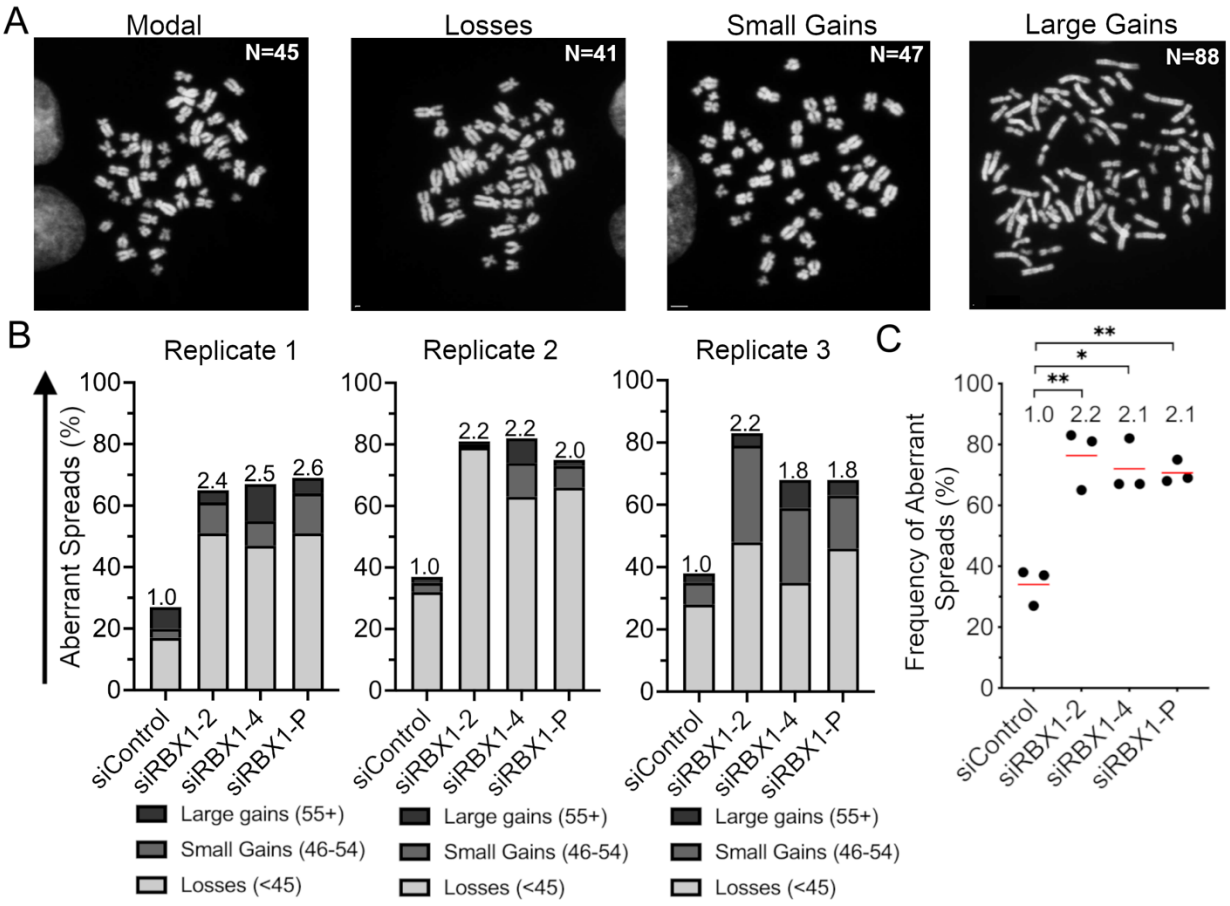

Figure 4-14. *RBX1* Silencing Underlies Increase in Aberrant Chromosome Numbers in HCT116.

(A) Mitotic chromosome spreads (DAPI-counterstained) depicting the modal number of 45 chromosomes, chromosome losses (<45 chromosomes), small scale chromosome gains (46-54 chromosomes) and large chromosome gains (≥55 chromosomes). **(*B*)** Bar graphs demonstrate the frequency of aberrant chromosome spreads after *RBX1* silencing. Each graph represents one biological replicate. Fold increases are indicated above each bar (N = 3; ≥100 spreads per condition). ***(C)*** Dot plot depicting significant increases in the frequencies of aberrant chromosome numbers after *RBX1* silencing in three replicates. Fold increases relative to siControl are displayed below statistical information (Student's t-test; N = 3, n ≥100 spreads/condition; * p-value < 0.05; ** p-value < 0.01). Red bars correspond to mean values.

CHAPTER 5. SUMMARY AND DISCUSSION

5.1. SUMMARY

To address the hypothesis and research aims of the present study, I employed siRNA-based gene silencing to assess the impact reduced *RBX1* expression has on CIN and the potential implications for early CRC development. Four individual siRNAs and one pooled siRNA were used to perform both research aims. In *Aim 1*, *RBX1* siRNA-based silencing resulted in overall reduction in RBX1 abundance in two distinct non-transformed/non-malignant karyotypically stable colonic epithelial cell lines (*i.e.* 1CT and A1309). In *Aim 2*, siRNA gene silencing also resulted in decreased *RBX1* expression and reduction of RBX1 levels in one transformed/malignant cell line (*i.e.* HCT116 cell line). Results from *Aim 1* demonstrate that reduced *RBX1* expression in 1CT and A1309 corresponded with statistically significant increases in CIN-associated phenotypes (*i.e.* nuclear areas, micronucleus formation and aberrant chromosome numbers). Similar results were observed in *Aim 2*, where diminished *RBX1* expression also resulted in statistically significant increases in nuclear areas, micronucleus formation and aberrant chromosome numbers in HCT116. Additionally, it has been observed a correlation between decreased *RBX1* expression and increased in Cyclin E1 abundance in all silenced conditions across both non-malignant and malignant colonic epithelial cell lines. Such increases are a strong indication of SCF complex on-target effects and elucidates potential mechanism by which reduction in RBX1 abundance may induce CIN. Thus, the data presented in this study identify *RBX1* as a novel CIN gene in non-malignant and malignant colonic epithelial cell lines, suggesting that reduced RBX1 abundance may be a mechanistic event that contribute to early CRC development.

5.2 DISCUSSION

5.2.1. *RBX1* Silencing Corresponds with Larger Increases in Nuclear Areas that may be Induced by Endoreduplication

CIN is the most prevalent genome instability phenotype in CRC, and it is defined by the increase of rate in which whole chromosomes or chromosome fragments are gain or lost, resulting in ongoing cell-to-cell heterogeneity[10, 11]. Accordingly, reduced *RBX1* expression is expected to result in gains or losses of chromosomes or chromosome complements, which would translate as increases or decreases in nuclear areas and chromosome numbers. In spite of that, *RBX1* induced silencing using siRNAs only corresponded to increases in nuclear areas when compared to siControl. Statistically significant increases in nuclear areas were observed in both non-malignant

(*i.e.* 1CT and A1309) and malignant (*i.e.* HCT116) cell lines, which were consistent across all biological replicates. Increases in nuclear areas are proposed to be a consequence of large-scale changes in DNA content; however, analyses of mitotic chromosome spreads determined that chromosome losses were the most frequent aberrant chromosome phenotype.

As demonstrated in the pilot siRNA-based screen (see *Section 1.3.1*), silencing of SCF complex core members and F-box proteins resulted in changes in nuclear areas that varied according to the silenced gene and corresponded mostly with increases in nuclear areas (including *RBX1* silencing); however, decreases in nuclear areas were also observed in some cases. Additionally, data from an *RBX1* silencing study in high-grade serous carcinoma (HGSC) using both siRNA and CRISPR-Cas9 also resulted in increases in nuclear areas in FT194 and FT246 cell lines[86], which are consistent with the findings of the present study and might be a result of polyploidy-related mechanisms. It has been established that large-scale chromosome gains (*i.e.* polyploidy) are well tolerated in nature as plants, animals and some types of human cells (*i.e.* megakaryocytes, hepatocytes and cardiomyocytes) and are able to have normal physiological function[133, 134]. Additionally, polyploidy can be observed in many different types of malignancies, including CRC, and it is proposed to participate in tumour initiation and treatment resistance[133, 135].

On the other hand, chromosome losses may reflect the loss of genes that are essential to regulate normal cellular processes. Studies using HeLa (cervical cancer) and T98G (glioblastoma) cell lines demonstrated that chromosome losses are less tolerated when compared to large-scale chromosome gains[136]. Thus, mitotic chromosome spreads containing less that 32 chromosomes were not identified in *RBX1* silenced cells on the present study. Therefore, large-scale gains of chromosomes are more likely to be tolerated by cells, which may partially explain the prevalence of increases (rather than decreases) in nuclear areas in CIN assays performed in *RBX1* silenced populations. Results from mitotic chromosome spreads enumeration performed in both non-malignant and malignant cell lines presented a high frequency of chromosome losses rather than large scale chromosome gains (*i.e.* $\geq$ 10 chromosomes). Discrepancies between increases in nuclear areas and prevalence of chromosome losses may be partially explained by limitations involving the assessment of asynchronous populations, distinct biological mechanisms and how CIN assays were performed. For instance, nuclear area analyses are performed on interphase cells (~95% of cells)[10], and automatically excludes mitotic cells as their nuclear envelop is not present, whereas to generate mitotic chromosome spreads, cells are submitted to a relatively short period

of Colcemid treatment to arrest cells that are undergoing mitosis. Thus, as cell populations are asynchronous, only cells capable of entering and remaining in mitosis are assessed (~5% cells)[10].

Increases in nuclear areas may also be a result of cells undergoing endoreduplication, when cells fail to enter mitosis and undergo additional rounds of DNA duplication[85]. Thus, cells undergoing endoreduplication may be better represented on the assays that assess nuclear areas rather than the analysis of mitotic chromosome spreads. Previous studies showed evidence that silencing of SCF complex members (*e.g., SKP1*, *SKP2* and *EMI1*) corresponded with increases in endoreduplication events in CRC context[10, 85, 99]. Accordingly, ~33% of large-scale chromosome gains observed upon *EMI1* silencing demonstrated evidence of endoreduplication[85], while ~50% - 90% of *SKP2* large-scale chromosome gains displayed a similar phenotype in colonic epithelial cell lines[10]. Therefore, increases in nuclear areas in *RBX1* silenced conditions may also be a result of endoreduplication.

Lastly, studies reveal an association between endoreduplication, and genomic amplification and ectopic overexpression of the *CCNE1*[10, 137]. Recall that decreased RBX1 abundance is associated with increases in Cyclin E1 levels in both non-malignant and malignant cell lines. Cyclin E1 is an oncoprotein and known target of the SCF complex and participates in DNA replication and genome stability and coordinates the G1 to S-phase transition in the cell cycle[10, 137]. Thus, increases in Cyclin E1 abundance are predicted to phenocopy genomic amplification and may induce endoreduplication. Interestingly, silencing of SCF complex core members in CRC and HGSC corresponded with increases in Cyclin E1 levels and endoreduplication[86, 99].

Collectively, data presented in this thesis support the hypothesis that decreased *RBX1* expression may play a role in CIN in CRC through mechanisms linked to endoreduplication. Additionally, CIN is a dynamic phenotype and differences between nuclear areas and mitotic chromosome spreads highlights the importance of distinct and complementary approaches to evaluate phenotypes associated with this genome instability markers.

5.2.2. *RBX1* Silencing Corresponds with Variable CIN Phenotypes in Non-Malignant and Malignant Colonic Epithelial Cell Lines

According to the data presented in this study, *RBX1* was identified as a novel CIN gene in both non-malignant and malignant colonic epithelial cell lines. However, differences in the occurrence and frequence of CIN phenotypes were observed between silenced conditions, biological replicates and across distinct colonic epithelial contexts, which may be a result of limitations regarding the techniques employed and distinct genetic profiles among the cell lines. It is also relevant to highlight that variations in phenotypes are a consequence of the chromosome dynamics that arise from CIN. Although semi-quantitative analyses revealed consistent *RBX1* silencing between distinct silencing conditions in all cell lines (< 6% of RBX1 abundance in the silenced condition relative to control), siRNA based silenced experiments revealed distinct CIN phenotypes.

While statistically significant results were observed for all three CIN phenotypes assessed in *RBX1* silenced conditions relative to siControl in both non-malignant and malignant cell lines (see *Section 4*), micronucleus formation analysis displayed distinct frequencies across all silenced conditions and replicates. More specifically, variations within non-malignant cell lines were observed, as the frequency of micronucleus formation in 1CT (~2% - 4%, ***Table S2***, page 73) was lower when compared to the A1309 cell line (~3% - 10%, ***Table S5***, page 75). Such discrepancies may arise from variabilities in siRNA transfection efficiency and RBX1 abundance, as variations in silencing efficiency are expected between cells within the same population and across distinct biological replicates. Additionally, semi-quantitative analysis of proteins from bulk populations fail to determine differences in RBX1 abundance between individual cells; therefore, differences in *RBX1* silencing and RBX1 abundance between cells could partially explain the variations observed in micronucleus formation assays.

Underlying mutations present in the cell lines (see ***Table 3-1***, page 20) may also impose a synergistic effect along with decreased *RBX1* expression, which may also result in differences in the frequency of micronucleus formation among colonic epithelial cell lines. For instance, 1CT exhibit wild type *KRAS*, *TP53* and *APC*, while A1309 (a cell line derivative of 1CT) exhibit mutation in the *KRAS* gene, as well as ~50% knockdown of *TP53* and truncated expression of *APC*[54]. Accordingly, previous studies[138, 139] revealed that expression of *KRAS* mutations may be linked to the onset of lagging chromosomes and contribute to defects in chromosome segregation and increase in the frequency of micronuclei in A1309. Additionally, *APC* mutation is linked not only to polyp formation in the colon but also plays an important role in microtubule stabilization

and normal chromosome segregation activity[140]. Therefore, the presence of truncated APC may play a role in the high levels of micronucleus formation observed in the silenced conditions in the A1309 cell line when compared to siControl. The *TP53* mutation in A1309 may also contribute to this phenotype, as the gene is involved in repairing double-strand DNA breaks and triggering apoptosis in response to DNA damage[141].

Regarding the malignant context, the frequency of micronucleus formation in HCT116 ranged from ~1% to 6% (***Table S8***, page 77); however, it was not determined as statistically significant in all biological replicates. Recall that HCT116 (see ***Table 3-1***, page 20) also expresses mutant *KRA*S and exhibit microsatellite instability (*MLH1* mutation); thus, mutant *KRAS* and the combination of two distinct genome instability phenotypes (microsatellite instability and CIN) may promote extreme levels of DNA damage, leading to decreased fitness and survival, and increased levels of apoptosis in those populations, which might explain the variations observed in micronucleus formation events in HCT116 cells when compared to non-malignant cell contexts.

Although decreased *RBX1* expression coupled with underlying mutations described in non-malignant and malignant cell lines alone do not contribute to increases in nuclear areas, micronucleus formation and aberrant chromosome numbers, the collective data presented in the literature and in this study suggest that they are strongly associated with the onset of dynamic CIN-associated phenotypes and the variations observed in the assays employed.

5.2.3. *RBX1* Silencing may Induce CIN-associated Phenotypes through Aberrant Increases in Cyclin E1

Data presented in this thesis revealed that *RBX1* silencing results in statistically significant increases in CIN phenotypes (*i.e.* nuclear areas, micronucleus formation and aberrant chromosome numbers) in colonic epithelial cell lines. A possible mechanism that could partially explain increases in CIN is Cyclin E1 accumulation, which phenocopies genomic amplification and may contribute to pathogenesis in many cancer types, including CRC[86, 100, 142, 143]. As previously described, decreased *RBX1* expression corresponded with increases in Cyclin E1 accumulation in both non-malignant and malignant cell lines. Although *RBX1* silencing resulted in Cyclin E1 accumulation in distinct cell lines, Cyclin E1 levels varied within distinct silencing conditions and cell lines. As a critical regulator of the cell cycle, this protein coordinates the G1 to S-phase transition[10, 137]. However, as it is cell cycle dependent, the prevalence of cell cultures with asynchronous populations may explain the variation in protein expression levels. Interestingly,

HCT116 displayed striking levels of Cyclin E1 accumulation (~1801%, Figure 4-11) when compared to the non-malignant cell lines (~534% in 1CT and ~223% in A1309, Figure 4-4). A possible explanation for such high increases in HCT116 may be associated with its genetic profile. Recall the HCT116 is a malignant colonic epithelial cell line that has a mutation in the *MLH1* gene (see *Table 3-1)*; thus, a possible synergistic mechanism may exist where inducing CIN in a malignant cell line with underlying genome instability mutation corresponds with high Cyclin E1 levels. Furthermore, increases in nuclear areas followed by silencing of SCF complex members in HGSC and CRC studies also corresponded with increases in Cyclin E1 levels and endoreduplication events[86, 99]. Additionally, others have shown that *CCNE1* overexpression results in genomic instability and was associated with replication stress, chromosome segregation defects, aneuploidy, defects in mitotic spindle and centrosome amplification in mice and human cells[144-147]. Thus, increases in Cyclin E1 levels in *RBX1* depleted colonic epithelial cell lines is not only an indication of impaired SCF complex function, but also a mechanism that may strongly contributes to CIN and the increases observed in CIN-associated phenotypes in CRC. To validate whether or not increased Cyclin E1 abundance plays a role in CIN, previous studies performed phenotypic rescue experiments[99]. Accordingly, CIN-associated phenotypes were assessed upon silencing of SCF complex members alone and also co-silenced with *CCNE1*. Results revealed that *CCNE1* co-silencing rescued ~50% of the aberrant CIN phenotypes when compared to silencing of an SCF complex member alone[99], which supports the possibility that Cyclin E1 accumulation is a contributing mechanisms underlying CIN in CRC and HGSC[86, 99]. It is important to highlight that the SCF complex is responsible to polyubiquitinate hundreds of protein substrates (see *Section 1.3*) whose misregulation and accumulation may also contribute to CIN and CRC pathogenesis[94].

In conclusion, the present thesis identifies *RBX1* as a novel CIN gene in both non-malignant and malignant colonic epithelial cell lines, providing new insights into how decreased *RBX1* expression impacts CIN and may contribute to early events associated with CRC development. However, future studies are required to obtain mechanistic insight into how decreased *RBX1* expression may impact cellular transformation phenotypes and how this genetic alteration may be exploited in the development of novel therapeutic strategies.

CHAPTER 6. FUTURE DIRECTIONS, CONCLUSIONS AND SIGNIFICANCE

6.1. FUTURE DIRECTIONS

The results of the present study identified *RBX1* as a novel CIN gene in CRC, as its reduced expression corresponded with increases in CIN associated phenotypes (*i.e.* increases in nuclear areas, micronucleus formation and increases in aberrant chromosome numbers) in karyotypically stable non-malignant and malignant colonic epithelial cell models. Moving forward, studies aimed at determining the long-term impact reduced *RBX1* expression has on CIN using clinically relevant models (*i.e.* *RBX1*$^{+/-}$ clones) are essential to assess the ongoing chromosome alterations that arise from CIN as well as how they impact CIN associated phenotypes and cellular transformation in CRC context. Lastly, as previously stated, ~34% of patients with CRC harbor *RBX1* shallow deletions[124, 128, 129]; therefore, understanding the molecular mechanisms giving rise to CIN may offer new perspectives into the development of novel therapeutic strategies that would potentially improve the lives of patients that exhibit *RBX1* shallow deletions.

6.1.1. Determining the Long-term Impact Reduced *RBX1* Expression has on CIN Using *RBX1*$^{+/-}$ Clones

According to publicly available TCGA data[124] accessed through cBioPortal (see *Section 4.1*), reduced *RBX1* expression is a clinically relevant phenomenon as ~34% of CRC patients harbour heterozygous loss, while only 3% of the cases correspond with gains in *RBX1* copy numbers[124, 128, 129]. Although transient siRNA-based silencing induced increases in CIN phenotypes in distinct colonic epithelial cell lines, CIN is a dynamic event that drives ongoing karyotypic heterogeneity[11, 85, 86]. Therefore, the use of *RBX1*$^{+/-}$ clones to perform long-term assays would provide novel understanding regarding CRC patients with a similar genetic profile. Accordingly, the McManus laboratory developed a research pipeline using a two-step CRISPR-Cas9 to generate heterozygote clones in colonic epithelial cell lines. CRISPR-Cas9 is a gene-editing technology that employs the use of guide RNAs and the Cas9 endonuclease[11, 85, 86]. Briefly, cells are transduced with lentiviral particles that contain guide RNAs targeting the gene of interest or a non-targeting guide RNA control, which are designed to co-express blue fluorescent protein (BFP)[11, 85, 86]. Cells that are BFP+ are isolated using fluorescence-activated cell sorting (FACS) and are subsequently transfected with a plasmid that co-expresses Cas9 and green fluorescent protein (GFP). Transfected cells are subjected to FACS, whereby BFP+/GFP+ cells are isolated and clonally expanded[11, 85, 86]. Semi-quantitative western blot can be used to evaluate the protein expression profiles of the clones and compared to a non-targeting control population. Potential *RBX1*$^{+/-}$ clones are identified and validated using PCR and

DNA sequencing, which can then be used in long-term CIN assays[11, 85, 86]. At least two distinct *RBX1*$^{+/-}$ clone populations and a non-targeting control would be selected to properly assess the ongoing dynamic changes that arise from *RBX1* heterozygote loss. Briefly, CIN phenotypes (*i.e.* nuclear area changes, micronucleus formation and aberrant chromosome numbers) would be assessed every two weeks (every four passages) for a total of ~2.5 months. Ultimately, long-term CIN assays would be used to provide novel insights into the molecular mechanisms that underly the ongoing chromosome alterations related to CIN in CRC pathogenesis.

6.1.2. Evaluating Cellular Transformation Phenotypes Using *RBX1*$^{+/-}$ Clones

Cellular transformation events represent biological processes that precede tumour initiation, progression and metastasis. It is a multistep process in which normal somatic cells acquire cancer-like genotypic and phenotypic alterations that enable changes in cellular growth, proliferation and metastasis[148, 149]. Colonic epithelial cell lines harboring *RBX1* heterozygote loss would also represent a relevant model to perform cellular transformation experiments, as they mimic the clinical status of ~34% of CRC patients[124, 128, 129]. Therefore, to evaluate cellular transformation phenotypes, experiments that investigate cell proliferation, contact inhibition, and 3D colony formation mechanisms in early (p0) and late passage (p20) cells would be highly beneficial[85]. Aberrant rates in cell proliferation constitute one of the known hallmarks of cancer, where cells exhibit high rates of growth and division[149]. Accordingly, following research pipelines for proliferation assays, *RBX1*$^{+/-}$ clones and a NT-Control would be seeded based on pre-determined cell densities and monitored overtime. For instance, assays such as CellTiter-Glo can determine the number of viable cells based on the levels of adenosine triphosphate (ATP), while Real-Time Cell Analysis (RTCA) uses non-invasive microelectronic sensors that monitor cell-proliferation in real-time. Non-targeting controls are seeded for both assays, which are based on pre-defined densities, and results are used to calculate and compare the correspondent proliferation rates[86, 150]. Contact inhibition experiments also play an important role for the evaluation of cellular transformation characteristics. These assays are based on regulatory mechanisms where non-transformed cells stop migrating and do not proliferate upon contact with surrounding cells, which can also be monitored by RTCA analysis[86, 151]. Lastly, 3D colony formation assays are also a valuable tool in cancer research which evaluates the anchorage-independent growth of cells. This assay relies on the ability transformed cells have to grow regardless of being on a solid surface[152]. To perform this experiment, cell culture plates receive a bottom layer of agarose diluted in cell media. Distinct *RBX1*$^{+/-}$ clonal isolates (*i.e.* p0 and p20) and a NT-Control (*i.e.* HCT116 cells) are seeded individually

on a second layer of agarose containing cell media and cell suspension with pre-determined seeding densities. Following that, plates receive a third layer of only cell media, which is regularly refreshed on a weekly basis for a total of four weeks[10, 152]. After that period, cells are fixed with PFA and stained with crystal violet prior to their assessment. Ideally, using *RBX1*$^{+/-}$ clones to perform cell proliferation, contact inhibition, and colony formation assays would provide novel insights into how decreased *RBX1* expression impacts cellular transformation phenotypes.

6.1.3. Exploiting Reduced *RBX1* Expression in Novel Diagnostic and Therapeutic Strategies

As presented in **Figure 4-1A** (see *Section 4*), *RBX1* heterozygote loss is present in several solid cancer types. Genome instability data revealed that CRC patients with *RBX1* copy number losses were associated with decreased mRNA expression and worse survival outcomes[124, 128, 129], suggesting that reduced *RBX1* expression may be implicated with early CRC development, cell survival advantages, and multi-drug resistance. As a novel treatment alternative, synthetic lethality (SL) represents a breakthrough in cancer therapy. Previous studies using *Drosophila melanogaster* and yeast model systems led to the discovery of synthetic lethal interactions, when cellular or organism lethality is caused by the combination of two distinct and viable gene mutations in a single cell[84]. More specifically, two genes are considered synthetic lethal when the deletion of either gene alone is viable, but the deletion of both genes leads to cell death[153]. For instance, *BRCA1/BRCA2* are tumour suppressor genes that are normally required to maintain genome stability as they play key roles in DNA homologous recombination repair (HR)[84, 153, 154]. SL interactors often share similar biological mechanisms; thus, only one functional *BRCA1/2* copy can still provide a compensatory HR function[84, 153, 154]. However, cancers harboring *BRCA1/2* mutations are forced to rely on PARP1 [poly (ADP-ribose) polymerase-1]-dependent repair mechanisms. PARP1 is an abundant nuclear protein whose expression is activated as a response to DNA breaks, leading to the recruitment of several DNA repair proteins. As one of the most relevant SL models, PARP inhibitors (*i.e.* Olaparib and Niraparib) are used to exploit breast and ovarian cancers harboring *BRCA1/2* mutations[155]. They represent a class of drugs that pharmacologically inhibits PARP enzymatic activity, preventing cells from repairing damaged DNA, which ultimately leads to reduction in cell growth and eventual cell death[84, 153, 154]. Accordingly, to provide new insights into SL mechanism targeting cells with decreased *RBX1* expression, *RBX1*$^{+/-}$ clones would also represent a relevant heterozygous model that could be used for the identification of novel SL drug interactions that selectively target and induce apoptosis. A recent study performed by the McManus laboratory identified and characterized a novel SL interaction between a CIN gene in CRC (*FBX07*) and *CHEK1*[156]. Accordingly, inhibition of *CHEK1* (either by siRNA or pharmacological

interaction) in human colonic epithelial cell lines that are FBX07-deficient resulted in an increase in DNA double-strand break and apoptosis, which are indicated by increases in γ-H2AX foci formation and cleaved caspase-3 signals[156]. Additionally, proteolysis targeting chimeras (PROTACs) represent an emerging cancer therapeutic strategy that in essence can virtually target any protein. PROTACs is a hetero-bifunctional molecule that works by selectively polyubiquitinating specific proteins for proteolytic degradation[157, 158]. Thus, *RBX1*$^{+/-}$ clones could also be employed on PROTAC assays that selectively target the accumulation of oncoproteins (*i.e.* Cyclin E1) resulting from decreased *RBX1* expression and SCF complex disfunction[86]. Therefore, the development of novel SL and PROTAC studies that specifically exploit *RBX1* heterozygous loss and associated mechanisms would ultimately improve the poor prognosis and increased mortality rates associated not only with CRC but also additional tumours harboring *RBX1* deficiency.

6.2. CONCLUSION AND SIGNIFICANCE

The collective data presented in this thesis along with the current literature provided new insights into the molecular mechanisms that drive CIN and offered a novel perspective of how reduced *RBX1* expression induces CIN and its potential impact on early CRC development. Thus, results presented on this research have identified *RBX1* as a novel CIN gene in both non-malignant and malignant colonic epithelial cell lines, as decreased *RBX1* expression corresponds with statistically significant increases in cell-to-cell heterogeneity, nuclear areas, micronucleus formation and aberrant chromosome numbers. These data also support that *RBX1* plays an important role on genome stability, cell cycle progression and CRC development. Recall that in 2025 ~ 26,400 patients were diagnosed with CRC in Canada and ~9,100 deaths were observed in that year[3]; thus, further investigation is necessary to gain novel perspective into additional underlying mechanisms associated with early CRC development and aberrant expression of *RBX1* and additional SCF complex members. Therefore, advancing the understanding into the etiological mechanisms that drive CIN and tumour development is critical for the development of novel therapeutic strategies that will eventually impact the lives of patients with *RBX1* copy number losses in cancers that harbor a similar genetic profile.

REFERENCES

1. Bray F, Laversanne M, Sung H, Ferlay J, Siegel RL, Soerjomataram I, et al. Global cancer statistics 2022: GLOBOCAN estimates of incidence and mortality worldwide for 36 cancers in 185 countries. CA Cancer J Clin. 2024;74(3):229-63.
2. Wu S, Zhang Y, Lin Z, Wei M. Global burden of colorectal cancer in 2022 and projections to 2050: incidence and mortality estimates from GLOBOCAN. BMC Cancer. 2025;25(1):1770.
3. Committee CCSA. Canadian Cancer Statistics 2025. Canadian Cancer Statistics Advisory Committee. 2025.
4. Commitee CCSA. Canadian Cancer Statistics 2019 [Available from: cancer.ca/Canadian-Cancer-Statistics-2019-EN.
5. Hahn MM, de Voer RM, Hoogerbrugge N, Ligtenberg MJ, Kuiper RP, van Kessel AG. The genetic heterogeneity of colorectal cancer predisposition - guidelines for gene discovery. Cell Oncol (Dordr). 2016;39(6):491-510.
6. Asghari-Jafarabadi M, Wilkins S, Plazzer JP, Yap R, McMurrick PJ. Prognostic factors and survival disparities in right-sided versus left-sided colon cancer. Scientific Reports. 2024;14(1):12306.
7. Baran B, Mert Ozupek N, Yerli Tetik N, Acar E, Bekcioglu O, Baskin Y. Difference Between Left-Sided and Right-Sided Colorectal Cancer: A Focused Review of Literature. Gastroenterology Res. 2018;11(4):264-73.
8. Toews KP, Auld FM, Moyana TN. Embryonic Signaling Pathways Shape Colorectal Cancer Subtypes: Linking Gut Development to Tumor Biology. Pathophysiology. 2025;32(4):52.
9. Ahmed S, Kaur H, Diab MO, Nadir A. Diagnostic Challenges in Sessile Serrated Lesions: Progression to Adenocarcinoma in a High-Risk Patient. Am J Case Rep. 2025;26:e950179.
10. Neudorf NM, Thompson LL, Lichtensztejn Z, Razi T, McManus KJ. Reduced SKP2 Expression Adversely Impacts Genome Stability and Promotes Cellular Transformation in Colonic Epithelial Cells. Cells. 2022;11(23).
11. Geigl JB, Obenauf AC, Schwarzbraun T, Speicher MR. Defining 'chromosomal instability'. Trends in Genetics. 2008;24(2):64-9.
12. Fearon ER, Vogelstein B. A genetic model for colorectal tumorigenesis. Cell. 1990;61(5):759-67.
13. Kuipers EJ, Grady WM, Lieberman D, Seufferlein T, Sung JJ, Boelens PG, et al. Colorectal cancer. Nat Rev Dis Primers. 2015;1:15065.
14. Campos Gudiño R, McManus KJ, Hombach-Klonisch S. Aberrant HMGA2 Expression Sustains Genome Instability That Promotes Metastasis and Therapeutic Resistance in Colorectal Cancer. Cancers (Basel). 2023;15(6).
15. Lewandowska A, Rudzki G, Lewandowski T, Stryjkowska-Góra A, Rudzki S. Risk Factors for the Diagnosis of Colorectal Cancer. Cancer Control. 2022;29:10732748211056692.
16. Mangas-Sanjuan C, Jover R. Familial colorectal cancer. Best Practice & Research Clinical Gastroenterology. 2022;58-59:101798.
17. Binefa G, Rodríguez-Moranta F, Teule A, Medina-Hayas M. Colorectal cancer: from prevention to personalized medicine. World J Gastroenterol. 2014;20(22):6786-808.
18. Goosenberg E KA, Babiker HM. A Review of Hereditary Colorectal Cancers. Treasure Island (FL): StatPearls Publishin. 2025.
19. Syngal S, Brand RE, Church JM, Giardiello FM, Hampel HL, Burt RW. ACG clinical guideline: Genetic testing and management of hereditary gastrointestinal cancer syndromes. Am J Gastroenterol. 2015;110(2):223-62; quiz 63.

20. Munemitsu S, Albert I, Souza B, Rubinfeld B, Polakis P. Regulation of intracellular beta-catenin levels by the adenomatous polyposis coli (APC) tumor-suppressor protein. Proc Natl Acad Sci U S A. 1995;92(7):3046-50.
21. Disoma C, Zhou Y, Li S, Peng J, Xia Z. Wnt/β-catenin signaling in colorectal cancer: Is therapeutic targeting even possible? Biochimie. 2022;195:39-53.
22. Ionescu VA, Gheorghe G, Bacalbasa N, Chiotoroiu AL, Diaconu C. Colorectal Cancer: From Risk Factors to Oncogenesis. Medicina. 2023;59(9):1646.
23. Sung H, Siegel RL, Laversanne M, Jiang C, Morgan E, Zahwe M, et al. Colorectal cancer incidence trends in younger versus older adults: an analysis of population-based cancer registry data. The Lancet Oncology. 2025;26(1):51-63.
24. Durko L, Malecka-Panas E. Lifestyle Modifications and Colorectal Cancer. Curr Colorectal Cancer Rep. 2014;10(1):45-54.
25. Ungvari Z, Fekete M, Varga P, Lehoczki A, Fekete JT, Ungvari A, et al. Overweight and obesity significantly increase colorectal cancer risk: a meta-analysis of 66 studies revealing a 25-57% elevation in risk. Geroscience. 2025;47(3):3343-64.
26. Institute NC. Alcohol and Cancer Risk. NCI. 2025.
27. Canada S. Cancer in Canada: Stage at diagnosis Health Reports. December 2018;29:21-5.
28. Prevention CfDCa. U.S. Cancer Statistics Colorectal Cancer Stat Bite. US Department of Health and Human Services. 2025.
29. Agrawal N, Lanjhiyana SK, Jaiswal M, Siddiqui MA, Gupta S. Colorectal cancer spectrum: From subtypes and epidemiology to oncotherapies. Gastroenterology & Endoscopy. 2025;3(2):55-64.
30. Dantas AAG, de Oliveira NPD, Costa GAB, Martins LFL, dos Santos JEM, Migowski A, et al. Multilevel analysis of social determinants of advanced stage colorectal cancer diagnosis. Scientific Reports. 2024;14(1):9667.
31. Shaukat A, Levin TR. Current and future colorectal cancer screening strategies. Nat Rev Gastroenterol Hepatol. 2022;19(8):521-31.
32. Canadian Cancer Society. How a stool test can help find colorectal cancer. CCS. 2026.
33. Gupta S. Screening for Colorectal Cancer. Hematol Oncol Clin North Am. 2022;36(3):393-414.
34. Shapiro JA, Soman AV, Berkowitz Z, Fedewa SA, Sabatino SA, de Moor JS, et al. Screening for Colorectal Cancer in the United States: Correlates and Time Trends by Type of Test. Cancer Epidemiol Biomarkers Prev. 2021;30(8):1554-65.
35. Society CC. When should I be screened for colorectal cancer? CCS. 2026.
36. team TACSmaec. American Cancer Society Guideline for Colorectal Cancer Screening. 2024.
37. Yang Y, Wang Y, Wang Z. Construction of a new clinical staging system for colorectal cancer based on the lymph node ratio: A validation study. Front Surg. 2022;9:929576.
38. AJCC. American Joint Committee on Cancer. Chapter 20 - Colon and Rectum. Springer. 2017.
39. Rosen RD SA. TNM Classification. StatPearls Publishing. 2025.
40. Singh H, Nugent Z, Demers AA, Kliewer EV, Mahmud SM, Bernstein CN. The Reduction in Colorectal Cancer Mortality After Colonoscopy Varies by Site of the Cancer. Gastroenterology. 2010;139(4):1128-37.
41. Canadian Cancer Society. Treatments for colon cancer. CCS. 2026.
42. Pathak PS, Chan G, Deming DA, Chee CE. State-of-the-Art Management of Colorectal Cancer: Treatment Advances and Innovation. American Society of Clinical Oncology Educational Book. 2024;44(3):e438466.
43. Canada CC. Understandinc Colorectal Cancer. CCC. Jan 2026.

44. Wu DM, Wang YJ, Fan SH, Zhuang J, Zhang ZF, Shan Q, et al. Network meta-analysis of the efficacy of first-line chemotherapy regimens in patients with advanced colorectal cancer. Oncotarget. 2017;8(59):100668-77.
45. Edwards MS, Chadda SD, Zhao Z, Barber BL, Sykes DP. A systematic review of treatment guidelines for metastatic colorectal cancer. Colorectal Dis. 2012;14(2):e31-47.
46. Casale J PPF. Fluorouracil. StatPearls Publishing. 2024.
47. Mohelnikova-Duchonova B, Melichar B, Soucek P. FOLFOX/FOLFIRI pharmacogenetics: the call for a personalized approach in colorectal cancer therapy. World J Gastroenterol. 2014;20(30):10316-30.
48. Neugut AI, Lin A, Raab GT, Hillyer GC, Keller D, O'Neil DS, et al. FOLFOX and FOLFIRI Use in Stage IV Colon Cancer: Analysis of SEER-Medicare Data. Clin Colorectal Cancer. 2019;18(2):133-40.
49. team TACSmaec. Targeted Therapy Drugs for Colorectal Cancer. ACS. Jan 2025.
50. Xie Y-H, Chen Y-X, Fang J-Y. Comprehensive review of targeted therapy for colorectal cancer. Signal Transduction and Targeted Therapy. 2020;5(1):22.
51. Mulet-Margalef N, Linares J, Badia-Ramentol J, Jimeno M, Sanz Monte C, Manzano Mozo JL, et al. Challenges and Therapeutic Opportunities in the dMMR/MSI-H Colorectal Cancer Landscape. Cancers. 2023;15(4):1022.
52. Jungwirth J, Urbanova M, Boot A, Hosek P, Bendova P, Siskova A, et al. Mutational analysis of driver genes defines the colorectal adenoma: in situ carcinoma transition. Scientific Reports. 2022;12(1):2570.
53. Cho KR, Vogelstein B. Genetic alterations in the adenoma--carcinoma sequence. Cancer. 1992;70(6 Suppl):1727-31.
54. Zhang L, Kim S, Jia G, Buhmeida A, Dallol A, Wright WE, et al. Exome Sequencing of Normal and Isogenic Transformed Human Colonic Epithelial Cells (HCECs) Reveals Novel Genes Potentially Involved in the Early Stages of Colorectal Tumorigenesis. BMC Genomics. 2015;16 Suppl 1(Suppl 1):S8.
55. De Palma FDE, D'Argenio V, Pol J, Kroemer G, Maiuri MC, Salvatore F. The Molecular Hallmarks of the Serrated Pathway in Colorectal Cancer. Cancers. 2019;11(7):1017.
56. Choi J, Park SY, Costantini F, Jho E-h, Joo C-K. Adenomatous Polyposis Coli Is Down-regulated by the Ubiquitin-Proteasome Pathway in a Process Facilitated by Axin*. Journal of Biological Chemistry. 2004;279(47):49188-98.
57. Saeed H, Leibowitz BJ, Zhang L, Yu J. Targeting Myc-driven stress addiction in colorectal cancer. Drug Resistance Updates. 2023;69:100963.
58. Hankey W, Frankel WL, Groden J. Functions of the APC tumor suppressor protein dependent and independent of canonical WNT signaling: implications for therapeutic targeting. Cancer Metastasis Rev. 2018;37(1):159-72.
59. Zhang L, Theodoropoulos PC, Eskiocak U, Wang W, Moon Y-A, Posner B, et al. Selective targeting of mutant adenomatous polyposis coli (APC) in colorectal cancer. Science Translational Medicine. 2016;8(361):361ra140-361ra140.
60. Strickler JH, Yoshino T, Stevinson K, Eichinger CS, Giannopoulou C, Rehn M, et al. Prevalence of KRAS G12C Mutation and Co-mutations and Associated Clinical Outcomes in Patients With Colorectal Cancer: A Systematic Literature Review. The Oncologist. 2023;28(11):e981-e94.
61. Woodford-Richens KL, Rowan AJ, Gorman P, Halford S, Bicknell DC, Wasan HS, et al. SMAD4 mutations in colorectal cancer probably occur before chromosomal instability, but after divergence of the microsatellite instability pathway. Proc Natl Acad Sci U S A. 2001;98(17):9719-23.

62. Zhao M, Mishra L, Deng CX. The role of TGF-β/SMAD4 signaling in cancer. Int J Biol Sci. 2018;14(2):111-23.
63. Aubrey BJ, Strasser A, Kelly GL. Tumor-Suppressor Functions of the TP53 Pathway. Cold Spring Harb Perspect Med. 2016;6(5).
64. Baker SJ, Fearon ER, Nigro JM, Hamilton SR, Preisinger AC, Jessup JM, et al. Chromosome 17 Deletions and p53 Gene Mutations in Colorectal Carcinomas. Science. 1989;244(4901):217-21.
65. Pikor L, Thu K, Vucic E, Lam W. The detection and implication of genome instability in cancer. Cancer Metastasis Rev. 2013;32(3-4):341-52.
66. Juo YY, Johnston FM, Zhang DY, Juo HH, Wang H, Pappou EP, et al. Prognostic value of CpG island methylator phenotype among colorectal cancer patients: a systematic review and meta-analysis. Ann Oncol. 2014;25(12):2314-27.
67. Toyota M, Ahuja N, Ohe-Toyota M, Herman JG, Baylin SB, Issa JP. CpG island methylator phenotype in colorectal cancer. Proc Natl Acad Sci U S A. 1999;96(15):8681-6.
68. Cisyk AL, Nugent Z, Wightman RH, Singh H, McManus KJ. Characterizing Microsatellite Instability and Chromosome Instability in Interval Colorectal Cancers. Neoplasia. 2018;20(9):943-50.
69. Trautmann K, Terdiman JP, French AJ, Roydasgupta R, Sein N, Kakar S, et al. Chromosomal instability in microsatellite-unstable and stable colon cancer. Clin Cancer Res. 2006;12(21):6379-85.
70. Lepage CC, Morden CR, Palmer MCL, Nachtigal MW, McManus KJ. Detecting Chromosome Instability in Cancer: Approaches to Resolve Cell-to-Cell Heterogeneity. Cancers (Basel). 2019;11(2).
71. Orr B, Compton DA. A double-edged sword: how oncogenes and tumor suppressor genes can contribute to chromosomal instability. Front Oncol. 2013;3:164.
72. Papaccio F, Cabeza-Segura M, García-Micó B, Gimeno-Valiente F, Zúñiga-Trejos S, Gambardella V, et al. Decoding chromosomal instability insights in CRC by integrating omics and patient-derived organoids. J Exp Clin Cancer Res. 2025;44(1):77.
73. Siri SO, Martino J, Gottifredi V. Structural Chromosome Instability: Types, Origins, Consequences, and Therapeutic Opportunities. Cancers (Basel). 2021;13(12).
74. Heng J, Heng HH. Two-phased evolution: Genome chaos-mediated information creation and maintenance. Progress in Biophysics and Molecular Biology. 2021;165:29-42.
75. Ganem NJ, Godinho SA, Pellman D. A mechanism linking extra centrosomes to chromosomal instability. Nature. 2009;460(7252):278-82.
76. Barber TD, McManus K, Yuen KW, Reis M, Parmigiani G, Shen D, et al. Chromatid cohesion defects may underlie chromosome instability in human colorectal cancers. Proc Natl Acad Sci U S A. 2008;105(9):3443-8.
77. Fujiwara T, Bandi M, Nitta M, Ivanova EV, Bronson RT, Pellman D. Cytokinesis failure generating tetraploids promotes tumorigenesis in p53-null cells. Nature. 2005;437(7061):1043-7.
78. Weyburne E, Bosco G. Cancer-associated mutations in the condensin II subunit CAPH2 cause genomic instability through telomere dysfunction and anaphase chromosome bridges. J Cell Physiol. 2021;236(5):3579-98.
79. Zhang X, Kschischo M. Distinct and Common Features of Numerical and Structural Chromosomal Instability across Different Cancer Types. Cancers (Basel). 2022;14(6).
80. Burrell RA, McClelland SE, Endesfelder D, Groth P, Weller MC, Shaikh N, et al. Replication stress links structural and numerical cancer chromosomal instability. Nature. 2013;494(7438):492-6.

81. Bakhoum SF, Kabeche L, Murnane JP, Zaki BI, Compton DA. DNA-Damage Response during Mitosis Induces Whole-Chromosome Missegregation. Cancer Discovery. 2014;4(11):1281-9.
82. Hosea R, Hillary S, Naqvi S, Wu S, Kasim V. The two sides of chromosomal instability: drivers and brakes in cancer. Signal Transduction and Targeted Therapy. 2024;9(1):75.
83. Cunningham CE, MacAuley MJ, Yadav G, Vizeacoumar FS, Freywald A, Vizeacoumar FJ. Targeting the CINful genome: Strategies to overcome tumor heterogeneity. Progress in Biophysics and Molecular Biology. 2019;147:77-91.
84. Setton J, Zinda M, Riaz N, Durocher D, Zimmermann M, Koehler M, et al. Synthetic Lethality in Cancer Therapeutics: The Next Generation. Cancer Discov. 2021;11(7):1626-35.
85. Campos Gudiño R, Neudorf NM, Andromidas D, Lichtensztejn Z, McManus KJ. Loss of EMI1 compromises chromosome stability and is associated with cellular transformation in colonic epithelial cell contexts. British Journal of Cancer. 2024.
86. Bungsy M, Palmer MCL, Jeusset LM, Neudorf NM, Lichtensztejn Z, Nachtigal MW, et al. Reduced RBX1 expression induces chromosome instability and promotes cellular transformation in high-grade serous ovarian cancer precursor cells. Cancer Lett. 2021;500:194-207.
87. Al-Hakim A, Escribano-Diaz C, Landry MC, O'Donnell L, Panier S, Szilard RK, et al. The ubiquitous role of ubiquitin in the DNA damage response. DNA Repair (Amst). 2010;9(12):1229-40.
88. Kimura Y, Tanaka K. Regulatory mechanisms involved in the control of ubiquitin homeostasis. J Biochem. 2010;147(6):793-8.
89. Willems AR, Schwab M, Tyers M. A hitchhiker's guide to the cullin ubiquitin ligases: SCF and its kin. Biochim Biophys Acta. 2004;1695(1-3):133-70.
90. Komander D, Rape M. The ubiquitin code. Annu Rev Biochem. 2012;81:203-29.
91. Sadowski M, Sarcevic B. Mechanisms of mono- and poly-ubiquitination: Ubiquitination specificity depends on compatibility between the E2 catalytic core and amino acid residues proximal to the lysine. Cell Div. 2010;5:19.
92. Kleiger G, Mayor T. Perilous journey: a tour of the ubiquitin-proteasome system. Trends Cell Biol. 2014;24(6):352-9.
93. Thrower JS, Hoffman L, Rechsteiner M, Pickart CM. Recognition of the polyubiquitin proteolytic signal. Embo j. 2000;19(1):94-102.
94. Iconomou M, Saunders DN. Systematic approaches to identify E3 ligase substrates. Biochemical Journal. 2016;473(22):4083-101.
95. Petroski MD, Deshaies RJ. Function and regulation of cullin-RING ubiquitin ligases. Nat Rev Mol Cell Biol. 2005;6(1):9-20.
96. Hussain M, Lu Y, Liu YQ, Su K, Zhang J, Liu J, et al. Skp1: Implications in cancer and SCF-oriented anti-cancer drug discovery. Pharmacol Res. 2016;111:34-42.
97. Qi J, Ronai ZA. Dysregulation of ubiquitin ligases in cancer. Drug Resist Updat. 2015;23:1-11.
98. Gorski JW, Ueland FR, Kolesar JM. CCNE1 Amplification as a Predictive Biomarker of Chemotherapy Resistance in Epithelial Ovarian Cancer. Diagnostics (Basel). 2020;10(5).
99. Thompson LL, Baergen AK, Lichtensztejn Z, McManus KJ. Reduced SKP1 Expression Induces Chromosome Instability through Aberrant Cyclin E1 Protein Turnover. Cancers (Basel). 2020;12(3).
100. Lepage CC, Palmer MCL, Farrell AC, Neudorf NM, Lichtensztejn Z, Nachtigal MW, et al. Reduced SKP1 and CUL1 expression underlies increases in Cyclin E1 and chromosome instability in cellular precursors of high-grade serous ovarian cancer. Br J Cancer. 2021;124(10):1699-710.
101. Thompson LL, Rutherford KA, Lepage CC, McManus KJ. The SCF Complex Is Essential to Maintain Genome and Chromosome Stability. Int J Mol Sci. 2021;22(16).

102. Chen BB, Mallampalli RK. F-box protein substrate recognition: a new insight. Cell Cycle. 2013;12(7):1009-10.
103. Zheng N, Wang Z, Wei W. Ubiquitination-mediated degradation of cell cycle-related proteins by F-box proteins. Int J Biochem Cell Biol. 2016;73:99-110.
104. Cepeda D, Ng HF, Sharifi HR, Mahmoudi S, Cerrato VS, Fredlund E, et al. CDK-mediated activation of the SCF(FBXO) (28) ubiquitin ligase promotes MYC-driven transcription and tumourigenesis and predicts poor survival in breast cancer. EMBO Mol Med. 2013;5(7):1067-86.
105. Fujii Y, Yada M, Nishiyama M, Kamura T, Takahashi H, Tsunematsu R, et al. Fbxw7 contributes to tumor suppression by targeting multiple proteins for ubiquitin-dependent degradation. Cancer Sci. 2006;97(8):729-36.
106. Jiménez-Izquierdo R, Morrugares R, Suanes-Cobos L, Correa-Sáez A, Garrido-Rodríguez M, Cerero-Tejero L, et al. FBXW7 tumor suppressor regulation by dualspecificity tyrosine-regulated kinase 2. Cell Death & Disease. 2023;14(3):202.
107. Jia L, Bickel JS, Wu J, Morgan MA, Li H, Yang J, et al. RBX1 (RING box protein 1) E3 ubiquitin ligase is required for genomic integrity by modulating DNA replication licensing proteins. J Biol Chem. 2011;286(5):3379-86.
108. Wei D, Sun Y. Small RING Finger Proteins RBX1 and RBX2 of SCF E3 Ubiquitin Ligases: The Role in Cancer and as Cancer Targets. Genes Cancer. 2010;1(7):700-7.
109. Duda DM, Scott DC, Calabrese MF, Zimmerman ES, Zheng N, Schulman BA. Structural regulation of cullin-RING ubiquitin ligase complexes. Curr Opin Struct Biol. 2011;21(2):257-64.
110. Seol JH, Feldman RM, Zachariae W, Shevchenko A, Correll CC, Lyapina S, et al. Cdc53/cullin and the essential Hrt1 RING-H2 subunit of SCF define a ubiquitin ligase module that activates the E2 enzyme Cdc34. Genes Dev. 1999;13(12):1614-26.
111. Tan M, Davis SW, Saunders TL, Zhu Y, Sun Y. RBX1/ROC1 disruption results in early embryonic lethality due to proliferation failure, partially rescued by simultaneous loss of p27. Proc Natl Acad Sci U S A. 2009;106(15):6203-8.
112. Yang Q, Zhao J, Chen D, Wang Y. E3 ubiquitin ligases: styles, structures and functions. Mol Biomed. 2021;2(1):23.
113. Ebadi P, Stratton CM, Olsen SK. E3 ubiquitin ligases in signaling, disease, and therapeutics. Trends in Biochemical Sciences. 2025;50(11):960-76.
114. Füzesi-Levi MG, Fainer I, Ivanov Enchev R, Ben-Nissan G, Levin Y, Kupervaser M, et al. CSNAP, the smallest CSN subunit, modulates proteostasis through cullin-RING ubiquitin ligases. Cell Death Differ. 2020;27(3):984-98.
115. Shteingart S, Hadar R, Cohen I, Ravid T, Tirosh B. Endoplasmic reticulum stress induces a caspase-dependent N-terminal cleavage of RBX1 protein in B cells. J Biol Chem. 2012;287(37):31223-32.
116. Henneberg LT, Singh J, Duda DM, Baek K, Yanishevski D, Murray PJ, et al. Activity-based profiling of cullin–RING E3 networks by conformation-specific probes. Nature Chemical Biology. 2023;19(12):1513-23.
117. Furukawa M, Zhang Y, McCarville J, Ohta T, Xiong Y. The CUL1 C-terminal sequence and ROC1 are required for efficient nuclear accumulation, NEDD8 modification, and ubiquitin ligase activity of CUL1. Mol Cell Biol. 2000;20(21):8185-97.
118. Xie Y, Liu Y-K, Guo Z-P, Guan H, Liu X-D, Xie D-F, et al. RBX1 prompts degradation of EXO1 to limit the homologous recombination pathway of DNA double-strand break repair in G1 phase. Cell Death & Differentiation. 2020;27(4):1383-97.
119. Fournier M, Rodrigue A, Milano L, Bleuyard J-Y, Couturier AM, Wall J, et al. KAT2-mediated acetylation switches the mode of PALB2 chromatin association to safeguard genome integrity. eLife. 2022;11:e57736.

120. Sy SM, Huen MS, Chen J. PALB2 is an integral component of the BRCA complex required for homologous recombination repair. Proc Natl Acad Sci U S A. 2009;106(17):7155-60.
121. Zhang F, Ma J, Wu J, Ye L, Cai H, Xia B, et al. PALB2 links BRCA1 and BRCA2 in the DNA-damage response. Curr Biol. 2009;19(6):524-9.
122. Kapetanaki MG, Guerrero-Santoro J, Bisi DC, Hsieh CL, Rapić-Otrin V, Levine AS. The DDB1-CUL4ADDB2 ubiquitin ligase is deficient in xeroderma pigmentosum group E and targets histone H2A at UV-damaged DNA sites. Proc Natl Acad Sci U S A. 2006;103(8):2588-93.
123. Kunishige T, Migita K, Matsumoto S, Wakatsuki K, Nakade H, Miyao S, et al. Ring box protein-1 is associated with a poor prognosis and tumor progression in esophageal cancer. Oncol Lett. 2020;20(3):2919-27.
124. Hoadley KA, Yau C, Hinoue T, Wolf DM, Lazar AJ, Drill E, et al. Cell-of-Origin Patterns Dominate the Molecular Classification of 10,000 Tumors from 33 Types of Cancer. Cell. 2018;173(2):291-304.e6.
125. Shao J, Feng Q, Jiang W, Yang Y, Liu Z, Li L, et al. E3 ubiquitin ligase RBX1 drives the metastasis of triple negative breast cancer through a FBXO45-TWIST1-dependent degradation mechanism. Aging (Albany NY). 2022;14(13):5493-510.
126. Xing R, Chen K-B, Xuan Y, Feng C, Xue M, Zeng Y-C. RBX1 expression is an unfavorable prognostic factor in patients with non-small cell lung cancer. Surgical Oncology. 2016;25(3):147-51.
127. Canadian Cancer Society. Colorectal Cancer Statistics: CCS; 2024 [Available from: https://cancer.ca/en/cancer-information/cancer-types/colorectal/statistics.
128. Cerami E, Gao J, Dogrusoz U, Gross BE, Sumer SO, Aksoy BA, et al. The cBio cancer genomics portal: an open platform for exploring multidimensional cancer genomics data. Cancer Discov. 2012;2(5):401-4.
129. Gao J, Aksoy BA, Dogrusoz U, Dresdner G, Gross B, Sumer SO, et al. Integrative analysis of complex cancer genomics and clinical profiles using the cBioPortal. Sci Signal. 2013;6(269):pl1.
130. Roig AI, Eskiocak U, Hight SK, Kim SB, Delgado O, Souza RF, et al. Immortalized epithelial cells derived from human colon biopsies express stem cell markers and differentiate in vitro. Gastroenterology. 2010;138(3):1012-21.e1-5.
131. Lepage CC, Thompson LL, Larson B, McManus KJ. An Automated, Single Cell Quantitative Imaging Microscopy Approach to Assess Micronucleus Formation, Genotoxicity and Chromosome Instability. Cells. 2020;9(2).
132. Campos Gudiño R, Rutherford KA, McManus KJ. Evaluating Chromosome Instability and Genotoxicity Through Single Cell Quantitative Imaging Microscopy. Methods Mol Biol. 2024;2825:309-31.
133. Liu P, Wang L, Yu H. Polyploid giant cancer cells: origin, possible pathways of formation, characteristics, and mechanisms of regulation. Front Cell Dev Biol. 2024;12:1410637.
134. Torres EM, Williams BR, Amon A. Aneuploidy: cells losing their balance. Genetics. 2008;179(2):737-46.
135. Was H, Borkowska A, Olszewska A, Klemba A, Marciniak M, Synowiec A, et al. Polyploidy formation in cancer cells: How a Trojan horse is born. Seminars in Cancer Biology. 2022;81:24-36.
136. Kops GJ, Foltz DR, Cleveland DW. Lethality to human cancer cells through massive chromosome loss by inhibition of the mitotic checkpoint. Proc Natl Acad Sci U S A. 2004;101(23):8699-704.
137. Trecourt A, Genestie C, Valent A, Devouassoux-Shisheboran M, Rouleau E, Yaniz-Galende E, et al. Assessing the Status of Cyclin E1 (CCNE1) From Gene to Protein Level in

Ovarian and Endometrial Carcinomas: A Systematic Review. Laboratory Investigation. 2025;105(12):104249.
138. Perera D, Venkitaraman AR. Oncogenic KRAS triggers MAPK-dependent errors in mitosis and MYC-dependent sensitivity to anti-mitotic agents. Scientific Reports. 2016;6(1):29741.
139. Timothy McKinnon RV, Brendan C. Dickson, Leah Kabaroff, Manon Alkema1, Li Chen5, Jack F. Shern5, Marielle E. Yohe5, Javed Khan5, Rebecca A. Gladdy. Kras activation in p53deficient myoblasts results in highgrade sarcoma formation with impaired myogenic differentiation. Oncotarget. 2015;6(16).
140. Zumbrunn J, Kinoshita K, Hyman AA, Näthke IS. Binding of the adenomatous polyposis coli protein to microtubules increases microtubule stability and is regulated by GSK3 beta phosphorylation. Curr Biol. 2001;11(1):44-9.
141. Zhang YX, Pan WY, Chen J. p53 and its isoforms in DNA double-stranded break repair. J Zhejiang Univ Sci B. 2019;20(6):457-66.
142. Li J, Zhou L, Liu Y, Yang L, Jiang D, Li K, et al. Comprehensive Analysis of Cyclin Family Gene Expression in Colon Cancer. Front Oncol. 2021;11:674394.
143. Fang Y, Zhang X, Guo Y, Dong Y, Liu W, Hu X, et al. PKMYT1: A Potential Target for CCNE1 Amplificated Colorectal Tumors. Cell Biochem Biophys. 2023;81(3):569-76.
144. Kok YP, Guerrero Llobet S, Schoonen PM, Everts M, Bhattacharya A, Fehrmann RSN, et al. Overexpression of Cyclin E1 or Cdc25A leads to replication stress, mitotic aberrancies, and increased sensitivity to replication checkpoint inhibitors. Oncogenesis. 2020;9(10):88.
145. Aziz K, Limzerwala JF, Sturmlechner I, Hurley E, Zhang C, Jeganathan KB, et al. Ccne1 Overexpression Causes Chromosome Instability in Liver Cells and Liver Tumor Development in Mice. Gastroenterology. 2019;157(1):210-26.e12.
146. Nakayama K, Nagahama H, Minamishima YA, Matsumoto M, Nakamichi I, Kitagawa K, et al. Targeted disruption of Skp2 results in accumulation of cyclin E and p27(Kip1), polyploidy and centrosome overduplication. Embo j. 2000;19(9):2069-81.
147. Kuhn E, Wang TL, Doberstein K, Bahadirli-Talbott A, Ayhan A, Sehdev AS, et al. CCNE1 amplification and centrosome number abnormality in serous tubal intraepithelial carcinoma: further evidence supporting its role as a precursor of ovarian high-grade serous carcinoma. Mod Pathol. 2016;29(10):1254-61.
148. Colacci A, Corvi R, Ohmori K, Paparella M, Serra S, Da Rocha Carrico I, et al. The Cell Transformation Assay: A Historical Assessment of Current Knowledge of Applications in an Integrated Approach to Testing and Assessment for Non-Genotoxic Carcinogens. Int J Mol Sci. 2023;24(6).
149. Hanahan D, Weinberg RA. Hallmarks of cancer: the next generation. Cell. 2011;144(5):646-74.
150. Riss TL MR, Niles AL, et al. Cell Viability Assays. Assay Guidance Manual [Internet] Bethesda (MD): Eli Lilly & Company and the National Center for Advancing Translational Sciences. 2013.
151. Leontieva OV, Demidenko ZN, Blagosklonny MV. Contact inhibition and high cell density deactivate the mammalian target of rapamycin pathway, thus suppressing the senescence program. Proc Natl Acad Sci U S A. 2014;111(24):8832-7.
152. Borowicz S, Van Scoyk M, Avasarala S, Karuppusamy Rathinam MK, Tauler J, Bikkavilli RK, et al. The soft agar colony formation assay. J Vis Exp. 2014(92):e51998.
153. Li J, Zhang L, Shang Y, Liu J, Zhao H. Synthetic lethality in cancer therapy: Mechanisms, models and clinical translation for overcoming therapeutic resistance. Clin Transl Med. 2026;16(1):e70586.

154. Chauhan R, Damerla RR, Dhyani VS. Synthetic lethality in cancer: a protocol for scoping review of gene interactions from synthetic lethal screens and functional studies. Syst Rev. 2025;14(1):81.
155. Kim JH, Kim SI, Park EY, Kim ET, Kim H, Kim S, et al. Comparison of survival outcomes between olaparib and niraparib maintenance therapy in BRCA-mutated, newly diagnosed advanced ovarian cancer. Gynecol Oncol. 2024;181:33-9.
156. Razi T, Farrell AC, Campos Gudiño R, Neudorf NM, Lichtensztejn Z, McManus KJ. CHEK1 is a synthetic lethal interactor of FBXO7 in colonic epithelial cells. Mol Ther Oncol. 2025;33(3):201028.
157. Rutherford KA, McManus KJ. PROTACs: Current and Future Potential as a Precision Medicine Strategy to Combat Cancer. Mol Cancer Ther. 2024;23(4):454-63.
158. Békés M, Langley DR, Crews CM. PROTAC targeted protein degraders: the past is prologue. Nat Rev Drug Discov. 2022;21(3):181-200.

APPENDIX A: SOLUTIONS

CELL CULTURE

1× McCoy's 5A Complete Culture Medium + 10% Fetal Bovine Serum (FBS)

Name	Amount
McCoy's 5A Medium (HyClone)	450.0 mL
FBS (Sigma-Aldrich)	50.0 mL
Total Volume	500.0 mL

1× X-Medium + 2% Cosmic Calf Serum (CCS)

Name	Amount
Dulbecco's Modified Eagle Medium (DMEM) with High Glucose (HyClone)	780.0 mL
Medium 199 (HyClone)	195.0 mL
Epidermal Growth Factor (EGF) (PeproTech; 20 ng/mL)	20.0 µL
Insulin (Sigma; 10 µg/mL)	5.0 mL
Apo-transferrin (Sigma; 2 µg/mL)	40 µL
Hydrocortisone (Sigma; 1 µg/mL)	50 µL
Sodium selenite (Sigma; 5 nM)	1.0 µL
CCS (HyClone)	20.0 mL
Total Volume	~1.0 L

Combine first seven ingredients

Cupric Sulfate Pentahydrate

Name	Amount
Cupric Sulfate Pentahydrate	26.0 g
Milli-Q Water	Up to 1.0 L
Total Volume	1.0 L

10× Phosphate-Buffered Saline (PBS; Stock Solution)

Name	Amount
NaCl	80.0 g
KCl	2.0 g
Na_2HPO_4	14.4 g
KH_2PO_4	2.4 g
Milli-Q Water	Up to 1.0 L
Total Volume	1.0 L

Titrate to pH 7.4

1×PBS (Working Solution)

Name	Amount
10× PBS (Stock Solution)	100.0 mL
Milli-Q Water	900.0 mL
Total Volume	1.0 L

GENE SILENCING

1× siRNA Buffer

Name	Amount
5× siRNA Buffer (Dharmacon)	100.0 µL
Diethyl pyrocarbonate (DEPC)-treated Water	400.0 µL
Total Volume	500.0 µL

WESTERN BLOT

Modified Radioimmunoprecipitation Assay (RIPA) Buffer

Name	Amount
50 mM Tris – pH 8.0	5.0 mL
150 mM NaCl	7.5 mL
SDS (Sodium Dodecyl Sulfate; 0.1% [w/v])	500.0 µL
Sodium Deoxycholate (0.5% [w/v])	0.5 g
NP40 (1% [w/v])	1.0 mL
Milli-Q Water	Up to 100 mL
Total Volume	100.0 mL

Protect from light and store at 4 ºC

25x Protease Inhibitor

Name	Amount
Protease Inhibitor Complete EDTA-free (Roche)	1 tablet
Milli-Q Water	2.0mL
Total Volume	2.0mL

Vortex tablet fully until dissolved
Store aliquots at -20 ºC

Protein Extraction Buffer

Name	Amount
Modified RIPA Buffer	955.0 µL
25× Protease Inhibitor	45.0 µL
Total Volume	1.0 mL

4× Tris-HCl/SDS, pH 6.8 (0.5M Tris-HCl Containing 0.4% SDS)

Name	Amount
Tris	6.05 g
SDS	2.0 g
Milli-Q Water	Up to 100 mL
Total Volume	100.0mL

Titrate to pH 6.8 with 1N HCl
Store at 4 ºC

6× SDS Sample Loading Buffer

Name	Amount
4× Tris-HCl/SDS	6.5 mL
Glycerol	3.0 mL
SDS	1.0 mL
β-mercaptoethanol	600.0 µL
Bromophenol Blue	1.2 mg
Total Volume	~10.0 mL

Store in 0.5 mL aliquots at -20 ºC; warm to RT before use

10× Running Buffer (Stock Solution)

Name	Amount
Tris Base	30.0 g
Glycine	144.0 g
SDS	10.0 g
Milli-Q Water	Up to 1.0 L
Total Volume	1.0 L

1× Running Buffer (Working Solution)

Name	Amount
10× Running Buffer (Stock Solution)	100.0 mL
Milli-Q Water	900.0 mL
Total Volume	1.0 L

1× Transfer Buffer

Name	Amount
10× Running Buffer (Stock Solution)	50.0 mL
Methanol	100.0 mL
Milli-Q Water	350.0 mL
Total Volume	500.0 mL

Copper Phthalocyanine 3,4’ ,4’’ ,4’’’-tetrasulfonic acid Tetrasodium Salt (CPTS)

Name	Amount
CPTS	50.0 mg
HCl	1.0 mL
Milli-Q Water	Up to 1.0 L
Total Volume	1.0 L

10× Tris Buffered Saline (TBS; Stock Solution)

Name	Amount
NaCl	80.0 g
KCl	2.0 g
1 M Tris – pH 7.5	250.0 mL
Milli-Q Water	Up to 1.0 L
Total Volume	1.0 L

1× TBS-Tween20 (TBST)

Name	Amount
10× TBS (Stock Solution)	100.0 mL
Tween20	1.0 mL
Milli-Q Water	Up to 1.0 L
Total Volume	1.0 L

Non-fat Milk Blocking Solution (5% [w/v])

Name	Amount
Non-fat Milk Powder (Carnation)	5.0 g
1× TBST	Up to 100.0 mL
Total Volume	100.0 mL

CHROMOSOME INSTABILITY ASSAY

Paraformaldehyde Fixative (4% [w/v])

Name	Amount
Paraformaldehyde (VWR Canlab)	0.4 g
1× PBS	10.0 mL
Total Volume	10mL

Bring to a slight boil to dissolve paraformaldehyde, cool to RT prior to use

Hoechst 33342 (1 mg/mL, Stock Solution)

Name	Amount
Hoechst 33342 (Thermo Scientific)	10.0 mg
1× PBS	Up to 10 mL
Total Volume	10 mL

Protect from light and store at -20 ºC

Hoechst 33342 (300 mg/mL, Working Solution)

Name	Amount
Hoechst 33342 (Stock Solution)	7.0 µL
1× PBS	Up to 25.0 mL
Total Volume	25mL

Protect from light and store at -20 ºC

Colcemid (100 ng/mL, Working Solution)

Name	Amount
KaryoMAX Colcemid (Gibco; 10 µg/mL)	10.0 µL
Complete Cell Culture Medium	990.0 µL
Total Volume	1.0 mL

KCl (1 M, Stock Solution)

Name	Amount

KCl	7.5 g
Milli-Q Water	Up to 100.0 mL
Total Volume	100.0 mL

KCl (75 mM, Working Solution)

Name	Amount
KCl (1 M, Stock Solution)	7.5 mL
Milli-Q Water	92.5 mL
Total Volume	100.0 mL

3:1 Methanol Acetic Acid (Fixative)

Name	Amount
Methanol	12.0 mL
Acetic Acid	4.0 mL
Total Volume	16.0 mL

4’,6-Diamidino-2-phenylindole (DAPI; 50 µg/mL Stock Solution)

Name	Amount
DAPI (Sigma-Aldrich; 5 mg/mL)	10.0 µL
1× PBS	990.0 µL
Total Volume	1.0 mL

Protect from light and store at 4 ºC

DAPI Mounting Media

Name	Amount
DAPI (Sigma-Aldrich; 5 mg/mL)	10.0 µL
1× PBS	990.0 µL
Total Volume	1.0 mL

Protect from light and store at 4 ºC

APPENDIX B: SUPLEMENTARY TABLES

Table S1. Two-sample KS Test Reveals Significant Increases in Nuclear Area Distributions Following *RBX1* Silencing in 1CT

Condition	n[A]	p-value[B]	Significance[C]
Replicate 1			
siControl	>1000	-	-
-siRBX1-2	>1000	<0.001	****
siRBX1-4	>1000	<0.001	****
siRBX1-Pool	>1000	<0.001	****
Replicate 2			
siControl	>1000	-	-
siRBX1-2	>1000	<0.001	****
siRBX1-4	>1000	<0.001	****
siRBX1-Pool	>1000	<0.001	****
Replicate 3			
siControl	>1000	-	-
siRBX1-2	>1000	<0.001	****
siRBX1-4	>1000	<0.001	****
siRBX1-Pool	>1000	<0.001	****

[A]Number of nuclei analyzed

[B]p-values calculated from two-sample KS tests for the listed condition relative to siControl (non-targeting siRNA)

[C]Significance level (**** p-value < 0.0001)

Table S2. MW Tests Identify Significant Increases in the Frequencies of Micronucleus Formation Following *RBX1* Silencing in 1CT

Condition	n[A]	Mean Nucleus Count[B]	Mean MN Count[C]	Mean% MNF	p-value[F]	Sig.[G]
Replicate 1						
siControl	6	1432	41	3	-	-
siRBX1-2	6	512	17	3	0.1548	ns
siRBX1-4	6	438	19	4	0.0130	*
siRBX1-Pool	6	450	18	4	0.0465	*
Replicate 2						
siControl	6	570	9	2	-	-
siRBX1-2	6	200	7	4	0.0043	**
siRBX1-4	6	282	8	3	0.0465	*
siRBX1-Pool	6	230	7	3	0.0465	*
Replicate 3						
siControl	6	2557	24	1	-	-
siRBX1-2	6	616	15	4	0.0011	**
siRBX1-4	6	880	21	2	0.0076	**
siRBX1-Pool	6	935	17	2	0.0022	**

[A]Number of wells analyzed

[B]Number of nuclei analyzed per well

[C]Mean number of micronuclei counted per well

[D]Mean percent of micronucleus formation (micronucleus count/nucleus count x 100)

[E]Median fold change in micronucleus formation relative to siControl

[F]Significance level (ns, not significant; * p-value < 0.05; ** p-value<0.01)

Table S3. Student's T-Tests Identify Significant Increases in the Frequency of Aberrant Chromosome Numbers Following *RBX1* Silencing in 1CT

Condition	n[A]	N[B]	p-value[C]	Significance[D]
siControl	300	3	-	-
siRBX1-2	300	3	0.0021	**
siRBX1-4	300	3	0.0327	*
siRBX1-Pool	300	3	0.0315	*

[A]Number of mitotic chromosome spreads analyzed
[B]Number of biological replicates
[C]p-values calculated from Student's t-tests for the listed condition relative to siControl (non-targeting siRNA)
[D]Significance level (* p-value < 0 .05; ** p-value < 0.01)

Table S4. Two-sample KS Test Reveals Significant Increases in Nuclear Area Distributions Following *RBX1* Silencing in A1309

Condition	n[A]	p-value[B]	Significance[C]
Replicate 1			
siControl	>1000	-	-
siRBX1-2	>1000	<0.001	****
siRBX1-4	>1000	<0.001	****
siRBX1-Pool	>1000	<0.001	****
Replicate 2			
siControl	>1000	-	-
siRBX1-2	>1000	<0.001	****
siRBX1-4	>1000	<0.001	****
siRBX1-Pool	>1000	<0.001	****
Replicate 3			
siControl	>1000	-	-
siRBX1-2	>1000	<0.001	****
siRBX1-4	>1000	<0.001	****
siRBX1-Pool	>1000	<0.001	****

[A]Number of nuclei analyzed
[B]p-values calculated from two-sample KS tests for the listed condition relative to siControl (non-targeting siRNA)
[C]Significance level (**** p-value < 0.0001)

Table S5. MW Tests Identify Significant Increases in the Frequencies of Micronucleus Formation Following *RBX1* Silencing in A1309

Condition	n[A]	Mean Nucleus Count[B]	Mean MN Count[C]	Mean% MNF[D]	p-value[E]	Significance[F]
Replicate 1						
siControl	6	1020	32	3	-	-
siRBX1-2	6	249	24	10	0.0011	**
siRBX1-4	6	288	27	9	0.0011	**
siRBX1-Pool	6	321	30	10	0.0022	**
Replicate 2						
siControl	6	7656	80	1	-	-
siRBX1-2	6	1500	41	3	0.0011	**
siRBX1-4	6	1777	60	3	0.0011	**
siRBX1-Pool	6	1491	50	3	0.0011	**
Replicate 3						
siControl	6	5615	111	2	-	-
siRBX1-2	6	1477	76	5	0.0011	**
siRBX1-4	6	2565	85	3	0.0076	**
siRBX1-Pool	6	2307	82	4	0.0043	**

[A]Number of wells analyzed

[B]Number of nuclei analyzed per well

[C]Mean number of micronuclei counted per well

[D]Mean percent micronucleus formation (micronucleus count/nucleus count x 100)

[E]Median fold change in micronucleus formation relative to siControl

[F]Significance level (** p-value < 0.01)

Table S6. Student's T-Tests Identify Significant Increases in the Frequency of Aberrant Chromosome Numbers Following *RBX1* Silencing in A1309

Condition	n[A]	N[B]	p-value[C]	Significance[D]
siControl	300	3	-	-
siRBX1-2	300	3	0.0002	***
siRBX1-4	300	3	0.0046	**
siRBX1-Pool	300	3	0.0049	**

[A]Number of mitotic chromosome spreads analyzed
[B]Number of biological replicates
[C]p-values calculated from Student's t-tests for the listed condition relative to siControl (non-targeting siRNA)
[D]Significance level (** p-value < 0.01; *** p-value < 0.001)

Table S7. Two-sample KS Test Reveals Significant Increases in Nuclear Area Distributions Following *RBX1* Silencing in HCT116

Condition	n[A]	p-value[B]	Significance[C]
Replicate 1			
siControl	>1000	-	-
siRBX1-2	>1000	<0.001	****
siRBX1-4	>1000	<0.001	****
siRBX1-Pool	>1000	<0.001	****
Replicate 2			
siControl	>1000	-	-
siRBX1-2	>1000	<0.001	****
siRBX1-4	>1000	<0.001	****
siRBX1-Pool	>1000	<0.001	****
Replicate 3			
siControl	>1000	-	-
siRBX1-2	>1000	<0.001	****
siRBX1-4	>1000	<0.001	****
siRBX1-Pool	>1000	<0.001	****

[A]Number of nuclei analyzed
[B]p-values calculated from two-sample KS tests for the listed condition relative to siControl (non-targeting siRNA)
[C]Significance level (**** p-value < 0.0001)

Table S8. MW Tests Identify Significant Increases in the Frequencies of Micronucleus Formation Following *RBX1* Silencing in HCT116

Condition	n[A]	Mean Nucleus Count[B]	Mean MN Count[C]	Mean% MNF[D]	p-value[E]	Significance[F]
Replicate 1						
siControl	6	1303	22	2	-	-
siRBX1-2	6	321	10	3	0.0130	*
siRBX1-4	6	314	17	5	0.1970	ns
siRBX1-Pool	6	442	22	5	0.0325	*
Replicate 2						
siControl	6	429	5	2	-	-
siRBX1-2	6	50	1	2	0.3301	ns
siRBX1-4	6	117	2	2	0.3496	ns
siRBX1-Pool	6	62	4	6	0.0898	ns
Replicate 3						
siControl	6	135	2	1	-	-
siRBX1-2	6	242	6	3	0.0076	*
siRBX1-4	6	185	5	3	0.0042	**
siRBX1-Pool	6	249	4	1	0.2273	ns

[A]Number of wells analyzed

[B]Number of nuclei analyzed per well

[C]Mean number of micronuclei counted per well

[D]Mean percent micronucleus formation (micronucleus count/nucleus count x 100)

[E]Median fold change in micronucleus formation relative to siControl

[F]Significance level (ns, not significant; * p-value <0.05; ** p-value<0.01)

Table S9. Student's T-Tests Identify Significant Increases in the Frequency of Aberrant Chromosome Numbers Following *RBX1* Silencing in HCT116

Condition	n[A]	N[B]	p-value[C]	Significance[D]
siControl	300	3	-	-
siRBX1-2	300	3	0.0027	**
siRBX1-4	300	3	0.0151	*
siRBX1-Pool	300	3	0.0091	**

[A]Number of mitotic chromosome spreads analyzed
[B]Number of biological replicates
[C]p-values calculated from Student's t-tests for the listed condition relative to siControl (non-targeting siRNA)
[D]Significance level (* p-value < 0.05; ** p-value < 0.01)